IEEE INSTRUMENTATION & MEASUREMENT SOCIETY

Received 10 June 2022; revised 5 July 2022; accepted 26 July 2022. Date of publication 5 August 2022; date of current version 19 August 2022.
The review of this article was arranged by Associate Editor Subhas Chandra Mukhopadhyay.

Digital Object Identifier 10.1109/OJIM.2022.3196746

A Review of Chipless RFID Measurement Methods, Response Detection Approaches, and Decoding Techniques

KATELYN R. BRINKER (Graduate Student Member, IEEE), AND REZA ZOUGHI (Fellow, IEEE)

Center for Nondestructive Evaluation, Iowa State University, Ames, IA 50014, USA

Department of Electrical and Computer Engineering, Iowa State University, Ames, IA 50014, USA

CORRESPONDING AUTHOR: K. R. BRINKER (e-mail: brinker@iastate.edu)

ABSTRACT Chipless RFID systems can be considered as a special case of passive RFID systems, where the tag contains no power source and no electronics. Instead, the tag's information is stored in its structure and accessed through its electromagnetic (EM) scattering response. However, robust response detection, which is primarily a function of the measurement method, measurement equipment, and processing method used, is still a major challenge in the chipless RFID field. The consequences of not properly capturing a tag response include, incorrectly assigning an ID or incorrectly reporting a sensing parameter. Due to the criticality of these challenges, this review seeks to provide an overview of the current measurement methods, equipment architectures, and processing methods as they relate to chipless RFID tag response detection and decoding. Since chipless RFID started gaining popularity around 2005, the developments in this area have been focused on three major categories: time-domain, frequency-domain, and spatial-domain systems. Frequency-domain systems have emerged as the most popular among these three categories, and thus, this review focuses on techniques used for these systems.

INDEX TERMS Chipless RFID, measurement, reader, notch detection, decoding.

I. INTRODUCTION

RADIO frequency identification (RFID) systems consist primarily of a reader with at least one reader antenna and a tag. Depending on how the tag operates, the systems can be primarily classified as either active or passive. Tags in active RFID systems have their own power source (e.g., a battery) that helps them broadcast their information back to the reader, while tags in passive RFID systems are powered by the electromagnetic wave that interrogates them. Both types of tags contain electronics, including ICs, that allow them to interpret reader requests and send back information, such as their ID or connected sensor data [1], [2], [3].

Chipless RFID tags hold their information in their structure (e.g., the resonators, antennas, microstrip lines, etc. that make up the tag) and scatter this information to the reader when they are interrogated with an electromagnetic (EM) wave. Chipless RFID can be considered as either a subset of passive RFID or as its own category. Chipless RFID systems can be classified based on how the tag's response is viewed as time-domain, frequency-domain, or spatial-domain [4], [5], [6], [7], [8]. Frequency-domain based systems are the most common since they tend to provide for the highest coding capacity, and therefore they are the focus of this review [4], [9], [10], [11].

In comparing and contrasting the different types of RFID systems, the absence of electronics and a power source distinguishes chipless RFID tags from active and passive tags. Another difference between active and passive tags and chipless tags, is that active and passive tags use their ICs to modulate their response to the reader (i.e., transfer stored information). This provides natural isolation of the tag response from its background environment [1]. However, chipless tags do not have this capability, which leads to various measurement challenges, such as limited read range and interference from reflections due to the background environment [1], [12], [13]. These challenges are further

exacerbated by the regulatory limits on the allowed transmit power for ultrawideband (UWB) interrogation of chipless tags and the relatively small size of tags at microwave frequencies, both of which limit the scattered power detected by the reader [14], [15]. All of these measurement challenges can result in not properly capturing a tag's response, which can then lead to incorrectly assigning an ID or incorrectly reporting a sensing parameter [16], [17], [18], [19].

Attempts to address these chipless RFID measurement and response detection challenges have been made both on the tag side and the reader side. However, robust response detection, which is primarily a function of the measurement method, measurement equipment, tag, environment in which the tag is, and processing method used, is still a major challenge in the chipless RFID field. Tag/reader misalignment can additionally intensify these issues and cause further challenges [19], [20], [21], [22], [23], [24], [25], [26], [27]. Due to the criticality of these challenges, this review seeks to provide an overview of the current measurement methods, equipment architectures, and processing methods as they relate to chipless RFID tag response detection and decoding for frequency-domain tags. This is done in one place and in a comprehensive manner so that interested readers can be fully informed of these issues and challenges, as well as of the variety of proposed solutions at their disposal. To this end, Section II discusses the quantities, namely radar cross-section (RCS) and S-parameters, that are commonly measured and considered as the chipless RFID tag response, while Section III discusses the roles polarization, desired reading distance, monostatic vs bistatic setups, and calibration techniques play in how the tag response is measured. Section IV provides an overview of the hardware, both off-the-shelf and custom, that has been used to measure and, in some cases, decode the tag response. Section V examines the techniques used to pre-process, detect response features of interest, analyze, and decode the tag response. Lastly, Section VI provides a comparison of some measurements that have been reported in the literature and showcases the diversity of chipless RFID measurement methods and response detection/decoding approaches.

II. MEASUREMENT QUANTITY SELECTION

When it comes to measuring a frequency-domain chipless RFID tag, there is a choice to be made primarily between measuring the S-parameter(s) (e.g., the complex reflection coefficient, S_{11}, or the complex transmission coefficient, S_{21}) of the tag or its radar cross-section (RCS) and whether to measure them in a monostatic or a bistatic configuration. RCS can be thought of as a target's equivalent area that would be seen by a radar, and it is proportional to the ratio of the power scattered by the target to the power that was incident on the target. As such, RCS is a scalar quantity (i.e., it does not contain phase information) and the units of RCS are m^2 or dB square meter (dBsm) [28], [29]. S-parameters are ratios of reflected and received waves to the transmitted wave. S-parameters are complex (i.e., have a real and imaginary component) and are unitless. Both the RCS and S-parameters are functions of the polarization, frequency, and incidence angle of the interrogating wave [28], [29], [30].

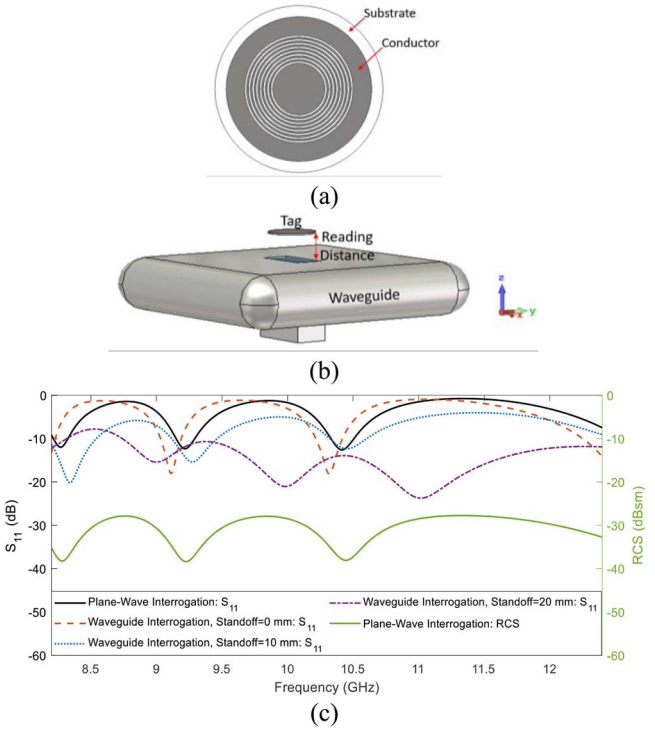

FIGURE 1. Simulation of tag response: a) model of eight circular slot tag, b) simulation setup used for waveguide interrogation, and c) tag responses generated with different simulation setups.

While there are similarities between RCS and S-parameter, there are also differences. The former is a far-field distance independent quantity while the latter is distance dependent. Another difference between RCS and S-parameters is that while S-parameters can be directly measured by a vector network analyzer (VNA), the RCS cannot. Instead, the RCS is calculated from measured quantities like received power or S-parameters in conjunction with some type of a calibration procedure [4], [29], [31]. Thus, determining RCS through measurement can be performed in several different ways [4]. Fig. 1 is provided to illustrate the relationship between RCS and S-parameters.

Fig. 1 shows simulated S_{11} and RCS responses of a tag with eight circular slot resonators, which was presented in more detail in [32], [33]. The responses were simulated using CST Studio Suite® in a couple of different ways. The first response was simulated using a waveguide port and by setting the boundary conditions such that plane-wave interrogation was performed and the complex reflection coefficient, S_{11}, response was generated. Next, a waveguide with an engineered flange was used to interrogate the tag at three different reading distances, namely: 0 mm, 10 mm, and 20 mm [34]. The setup for this simulation case is shown in Fig. 1b. Lastly, plane-wave interrogation was used with a RCS probe placed at a distance of 100 mm to extract the RCS vs. frequency

response of the tag. In comparing the responses in Fig. 1c, the distance dependence of the S_{11} responses and the similarities in terms of number of notches between the S_{11} and RCS responses can be seen. These notches, as well as other response features, could be used to assign a binary code or determine a sensing parameter (i.e., decode the response) depending on the application. The response feature detection and decoding mechanisms used in the chipless RFID field are discussed in more depth in Section V. It should also be noted that the difference in magnitude between the S_{11} and RCS responses is due to a difference in quantity definitions (voltage vs. power) and units (dB vs dBsm), rather than reading distance.

One approach to determining the RCS is to measure the received power (P_r) and use the radar range equation to solve for the RCS (σ) of a tag as [14], [31], [35]:

$$P_r = \frac{G_r P_t G_t \sigma \lambda^2}{(4\pi)^3 R^4} \tag{1}$$

$$\sigma_{target} = \frac{P_r}{P_t} \frac{(4\pi)^3 R^4}{G_t G_r \lambda^2} \tag{2}$$

In this equation P_r and P_t represent the received and transmitted powers, respectively, while R represents the distance to the target (i.e., tag), λ represents the operating wavelength, and G_r and G_r represent the gain of the transmit and receive antennas (i.e., reader antenna) that are used to interrogate the target. This approach requires the careful measurement of power, gain, and distance in order to accurately determine the RCS [14], [31], [35]. It should also be noted that this is a simplified version of the radar range equation that does not take into account parameters like receiver noise, polarization losses, and required SNR for detection [15], [36].

A second method relies on the relationship between S-parameters and RCS and again employs the radar range equation. Assuming that the gain of the transmit and receive antennas are equal (G), this relationship can be expressed for S_{21} (the complex transmission coefficient/the S-parameter measured at port 2 when a signal is transmitted from port 1) as follows [29], [37], [38], [39], [40], [41]:

$$|S_{21}| = \sqrt{\sigma} \frac{G\lambda}{\left(2\sqrt{\pi}\right)^3 R^2} \tag{3}$$

This approach can also be done with a S_{11} (the complex reflection coefficient/the S-parameter measured at port 1 when a signal is transmitted from port 1) measurement using the following equation:

$$|S_{11}| = \frac{G^2 \lambda^2}{(4\pi)^3 R^4} \sigma \tag{4}$$

Equations (3) and (4) reveal that while it is possible to determine RCS from a complex S_{21} or S_{11} measurement, it is not possible to determine the complex S_{21} or S_{11} from RCS (i.e., only the magnitude of S_{21} or S_{11} can be determined) [29], [37], [38], [39], [40], [41]. Similar to the previous method, this approach is contingent upon the accurate knowledge of antenna gain and target distance and also relies on accurate measurement of the target's S_{21} or S_{11} response [29], [31], [37], [42].

Another method combines S_{21} measurements of a target and a calibration standard with the radar range equation. In this approach, the calibration standard, such as a metal plate or sphere, is used to help achieve more accurate RCS measurement results [35]. The S_{21} response of a target can be related to the power as follows:

$$P_{target} = P_t * 10^{\left(\frac{S_{21_{target}}}{20}\right)} \tag{5}$$

In equation (5), P_{target} is the power received from the target and S_{21} is measured in dB. By combining equations (5) and (1) and using the following relationship, the RCS of the target can be expressed in terms of the RCS of the calibration standard and the S_{21} measurements of the target and the calibration standard:

$$\frac{P_{target}}{P_{std}} = \frac{\sigma_{target}}{\sigma_{std}} \tag{6}$$

$$\sigma_{target} = \sigma_{std} * 10^{\left(\frac{S_{21_{target}} - S_{21_{std}}}{20}\right)} \tag{7}$$

In equation (7), both S_{21} measurements are in units of dB [35]. The RCS of the selected calibration standard (σ_{std}) should be well-defined analytically so that it can be used in equation (7) [35], [36], [43]. One challenge of this approach is ensuring that the target and calibration standard are measured at the exact same location so that when their S_{21} responses are subtracted coherently there is no unwanted constructive or destructive interference.

A fourth method that was derived in [44] and discussed in [45] utilizes S_{21} measurements of a reference target and of its background environment in conjunction with an S_{21} measurement of the tag to determine its RCS. This method can be expressed analytically as:

$$\sigma_{target} = \left[\frac{S_{21}^{target} - S_{21}^{support}}{S_{21}^{std} - S_{21}^{support}} \right]^2 * \sigma_{std} \tag{8}$$

In equation (8), $S_{21}^{support}$ refers to the S_{21} response of the background/tag measurement setup (e.g., the anechoic chamber with a stand to hold the tag during measurements) without the tag. The assumption is that the reference standard is measured with the same setup as the tag [44], [45]. It should be noted that in both the numerator and denominator of equation (8), coherent subtraction is performed with the linear form of the S-parameters (not dB). Implementing this method results in a complex RCS, which differentiates this method from the others. This approach has gained popularity in the chipless RFID field and has also been modified for monostatic rather than bistatic measurement setups [4], [9], [46], [47], [48], [49], [50], [51].

A fifth method was designed specifically for monostatic setups and again combines S-parameter measurements to

obtain the RCS, as [50]:

$$\sigma_{target} = \left|S_{11_{target}} - S_{11_{support}}\right|^2 \frac{(4\pi)^3 R^4}{G^2\lambda^2\left(1 - \left|S_{11_{Tx/Rx}}\right|^2\right)^2} \quad (9)$$

In equation (9), $S_{11_{Tx/Rx}}$ is the S_{11} of the reader antenna in free-space. Just as in the previous approach, this approach also requires that coherent subtraction be performed with the S-parameters in linear form [50].

A sixth method was proposed for cross-polar tags (i.e., tags that produce a response with polarization that is orthogonal to that of the interrogating wave). This method, which is very similar to the previous one, uses a background reference measurement to subtract out the effects of the background environment, but does not account for the antenna effects (e.g., coupling and aperture reflections) like the previous method [52]:

$$\sigma_{tag_{cross-pol}} = \frac{(4\pi)^3 R^4}{G^2\lambda^2}\left|S_{21_{tag}}^{cross-pol} - S_{21_{support}}^{cross-pol}\right|^2 \quad (10)$$

Equation (10) assumes that a dual-polarized reader antenna is used in the measurements so that the transmit and receive gain are the same (G) [52].

The methods depicted above demonstrate the relative complexity of measuring the RCS of a tag as compared to measuring its S-parameters. As was pointed out, inaccuracy in the measurement of any of the measured parameters is propagated into the calculation of the RCS [42], [53]. Additionally, the reference measurements are distance specific so if a tag were to be measured at a different distance, the reference measurements would also need to be repeated. It should also be noted that many of these methods are not feasible outside of a laboratory setting, especially in sensing applications. For example, a tag couldn't be replaced with a calibration target to determine its RCS in an embedded materials characterization scenario [4], [32], [54], [55], [56], [57]. Due to the relationship between RCS and S-parameters, which has also been depicted in Fig. 1c, both are frequently used in the design and measurement of chipless RFID tags [4], [58], [59].

While S-parameters and RCS are the most commonly used chipless RFID measurement quantities, others such as power, voltage, and electric field have also been measured. This is especially done when custom readers, radars, or software defined radios are used to make the measurements rather than VNAs [60], [61], [62], [63], [64], [65].

III. CHIPLESS RFID MEASUREMENT APPROACHES

The choice of technique used to measure the quantity of interest is influenced by the tag design, the desired application, and the available equipment [4]. When it comes to the tag design, how the tag is designed to interact with the polarization of the interrogating wave is a major measurement approach determinant. In terms of their polarization response, tags can be categorized as co-polarizing or cross-polarizing. Co-polar tags are designed so that their response has the same polarization as the interrogating wave, while cross-polar tags are designed to have their response in the polarization orthogonal to that of the interrogating wave. In general, co-polar tags have a higher RCS and data capacity than cross-polar tags, but cross-polar tags tend to perform better in real (i.e., non-anechoic) environments. This is because background objects generally reflect with the same polarization as the interrogating wave, while a cross-polar tag produces a cross-polar response, providing for natural isolation of the cross-polar tag response from the background environment [66], [67]. Both co-polar and cross-polar tags can be categorized as Tx/Rx tags or backscatter/RF encoding particle (REP) tags. Tx/Rx generally consist of two patch antennas connected by a microstrip line loaded with resonators, while backscatter tags consist just of resonating elements [68].

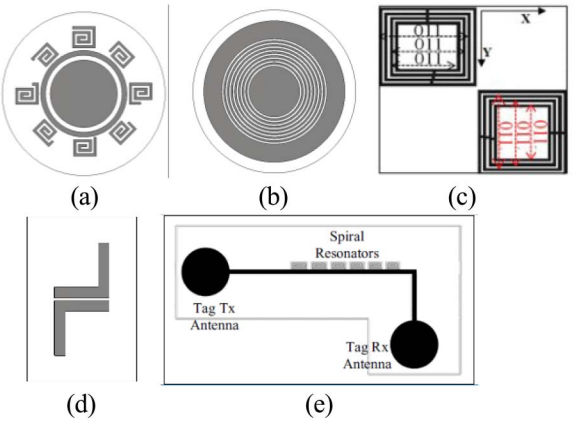

FIGURE 2. Models of different types of frequency-domain chipless RFID tags: a) co-polar linearly polarized tag [58], b) co-polar orientation insensitive tag [32], c) co-polar dual-polarized tag (©*2017, IEEE*), [76], d) cross-polar tag [69], and e) cross-polar Tx/Rx tag (©*2008, IEEE*), [79].

Co-polar tags can further be delineated as either linearly-polarized or orientation insensitive tags, where linearly-polarized tags require precise polarization alignment between the tag and the reader antenna, while orientation insensitive tags do not [20], [27], [40], [45], [69], [70], [71], [72], [73], [74]. There are also dual-polarized tags that are a special case of co-polar tags; they are designed to be read in two orthogonal polarizations that are co-polar with the polarization of the reader antenna. In the case of dual-polarized tags, the reader antenna is typically either dual-polarized, or the orientation of the reader antenna relative to the tag is changed to measure the tag in the two polarizations [69], [72], [75], [76], [77], [78]. Fig. 2 shows models of the different types of co-polar and cross-polar tags discussed above. A reference for each tag model is provided which gives more details on the dimensions, substrate material, response, frequency of operation, etc. of each tag [32], [58], [69], [76], [79].

There are numerous configurations with which co-polar and cross-polar tags can be interrogated. These include the following:

- A single linearly-polarized antenna (i.e., a monostatic setup), such as a horn or open-ended waveguide, used to interrogate a co-polar tag.
- A bistatic configuration of linearly co-polarized antennas used to interrogate a co-polar tag.
- A single dual linearly-polarized antenna used to interrogate a co-polar, cross-polar, or dual-polarized tag. This is the case of having a bistatic reader with a monostatic reader antenna.
- A bistatic configuration of linearly cross-polarized antennas used to interrogate a cross-polar tag.

From the list above, it can be seen that having a cross-polar or dual-polarized tag does necessarily imply a bistatic setup because of the use of dual-polarized antennas, such as dual-polarized horn antennas or specialized patch antenna arrays [15], [67], [69], [75], [80], [81]. In general, a monostatic configuration is limited by the directivity of the reader antenna. Using a bistatic configuration helps overcome this and improves the signal-to-noise ratio (SNR) of the received signal. However, bistatic configurations can suffer from misalignment issues and coupling between the two reader antennas [45], [69], [78], [82], [83], [84], [85], [86], [87].

Fig. 3 shows schematics of some of the measurement configurations that have been discussed in this section. This figure is not comprehensive due to the breadth of possibilities, and instead provides illustrative examples from which the mechanics of other setups can be extrapolated. In Fig. 3, the polarization of the reader antenna and the tag are indicated with red arrows and the polarization of the transmitted and received wave are described with text. In the case of the cross-polarized tag, the tag polarization is represented by two orthogonal red arrows with a yellow arrow between them to represent the polarization conversion performed by the tag. In the case of monostatic dual-polarized measurement, two lines are used to connect the reader to the antenna to represent that this is a two-port measurement (i.e., a bistatic reader with monostatic measurement setup). While a horn antenna is used in the schematics of Fig. 3 for illustrative purposes, there are many different types of reader antennas that are used for making measurements of chipless RFID tags. The reader antenna landscape will be discussed in more detail in Section IV-B.

Co-polar and cross-polar tags can also be interrogated with a circularly-polarized wave [69], [85], [88], [89]. When a circularly-polarized wave impinges on a surface and is reflected, the polarization sense changes (i.e., right-hand polarized becomes left-hand polarized and vice versa). In general, a reader antenna that is circularly-polarized can only send and receive with a single sense [90], [91]. This means that if tags can produce a circularly-polarized response with the same polarization sense as the reader, then the tag response becomes naturally isolated from the environment. This is similar to the concept of cross-polar tags, but it does not require precise alignment between the polarization of the tag and the reader. In other words, by using circular polarization to interrogate a tag, orientation independence can be achieved along with potential background isolation assuming appropriate tag design [69], [81], [89], [92], [93], [94], [95]. It should be noted that while circular polarization can help overcome sensitivity to roll-based rotations, it does not necessarily help with pitch- and yaw-based rotations [20], [62], [93], [96]. The reader setups used to implement circularly-polarized orientation insensitive reading can be either bistatic or monostatic and vary in complexity [85], [89], [93]. Additionally, some of these circular polarization reading setups require specifically-designed tags while others are able to read tags with any of the polarization schemes discussed above [69], [85]. Relatedly, measurement setups that achieve orientation independence with linearly-polarized antennas have also been proposed [23], [97], [98].

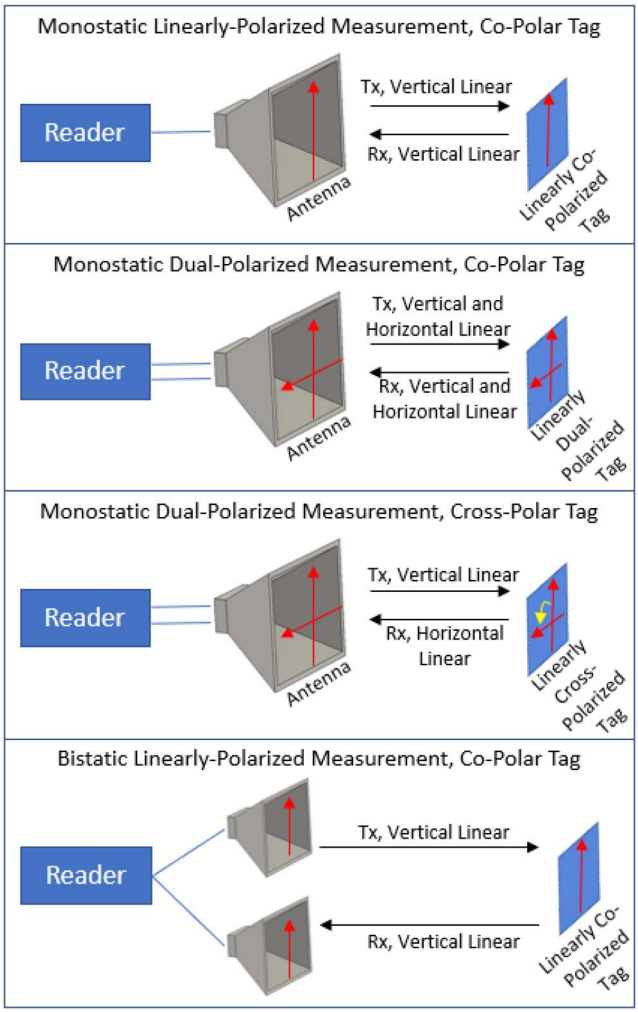

FIGURE 3. Examples of possible measurement configurations for different types of tags.

A. DESIRED READING DISTANCE

Interrogation with the polarization schemes described above has been performed in both the near-field and far-field of a reader antenna. The far-field is typically defined as starting at a distance of $2D^2/\lambda$ away from the antenna, where D is the primary dimension of the antenna. It should be noted that near-field chipless RFID measurements are typically done in a monostatic configuration. The exception to this is transmission line-based near-field readers where the tag is placed between two waveguides or on a microstrip line [33], [69], [99], [100], [101], [102], [103], [104]. The desired reading distance, and consequently whether the tag is read in the near-field or far-field, is dictated by the application and plays a role in determining the optimal measurement approach. As such, the reading distance has not necessarily increased over the evolution of chipless RFID systems. This is demonstrated in Fig. 4a where the reported reading distance is plotted against the year published for 172 different reported works, which have compiled in the dataset available in [105]. The different symbols represent whether the measurement was done with a monostatic or bistatic setup and the different colors represent whether a co-polar or cross-polar tag was measured. In works where multiple reading distances were reported, the highest one at which the tag was successfully read according to the authors of that work is reported in Fig. 4a. Furthermore, it should be noted that "success" is somewhat subjective and the criteria for success are often not provided. Therefore, some caution needs to be taken when comparing reading distances. From Fig. 4a it can also be seen that the reading distance is typically below 1 m.

There is also a relationship between the operational frequency range of the tag and the reading distance. This is illustrated in Fig. 4b. In Fig. 4b, the colors are used to help distinguish the 172 cases reported in [105] from each other (i.e., each case is represented by one vertical line) and illustrate the frequency ranges that have been used in chipless RFID measurements in the literature. Fig. 4b shows that the higher reading distances tend to be for tags operating at lower frequencies. Note the concentration of data along the bottom of the plot between reading distances of 30 cm and 100 cm. The intuition behind this is that as the frequency decreases, the tag tends to get larger, which is associated with a larger RCS. Relatedly, increasing the RCS has been demonstrated to be necessary for increasing the read range [15], [106]. One way to increase the RCS of a tag is by creating an array of tags [47], [106]. Additionally, at lower frequencies there is less path loss, which results in a larger tag response magnitude relative to that of tags that operate at higher frequencies [15]. Fig. 4b also shows that there is a concentration of designed and measured tags in the 3.1-10.6 GHz range (i.e., 35 of the 172 cases considered fall in this range and 131 of the 172 cases considered were measured at frequencies less than 10.6 GHz). This is largely due to Federal Communications Commission (FCC) and European Telecommunications

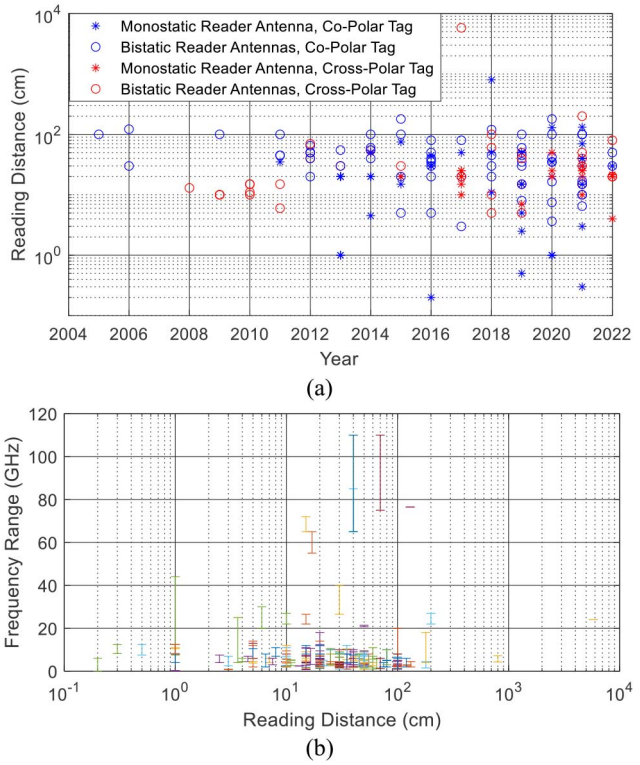

FIGURE 4. Relationship between the reported reading distance, frequency range, and year published for [9, 11, 12, 16, 19, 20, 22, 32, 33, 37-39, 45-48, 51-54, 57, 58, 60-62, 65-67, 69, 70, 73, 75, 76, 79, 80, 87, 93, 96, 99-105, 107-234]: a) Reading distance vs year, and b) Frequency range vs reading distance.

Standards Institute (ETSI) requirements for ultrawideband (UWB) applications which restrict the equivalent isotropic radiated power (EIRP) [61], [67], [235], [236]. An exception to both the frequency range and reading distance trends is reported in [157], where a combination of a 24 GHz Van Atta Array cross-polar tag, bistatic measurement setup, and a high gain transmit antenna with beam scanning capabilities is used to achieve a reading distance of 58 m.

Table 1 breaks down the number of each type of tag and type of measurement setup considered across the 172 cases in [105] and also shows the average reading distance for the different tag/reader configurations considered in Fig. 4a. From Table 1 it can be seen that cross-polar tags and bistatic reading setups, on average, tend to have higher reading distances. However, if the 58 m reading distance case from [157] is removed from the data set, the average cross-polar tag reading distance drops to 30.0 cm, the average bistatic reading distance drops to 44.8 cm, and the average bistatic cross-polar reading distance drops to 34.8 cm. This means that while cross-polar tags can be theoretically read at larger distances than co-polar tags, practitioners are not always leveraging this advantage to its fullest potential [15], [237].

Read range is defined as the largest possible distance at which a tag can be read. While the reading distance is

TABLE 1. Average reading distances for different measurement scenarios using the 172 cases in [105].

Parameter	Value
Number of Co-Polar Measured Tags	118
Number of Cross-Polar Measured Tags	54
Number of Monostatically Measured Tags	73
Number of Bistatically Measured Tags	99
Number of Monostatically Measured Co-Polar Tags	53
Number of Bistatically Measured Co-Polar Tags	65
Number of Monostatically Measured Cross-Polar Tags	20
Number of Bistatically Measured Cross-Polar Tags	34
Average Reading Distance for Co-Polar Tags	45.5 cm
Average Reading Distance for Cross-Polar Tags	136.9 cm
Average Reading Distance of Monostatic Measurements	35.2 cm
Average Reading Distance of Bistatic Measurements	103.0 cm
Average Reading Distance for Monostatically Measured Co-Polar Tags	40.1 cm
Average Reading Distance for Bistatically Measured Co-Polar Tags	49.9 cm
Average Reading Distance for Monostatically Measured Cross-Polar Tags	22.1 cm
Average Reading Distance for Bistatically Measured Cross-Polar Tags	204.4 cm

typically shorter than the read range, they can be the same. Read range is often measured or defined based on specific conditions (e.g., measuring in an anechoic chamber or with an antenna with a specific gain). In practice, the reliable reading distance is typically degraded from the read range due to a number of factors, such as polarization mismatch between the tag and reader antenna, reflections from the background environment of the tag, dynamic range of the receiver, and reader antenna performance (e.g., gain, beamwidth/reading zone, and bandwidth) [12], [15], [61], [85], [188], [237]. In order to increase the read range, the RCS of the tag relative to the background must increase, as simply increasing the transmit power also increases the scattering from the background environment [9], [15], [16], [82].

B. CALIBRATION PROCEDURES

Calibration procedures can help in isolating the tag response, which can also impact the achievable read range and reliable reading distance. Here, calibration procedures describe those that require specific steps be taken during the measurement process. Signal processing procedures that are implemented post measurement will be described in Section V. Based on this convention, there are a number of primary ways by which calibration is performed. The first, involves measuring the background response in the absence of the tag and then coherently subtracting this response from that of the tag [29], [32], [238], [239]. While this helps remove "clutter" (i.e., response due to the background environment) from the measurement, it does not help remove the effect of the reader antenna. Additionally, it has been shown that background subtraction is most effective for large reading distance measurements with there being miniscule effects for small reading distance measurements [234]. In order to remove the effect of the reader antenna, a reference target, typically a large metal plate, is often used. The reference target is measured at the same location as the tag is to be measured and then is used to calibrate the response. This is done either through the procedures described for RCS measurement in the previous section or by dividing the result of subtracting the background response from that of the tag by the Fourier transform of the time-gated metal plate response [35], [38], [45], [123], [134]. By using a reference target in this manner, the calibration procedure becomes distance specific (i.e., it only allows for tags to be measured at the specific distance at which the reference target was measured) [240]. While these approaches can be effective in static environments where the background is not changing significantly from one measurement to the next, they do not work as effectively when the environment becomes dynamic (e.g., the tag and other objects in the scene are moving) [241].

Another calibration approach that suffers from the same distance-specific limitation, is the use of calibration tags. For this approach, a calibration tag, which is typically a tag with the same form factor as the tag of interest and all the resonators removed or shorted, is measured at the same distance as the tag of interest. The responses of the tag of interest and the calibration tag are coherently subtracted and this magnitude difference is examined. In dynamic systems (e.g., sensing applications where the response is changing over time), a measurement from a specified increment of time in the past can be used as the calibration tag/reference measurement and subtracted from the current response. The responses measured from calibration tags can also be used to create a threshold of detection for the response. Furthermore, the use of a calibration tag can also be combined with background environment response subtraction and time gating [65], [100], [121], [129], [142], [160], [222].

Time gating has also been used by itself as a calibration procedure to help reduce the effects of multi-path and isolate the tag's antenna mode from its structural mode. A more detailed explanation of antenna and structural modes is provided in Part A of Section V. Time gating can be implemented directly on some VNAs, which are frequently used to read frequency-domain chipless RFID tags, or in post processing [39], [57], [94], [124]. Similarly, averaging can also be implemented on a VNA to help increase the fidelity of the tag response [51], [137]. Another approach, is to calibrate a VNA either up to the connectors or up to the aperture of the antenna, which can be done with port extension or with calibration standards when standardized antennas like waveguides are used as the reader antenna [54], [58], [69], [119], [120], [194].

Another approach geared towards systems with dual-polarized or cross-polar tags involves measuring a tag and/or the background in multiple orthogonal polarizations. The background environment responses can either be individually subtracted from their associated tag response or they can be combined with each other. For example, by subtracting the two background measurements made with

orthogonal polarizations, an estimate of the mutual coupling between the two orthogonally-polarized ports of the reader antenna can be obtained [52], [142]. Just as with some of the calibration procedures discussed previously, this multiple polarization approach can also be combined with time gating. As an example, in [75] a dual-polarized tag and the background responses were both measured in orthogonal polarizations and then the associated background response was subtracted from each tag response. These background-subtracted responses were then individually time-gated and then subtracted from each other in the frequency domain [75].

An approach which is not distance specific has also been developed [240]. This approach involves performing a measurement of the background environment and of a large metal plate at a known distance. The metal plate response is then subtracted from the background response and the result is inverse Fourier transformed into the time-domain so it can be time windowed. From this time-domain response the time of arrival from the metal plate can be computed. Subsequently, the tag response is measured and the background response is subtracted from it. This background-subtracted response is also inverse Fourier transformed for time windowing purposes and from it the time of arrival of the tag response is computed. From the time of arrival of the tag and metal plate responses and the known distance at which the plate was measured, the distance at which the tag is measured can be computed. Consequently, by knowing all of these parameters the tag transfer function can be estimated. This process is described and demonstrated in more detail in [240]. The benefit of this process is that only one set of calibration measurements is necessary in order to measure tag response at any distance from the reader.

In general, the number of measurements required to measure a tag, including those associated with the calibration process, can be used as a metric to indicate practicality when comparing measurement approaches. Additionally, some measurement approaches with associated post processing procedures have been developed that explicitly do not require calibration [241], [242], [243], [244], [245]. In [193], a table (Table 1) is provided which shows whether one or two measurements are needed in the measurement approach. In Section VI of this work, the number of required measurements for a given approach is implied by the calibration technique and measurement parameter.

C. APPLICATION-SPECIFIC MEASUREMENT APPROACHES

Another aspect that dictates the measurement approach is the application for which a tag is designed. For example, for the purpose of assessing and mitigating the effects of tag/reader misalignment several approaches have been proposed, including: 1) characterizing the reading volume of the tag using a 3D raster scanner, 2) using a specific slot resonator tag with a reader architecture consisting of two orthogonally located linearly co-polarized antennas, and 3) employing a reader capable of tag polarization recognition [19], [62], [98], [246]. Determining the position of tags (i.e., tag localization) can also require the use of multiple reader antennas arranged at specific known locations [26], [247], [248]. Another application where a specific measurement setup may be required is sensing of environmental parameters, such as temperature, humidity or pressure. In these cases, a chamber is used to produce specific conditions and the measurement setup is adjusted to meet the constraints imposed by the chamber [159], [249], [250]. For Internet-of-Things (IoT) applications, high read range in real environments is cited as an important system requirement [251], [252].

The polarization schemes, reading distances, calibration procedures, and application specific measurement approaches discussed in this section provide some insight into the breadth and lack of standardization in the chipless RFID field. This will be further demonstrated in Section VI where an additional comparison of reported chipless RFID measurements are provided. Table 2 provides a summary of the pros and cons of the various chipless RFID measurement approach related choices that are made when determining how to measure a tag (e.g., measuring with a monostatic or bistatic setup). These choices are largely independent from each other and can be made based on the application and available equipment. As such, no one combination of measurement approach choices is inherently superior to another.

IV. MEASUREMENT HARDWARE

When it comes to the measurement hardware used to implement the measurement approaches previously discussed, there is a mix of off-the-shelf and custom solutions for both the reader itself and the reader antenna. Factors involved in selecting measurement hardware include, the operating frequency, bandwidth, dynamic range, sensitivity, cost, desired read range, and measurement speed, which can all affect the system response detection and decoding capabilities.

A. READER ARCHITECTURE SELECTION

While this work focuses on the measurement of frequency-coded tags, where the tag information is encoded and viewed in the frequency-domain, the tag response can be acquired either directly with a frequency-domain reader or indirectly with a time-domain reader, such as a ultra-wideband (UWB) impulse radio (IR-UWB) system. The time-domain response can be translated to its frequency-domain response through a Fast Fourier Transform (FFT) operation [253], [254]. A brief description of the off-the-shelf and custom frequency-domain and time-domain readers and their respective limitations is provided here. Fig. 5 shows schematics of one custom frequency-domain reader and one custom time-domain reader for basic comparison purposes. However, many different architectures of frequency-domain

TABLE 2. Pros and cons of different measurement approach choices.

Measurement Approach Decision	Pros	Cons
Measurement Quantity: RCS	Distance independent.	Derived quantity that often requires multiple measurements to calculate, is only valid for far-field measurements, and is not universally practical outside of a laboratory setting.
Measurement Quantity: S-parameter	Can be directly measured.	Distance dependent.
Tag Polarization: Co-Polar	Wide variety of tag design options and only requires antennas with one polarization to measure. Tend to have a higher RCS and coding capacity than cross-polar tags.	Can be very sensitive to tag/reader polarization misalignment and the response can be overwhelmed by background reflections.
Tag Polarization: Cross-Polar	Response is naturally isolated from the background.	Measurement hardware can be more complex and can still be sensitive to tag/reader polarization misalignment.
Reader Polarization: Linear	Simple reader equipment with many different off-the-shelf options for reader antennas.	Can be sensitive to tag/reader misalignment issues.
Reader Polarization: Circular	Can help mitigate tag/reader misalignment issues and potentially provide isolation of the tag response from the background.	Requires more specialized reader equipment.
Measurement Setup: Monostatic	Simple hardware as compared to bistatic setups.	Limited by the directivity of the reader antenna.
Measurement Setup: Bistatic	Higher SNR than monostatic setups.	Can have misalignment and mutual coupling issues. Not generally suitable for near-field measurements.
Desired Reading Distance: Near-field	Less affected by background reflections and the tag response generally has a higher SNR.	Some antennas, such as horn antennas, are not well suited for use in the near-field due to high phase variation.
Desired Reading Distance: Far-field	Can use a wide variety of reader antennas and well suited for applications where close proximity to the tag is not possible.	Tag response is small due to propagation loss and can be more easily overwhelmed by background reflections than in the near-field.
Performing Calibration	Can remove the effects of background reflections and make the tag response easier to detect and decode.	Requires additional measurements and processing to determine the tag response.

and time-domain readers have been proposed and therefore, interested readers can refer to the block diagrams of frequency-domain and time-domain reader architectures with more in-depth descriptions of the individual components that can be found in [63], [236], [254], [255], [256].

Pertaining to frequency-domain readers, VNAs are the most common off-the-shelf option [105]. While VNAs can

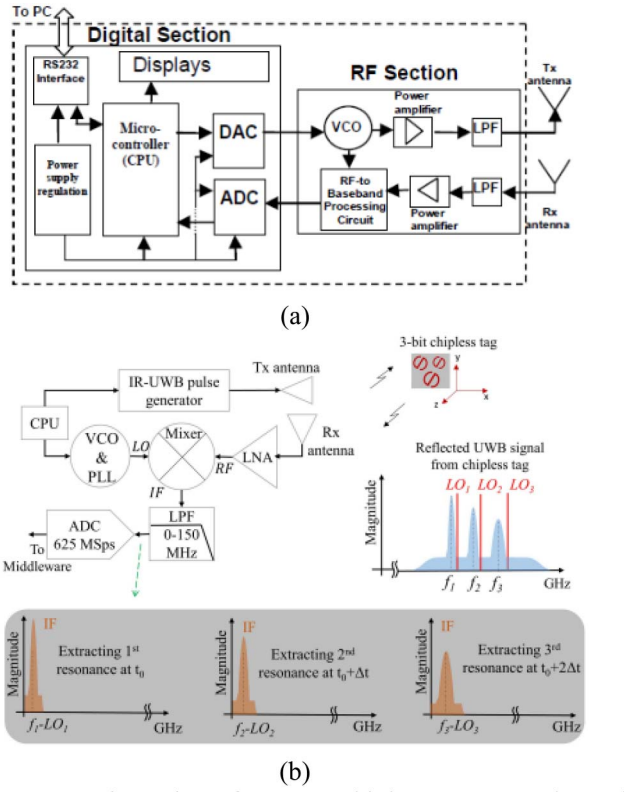

FIGURE 5. Schematics of custom chipless RFID readers: a) frequency-domain reader (©*2009, IEEE*) [65], and b) time-domain IR-UWB reader (©*2021, IEEE*) [61].

support UWB operation with high frequency resolution and accuracy, they can be costly and bulky which has prompted interest in the development of custom-designed and economical readers. However, it should be noted that with the current developments in the design and commercialization of microwave components, relatively low-cost and handheld VNAs have appeared in the market in recent years [110], [257]. Software defined radios, which tend to be less expensive than VNAs, and a combination of an RF signal generator and spectrum analyzer have also been used for reading chipless RFID tags [86], [187], [216], [242]. When it comes to custom-designed frequency-domain systems, scalar, homodyne, and superheterodyne architectures have also been proposed. All of these architectures have faced some common challenges, namely: balancing voltage-controlled oscillator (VCO) performance and cost (i.e., having a VCO with a wide enough bandwidth to read the tags of interest), managing transmit power regulations, achieving a high read range, reducing read time/system latency, and mitigating self-interference due to signals from the transmitter leaking into the receiver sub-section of the reader. By the virtue of lacking phase information, scalar readers also suffer from calibration-based limitations and high receiver noise power [82], [86], [186], [254], [258], [259], [260], [261], [262], [263]. In addressing the issue of self-interference, self-interference cancellation boards [86], an UWB compensation unit based on a polyphase power divider [186], [235],

a compensation unit based on wideband differential phase shifters [264], and a wideband directive filter have been proposed [260]. For the issue of noise, various techniques, such as a moving average filter, has been proposed and implemented on-board the reader [265], [266].

With respect to off-the-shelf time-domain readers, high-speed digital oscilloscopes with impulse generators and radar systems have been used [67], [170], [244], [267], [268], [269]. The main benefit of using a time-domain reader system is the spreading of the transmitted power over the frequency band of interest with a short single pulse, which provides for high peak power with a low average power. In this way, these systems effectively increase the power of the signal used to interrogate the tag while still being compliant with FCC and ETSI regulations, which theoretically increases the maximum read range of time-domain readers over that of frequency-domain readers for some types of tags [61], [82], [255], [270]. However, the amplitude of the interrogation pulse is not constant over frequency; rather, it takes a gaussian shape. Therefore, additional signal processing is often recommended to interpret and decode the tag response in the frequency-domain. One alternative to this uses a set of pulses with different center frequencies to create a more even spectrum amplitude across the overall interrogation signal [271].

There are two primary custom-designed time-domain reader architectures, namely: IR-UWB and chirped pulse Fourier transform microwave (CP-FTMW). IR-UWB readers can theoretically capture the entire tag response simultaneously in the backscattered short-duration pulse because they do not need to sweep the frequency. This makes this approach very fast, but it also means that the resulting frequency resolution will suffer after the Fourier transform due to the short duration of the pulse. CP-FTMW readers, in contrast to IR-UWB readers, use a broadband chirped pulse that is stretched in time while still generally having a shorter reader time than IR-UWB readers. This longer duration pulse provides for the transmitted power to be more evenly distributed over the frequency range of interest and provides for better frequency resolution post Fourier transform [203], [236], [254].

For both IR-UWB and CP-FTMW readers, a high-performance high-speed analog-to-digital converter (ADC) is needed to sample the signal that is scattered from the tag [61], [203], [236], [254]. To reduce the cost associated with high-performance ADCs in custom solutions, a method that uses multiple ADCs and an equivalent time approach method have been proposed [236], [272]. In the equivalent time approach, multiple UWB impulses are used to interrogate the tag and the reader incrementally samples a few points from each backscattered pulse. While cost effective, this approach can experience drawbacks as a result of sampling clock jitter. However, these issues can be mitigated with increased hardware complexity [236], [268], [273]. In practice, the pulse repetition rate can be increased and averaging can also be implemented to increase the SNR [203]. Additional recent developments of custom time-domain readers include, a fully-tunable ultra-low jitter baseband pulse generator [274], reduction in read time through FPGA implementation optimization [236], a dual-comb technique for increasing the frequency resolution while reducing the complexity of the receiver portion of the reader design [203], a combined IR-UWB transmitter/frequency translation reading method [61], and a multicarrier-based receiver with a pulse distortion decoding approach [275].

For both frequency-domain and time-domain readers, numerous techniques have been proposed in the literature for increasing performance. These include implementing features like a handshaking algorithm for detecting if a tag is present in order to reduce power consumption [276], selectively silencing the transmitter to allow for increased radiated power while interrogating the tag [235], using a fast locking phase-locked loop (PLL) to allow for higher transmitted power [186], including adaptive frequency hopping and adaptive sliding window methods to reduce read time [262], [263], and using ZF equalization to improve the tag detection rate [277]. Increasing the number of receiver antennas to increase receiver diversity, using a Selective-RAKE receiver to filter clutter, using dual signal sources to intentionally create different interrogating wave polarizations, and creating a reader that can read tags in two polarizations without changing the orientation of the reader antenna have also been proposed [98], [242], [278], [279]. Additionally, using a bank of bandpass filters in the receiver with each filter having a center frequency corresponding to a resonance frequency of the tag has been proposed. While this approach reduces the reader receiver complexity and lowers the ADC performance requirements, it also is limited in terms of the tags it can read [63].

In comparing frequency-domain and time-domain readers, frequency-domain readers tend to be more sensitive to the tag response due to their input noise bandwidth and they tend to provide higher frequency resolution. This is primarily due to the short duration of IR-UWB pulses, which determines the frequency resolution. However, IR-UWB readers tend to have a faster read time than frequency-domain readers and as discussed previously, have transmitted power advantages that result in stronger received signals and therefore greater potential reading distances [63], [82], [236], [254], [255]. It should be noted that read time is dependent on the bandwidth, number of frequency points, and reader architecture. Therefore, as a metric read time needs to be considered in the context of the application and one-to-one comparisons of read times can only be made when similar tags are read by both readers. This points to the potential benefit of the chipless RFID field agreeing on specific tag standards for testing and comparing reader performance, which do not currently exist.

The reader hardware for the 172 cases reported in [105] is compared in Fig. 6. This plot depicts the highest reported reading distance vs. the center frequency of the range over which the tag was measured for three categories of readers,

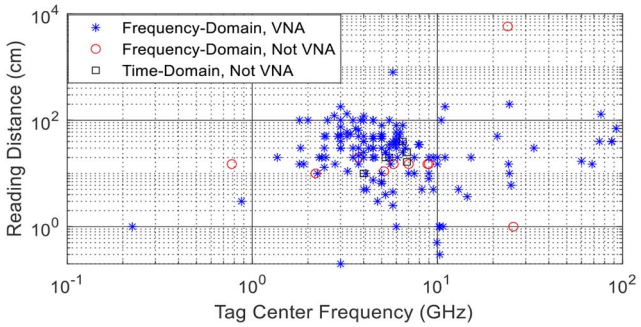

FIGURE 6. Comparison of time-domain and frequency-domain readers in terms of reading distance and center frequency of the measured operational frequency range [9, 11, 12, 16, 19, 20, 22, 32, 33, 37-39, 45-48, 51-54, 57, 58, 60-62, 65-67, 69, 70, 73, 75, 76, 79, 80, 87, 93, 96, 99-105, 107-234].

namely: VNAs, non-VNA frequency-domain readers, and time-domain readers. Fig. 6 demonstrates the similar reading distances that are achieved in practice for frequency-domain and time-domain readers, despite time-domain readers theoretically providing longer read ranges [61], [255]. However, of the 172 cases considered, only six were done with time-domain readers, while 156 were done with a VNA and ten were done with other types of frequency-domain readers. This provides evidence for both the lack of prevalence of time-domain readers for frequency-domain chipless tags and the potential to better leverage the advantageous features of time-domain readers.

The evolution of the custom-designed chipless RFID reader development landscape is depicted in Table 3. Table 3 lists the readers that have been proposed and tested in the literature over time, and allows for comparison across architectures, required calibration complexity, bandwidth, and cost when possible. It should be noted that some of the entries represent incremental improvements over others and that only readers that were prototyped were included in this table. As can be seen from Table 3, most of the readers operate in the 3.1 – 10.6 GHz range, which is in line with the trends shown in Figs. 4 and 6. As previously discussed, this frequency range is popular due to the desire for developed readers and tags to comply with FCC and ETSI regulations. There is also a tradeoff to consider when it comes to higher frequency tags: as tags are designed to operate at higher frequencies, they tend to become smaller and then have a smaller average RCS over frequency and smaller read range [54]. This means that in order to read a higher frequency tag, readers generally need to have a higher sensitivity to lower level signals so that they are able to detect the minimum RCS value of the tag [82].

Another point of interest in Table 3 is that there is a mix of both monostatic and bistatic setups for both frequency-domain and time-domain readers. Cost is potentially another metric across which readers can be compared. However, cost is not always discussed in the published technical literature, and when it is mentioned, the currency is not always specified and there are inconsistencies in terms of whether or not the cost of the antennas is included in the total reported price of the reader. The performance of custom readers like these in terms of measuring tags will be further demonstrated in the comparison provided in Section VI.

B. ANTENNA SELECTION

Similar to reader hardware, the antennas used to interrogate a tag can be off-the-shelf or custom and depend on factors, such as the polarization scheme and desired read range. Additional factors for consideration include desired gain, half power beam width (HPBW), form factor, cost, and calibration potential. Notably, read range been shown to be affected by the gain, beamwidth, and polarization of the reader antenna [12], [85], [157], [280]. Ultimately, however, the driving requirement for chipless RFID reader antennas is the operational frequency range of the tags of interest. In other words, the reader antenna needs to be able to interrogate the tag over a range of frequencies that captures all of the response features of interest (e.g., all of the resonances) [63], [85].

When it comes to off-the-shelf solutions, rectangular waveguides and horn antennas are popular choices. Some benefits to using rectangular waveguides are that they can be calibrated up to their aperture with well-known standards (e.g., short, shifted short, and matched load) and are inherently wideband as compared to basic patch antennas. However, waveguides have a smaller gain than some other types of antennas, such as horn antennas, and measurements made with waveguides can suffer from flange effects. To mitigate flange effects, engineered flanges that approximate infinite flanges have been developed and used in the measurement of chipless RFID tags [20], [34], [54], [58], [103]. Horn antennas, on the other hand, have higher gains than open-ended waveguides and can be more wideband (e.g., ridged horns). However, there is a lot of phase variation in the near-field of horn antennas and therefore, they are typically only used in far-field measurements [90]. Horn antennas can also be dual-polarized and are therefore often used for the interrogation of cross-polar tags when a monostatic antenna setup is desired [66], [67].

Custom options have been proposed mainly because of the larger form factors and costs of standard off-the-shelf options, such as horn antennas, that are commonly used in laboratory settings and would not necessarily be suitable for large scale commercial use [63], [236], [285]. Custom-designed antennas can be categorized by whether they are planar or nonplanar, their polarization characteristics, their operational frequency range, gain, and other pertinent parameters. Table 4 provides a comparison of antennas that have been custom-designed specifically for chipless RFID applications. It should be noted there are many other UWB antennas in the literature that could be suitable for chipless RFID applications, but all cannot be explored comprehensively within the scope of this work. Based on the custom-designed reader antennas reported in Table 4 there are a few trends that can be identified, namely: 1) custom-designed reader

TABLE 3. Comparison of custom chipless RFID readers that have been fabricated and tested.

Time- or Frequency - Domain	Monostatic or Bistatic	Noted Features	Calibration	Frequency Range (GHz)	Cost	Year	Reference
Freq.	Bistatic	Designed for near-field applications, the reader can process the tag response after the tag has left the interrogation zone.	Reference tags	1.9-2.5	AUD $300	'09	[65]
Freq.	Bistatic	The digital section can be connected to multiple RF sections for reading multiple tags in conveyor belt type situations simultaneously.	Reference tags	4-6		'10	[281]
Freq.	Bistatic	Considered to be the 2nd generation version of the reader in [65].	Reference tags	5-9	AUD $4500	'10	[114]
Freq.	Bistatic	Designed for near-field applications.	Reference tags	5-10.7		'10	[115]
Freq.	Bistatic	Uses only one VCO to generate a wideband linear chirp signal and uses a Hilbert transform complex analytical sign-processing technique. 3rd generation of the reader in [65].		4-8	$650	'12	[258]
Time	Bistatic	Uses equivalent time approach and has a design that decreases sampling noise		3.1-10.6	€2000	'15	[273]
Time	Bistatic	Uses equivalent time approach		3-7.5	€2000	'15	[143]
Freq.	Monostatic	Only has 1 VCO and tag resonance information appears as a low-frequency signal superimposed on the bias current of the VCO.	Reference tags	2-3.4		'16	[282]
Time	Bistatic	Uses equivalent time approach, reduction in sampling noise as compared to [143] and fixes synchronization issue from [273].		3-7		'17	[268]
Freq.	Bistatic	Has dual signal sources and controllable attenuators in order to control the polarization interrogating the tag.		12.4-18		'17	[98]
Freq.	Monostatic	Implements a self-interference cancellation circuit with a software defined radio to increase the read range		2.57-2.69		'18	[86]
Freq.	Bistatic	Uses a handshaking algorithm with single frequency interrogation to reduce power consumption.	Reference tags	4-8		'18	[276]
Freq.	Monostatic	Uses an ultra-wideband compensator for interference isolation	Background measurement	4.3-7.3	$600	'19	[186]
Freq.	Bistatic	Low cost solution		4-8	$600	'19	[283]
Freq.	Bistatic	Designed to be used with cross-polar tags		2-2.5	$120	'19	[259]
Freq.	Monostatic	Reader is based on the one in [186] and Implements the adaptive wavelet based detection algorithm in hardware.	Established detection thresholds by measuring a tag 100 times.	4-7.5		'20	[190]
Freq.	Bistatic	Designed for use with cross-polar tags and dual-polarized antenna.	Startup procedure for finding optimum coefficients for the vector modulator.	4.6-5.6	$1000	'20	[284]
Time	Bistatic	Uses a frequency translation method in the receiver which reduces the noise bandwidth, cost, read time, and complexity of the receiver, while still providing for a VNA competitive read range. Preliminary information about the tag must be known prior to measurement.	Background measurement	3.1-10.6	$600	'21	[61]
Freq.	Bistatic	Employs a directive filter and a modified gain-phase detector for leakage cancelation and accurate phase detection, respectively.	Startup procedure for finding optimum coefficients for the vector modulator and then background measurement	4-8	$800	'22	[261]
Time	Bistatic	Multicarrier system that uses pulse distortion for decoding the tag response.		4.3-7.5		'22	[275]

antennas tend to be planar (i.e., microstrip patch antennas), 2) they tend to operate in the UWB 3.1-10.6 GHz range in order to be compatible with the proposed custom-designed readers and regulations, and 3) the gain varies widely from 2.6 to 26 dBi.

A consequence of many planar custom-designed reader antennas is that they are often fabricated using printed circuit boards (PCB). However, 3D printing has also been employed for fabrication [69], [188]. Table 4 also shows that linear polarization and dual linear polarization are the dominant polarization schemes for custom reader antennas. However, since the use of circular polarization for chipless RFID applications is relatively new, more circularly-polarized reader antenna designs could be on the horizon [69], [92], [93].

V. RESPONSE PROCESSING

Detecting tag response features (e.g., notches, peaks, and phase jumps) is critical for assigning a binary code or sensing parameter. Due to factors, such as noise, misalignment, multipath, overwhelming background reflections, and tag response collisions, a number of post processing methods have been developed in order to extract the tag response from the measurement and assign binary codes and sensing parameters as appropriate. Post processing needs and requirements are driven by the choice of the parameter being measured, the environment the tag is measured in, the hardware used to make the measurements, and the calibration techniques employed [57], [290], [291], [292].

Analysis of a tag response begins with how the response is considered, which is limited by the measurement parameter (e.g., if RCS is measured then there will generally not be phase information available to examine). For example, the interpretation and analysis of a response considered in magnitude and phase form may be different than that viewed in group delay form or as the amplitude difference between the tag of interest and a reference tag. To this end, this

TABLE 4. Custom chipless RFID reader antennas.

Antenna Type	Planar or Non-Planar	Polarization	Freq. (GHz)	Max Gain (dBi)	Year	Ref.
Log Periodic Dipole Array	Planar	Linearly-polarized	2-2.5	~5.8	'09	[65]
2x2 array of dipole reflector antennas	Non-Planar	Dual linearly-polarized	4.8-5.4	13.6	'10	[12]
UWB Monopole Patch	Planar	Linearly-polarized	3.1-10	2.6	'10	[12]
4x4 aperture coupled patch antenna array	Planar	Linearly-polarized	21-27	20	'12	[285]
Microstrip line for near-field coupling with tag	Planar	Linearly-polarized	5-10	NA	'13	[104]
2x2 elliptical leaf dipole array	Non-Planar	Linearly-polarized	4-6	15	'13	[63]
Reflectarray with horn antenna feed	Non-Planar	Linearly-polarized	4.9-7.1	~22.5	'14	[286]
Single element dual-polarized aperture coupled microstrip patch antenna (ACMPA)	Planar	Dual linearly-polarized	6.4-10.6	~7	'15	[147]
4x4 ACMPA	Planar	Dual linearly-polarized	22-26.5	16	'15	[80]
Single element linearly-polarized ACMPA	Planar	Linearly-polarized	6.4-10.6	~7	'16	[70]
Reflectarray with horn antenna feed	Non-Planar	Linearly-polarized	4-6	19.5	'18	[287]
8x8 interleaved ACMPA with back reflectors	Planar	Dual linearly-polarized	4.2-7.1	26	'18	[188]
Quadrifilar spiral antenna	Planar	Circularly-polarized	1.2-12.4	5.5	'18	[288]
Quasi-Yagi antenna	Planar	Linearly-polarized	1.7-5.5	5.3	'19	[289]
Septum polarizer with waveguide feeds	Non-Planar	Dual circularly-polarized	8..2-12.4	NA	'20	[69]
2x2 ACMPA with back reflector	Planar	Linearly-polarized	4.15-8	15.5	'20	[233]
4x4 dual-polarized ACMPA	Planar	Dual linearly-polarized	4.4-6.8	21	'20	[232]
UWB monopole patch	Planar	Linearly-polarized	2-8	5.7	'21	[11]
8x8 ACMPA array	Planar	Linearly-polarized	22-27	22	'21	[204]
2x2 circularly-polarized array	Planar	Circularly-polarized	7.05-8.48	15	'21	[93]

section will examine and analyze the components of a tag response, how the resonance frequencies are determined, how binary codes and sensing parameters are assigned, the metrics used to compare post processing and decoding methods, and application specific post processing methods.

A. ANALYSIS AND PRE-PROCESSING OF THE BACKSCATTERED RESPONSE

When a tag is measured in a real environment (i.e., not in an anechoic chamber environment), the response often contains interfering signals, such as noise and unwanted reflections from background objects. Additionally, as the reading distance increases, so does the path loss. This results in weaker signals that can be more easily overwhelmed by the aforementioned interfering signals (i.e., clutter) and is prohibitive to increasing the quantity of information coded in the tag (i.e., it is unproductive to increase the number of notches in a response if they cannot be detected and decoded). Consequently, pre-processing is often necessary to enhance the signal quality prior to detecting response features for the purpose of decoding (i.e., assigning a binary code or a sensing parameter) [240], [293], [294]. Additionally, sometimes pre-processing is needed to get the measured response into a desired format (e.g., using the Hilbert transform to get the amplitude and phase responses from a custom reader without the need for a calibration tag) [240], [258], [295]. Some popular approaches to pre-processing include, analysis of the backscattered signal components in the time-domain (reader mode, structural mode, and tag mode), channel estimation, and general filtering.

The response of a tag can be broken down into three general components in the time-domain: the reader mode (also referred to as the rejection mode), the structural mode, and the tag mode (also referred to as the antenna mode). The reader mode occurs first temporally and captures the aperture reflections and coupling of the reader antenna(s). This is usually the largest mode and contains most of the signal's energy. The structural mode occurs second temporally and consists of the immediate reflections from the tag structure (e.g., the substrate and the metallic resonators). In these reflections, the frequency content of the interrogating wave is not altered. In other words, the spectrum of the structural mode is effectively the same as that of the interrogating pulse. Additionally, in the case of cross-polar tags, the structural mode is greatly reduced with respect to that of co-polar tags [11], [216], [241], [245], [271], [294], [296], [297]. The tag mode occurs third and consists of information related to the tag's resonances. It is considered to be the late time, source-free portion of the response according to complex natural resonance (CNR) theory [298], [299]. The tag mode usually lasts for tens of nanoseconds while decaying exponentially and is smaller in amplitude than both the reader mode and the structural mode. There can also be additional components in the response, such as reflections from background objects and multipath reflections. Therefore, various filtering, subtraction, and time gating procedures have been proposed for isolating the tag mode, which can then be transformed to the frequency-domain for decoding [216], [241], [271], [296], [297].

Fig. 7 provides an example of the three different modes of a tag response and the process of extracting the tag mode. For this, the process outlined in [216] was followed. For Fig. 7, the eight circular slot tag shown in Fig. 1 was simulated in front of a horn antenna at a distance of 30 cm. Fig. 7a, shows the time-domain response of the tag that was obtained through an inverse FFT (IFFT) with the reader mode (y_r), structural mode (y_s), and tag mode (y_t) are designated. The

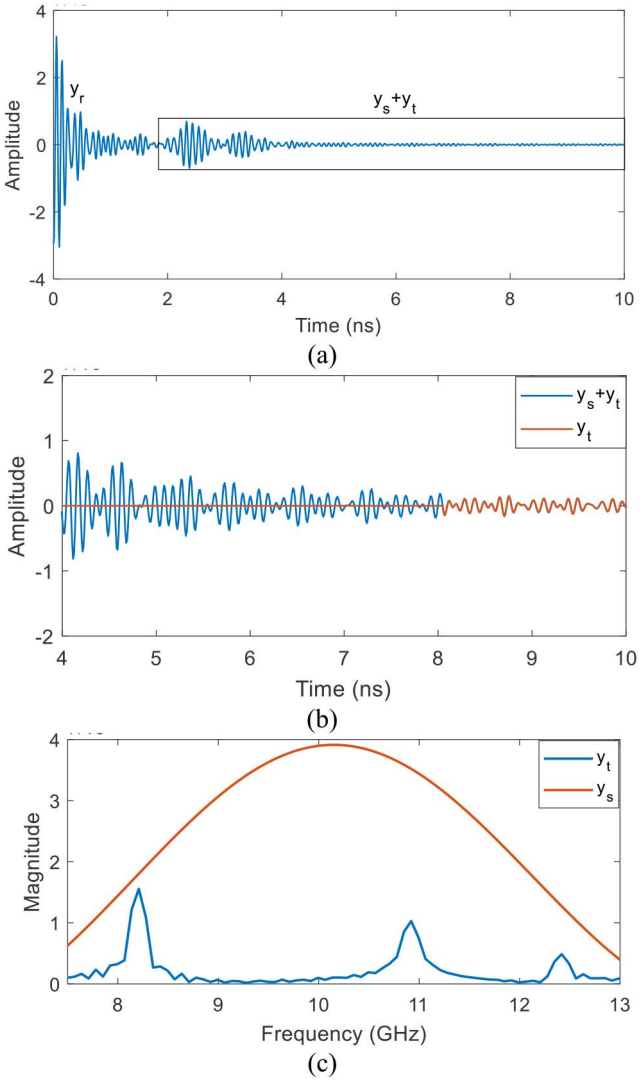

FIGURE 7. Example of 3 components of a tag response: a) reader mode (y_r), structural mode (y_s), and tag mode (y_t) of a tag in the time-domain, b) time-gated tag mode after the reader mode is subtracted, and c) structural mode and tag mode of a tag in the frequency-domain after time-gating to separate them.

horn antenna was then simulated without the tag and its response was also transformed to the time domain. The two signals were then subtracted to obtain the response shown in Fig. 7b, which was then time-gated using a rectangular window to extract the tag mode. The time window start and stop times were determined through trial-and-error. The FFT was taken of the structural mode and the extracted tag mode to obtain the spectrums shown in Fig. 7c. In Fig. 7c, the three peaks in the tag mode correspond to the three resonances of the tag that occur in the considered frequency range (see Fig. 1c).

One challenge when trying to isolate the tag mode from the structural mode is determining at what time the tag mode begins, assuming the tag mode and structural mode are not completely overlapped with each other or the reader mode [241], [298]. Additionally, the performance of time gating to isolate the tag mode is reduced for higher frequency resonators [15]. For this reason, isolating the antenna mode is only really possible when the tag is being measured at a large distance from the reader antenna (i.e., at least 15 cm according to [300]) and the tag is operating at sufficiently low frequencies [241]. Approaches previously proposed for determining the start time of the tag mode include, trial and error [297], having a Tx/Rx tag with a meandering transmission line between the tag antennas to create enough temporal separation to distinguish between the structural and tag modes easily [296], using the reading distance and system parameters like the cable lengths to estimate the starting time of the tag mode [57], examining the spectral norm of the impulse response data matrix over a sliding window [301], using the half Fourier transform [302], and examining the time-frequency plot after employing the short-time matrix pencil method (STMPM) [134], [303], [304]. Another challenge is making sure that the window isn't too long since this can introduce unwanted noise into the response. Methods, such as using knowledge of the lowest frequency pole or estimating it from the dimensions of the tag, have been proposed for this purpose [245], [304].

After determining the start and stop times of the window for isolating the tag mode, a variety of different types of windows can be used to extract the tag mode. For example, raised cosine window was used in [216] and [270], a Hamming window was used in [245], and a Tukey window was used in [304], while the example in Fig. 7 used a rectangular window. It should also be noted, that windowing can be applied to a background-subtracted response to further reduce the effects of noise or it can be combined with the use of a narrow beam antenna to achieve volume gating [266], [300]. Once the tag mode is "windowed" out, a Fourier transform can be performed to view the response in the frequency-domain and perform further processing and decoding [241].

Beyond analyzing the tag backscattered response, the wireless channel can be estimated and analyzed. This estimation can take into account many different factors, including the angles of arrival and departure of the interrogating wave and the spatial gain of the tag [25], whether the tag is being read in the near-field or the far-field with varying levels of noise [305], multipath components [57], fading [277], calibration accuracy [306], polarization dependence [293], and estimation of the residual environment [15]. In order to mitigate channel effects, zero forcing (ZF) equalizers have been proposed [277], [293].

While denoising and decluttering techniques, like moving average filters, have been implemented in hardware, they can also be implemented on a computer in the pre-processing stage [265], [266], [281], [307]. Other examples of improving the tag response signal quality include, the use of a prolate spheroidal wave function-based filter in [308], using a general matched filter [309], using a continuous wavelet transform as a matched filter in [244], using the

least mean square error algorithm to do adaptive direct path cancellation [310], and detrending the response followed by denoising with a discrete wavelet transform [311].

B. DETECTION OF RESPONSE FEATURES AND RESPONSE DECODING

The first step in decoding the tag response is to identify the features of interest in the response. These features of interest are often notches or peaks in the magnitude vs. frequency response of the measured quantity (e.g., S_{21} or RCS). These features are created by the designed resonant properties of the tag, but they can vary depending on the reader architecture, how the response is viewed, and the decoding method being used. For example, while the RCS magnitude or the magnitude or phase of S-parameters are typically directly examined for decoding, in [56] and [77] the tag is measured in two orthogonal polarizations and the two responses are subtracted which creates sharp amplitude changes that can be used to identify the resonance frequencies and assign a binary code. Other examples of unique response viewing approaches include, determining the zeros in the derivative of the group delay which is itself the derivative of the phase vs. frequency response [308] and examining the pulse distortion in the response of an IR-UWB reader [275]. Decoding can then be performed either onboard the reader, as in [65], or in post processing on a computer. The common methods used for decoding in chipless RFID applications are detailed below.

Some of the proposed methods for binary code assignment, which is primarily done for identification applications but has also been done for sensing applications, include the following:

1) Method 1: Specified response features (e.g., a peak or a notch) are 0's. Removing an instance of the specified response feature results in a 1 in the code [110].
2) Method 2: Specified response features are 1s. Removing an instance of the specified response feature results in a 0 in the code [46].
3) Method 3: Specified response features are 1s and removing an instance shortens the code [312].
4) Method 4: Encoding multiple bits per resonator state in conjunction with encoding the phase deviation and frequency position in a frequency channel [116], [117].
5) Method 5: Frequency shift coding. The bandwidth is divided into sections and the sections are divided into sub-sections. Each sub-section represents a possible position of a resonance and has a different binary bit sequence. In this way, each resonance is encoded by multiple bits [67], [135].
6) Method 6: Concatenating the codes generated using Method 2 when the tag is measured in two different polarizations [139].
7) Method 7: Concatenating the codes generated by Method 4 when the tag is measured in two different polarizations [144].
8) Method 8: Phase position modulation [128].
9) Method 9: Division into windows and assigning 1's where the response is primarily above the threshold (determined via integration) and assigning 0's where the response is primarily below the threshold [32], [194].

Methods 6 and 7 can be considered as hybrid methods since at least two parameters are combined to create the full code [69], [313], [314].

In terms of sensing parameter assignment, a variety of methods beyond binary code assignment have also been proposed [4], [194], [315]. These include the following:

1) Correlating a resonance frequency shift to a sensing parameter [169], [315].
2) Relating a change in response magnitude to a sensing parameter [316], [317].
3) Associating a calculated value, such as an error estimator, with a sensing parameter [157].
4) Matching response shapes to a sensing parameter [154].
5) Correlating changes in tag parameters, such as gain, impedance, or max RCS with a sensing parameter [318], [319].

From the decoding methods outlined above, it can be inferred that the more response features the decoding method relies on, the more accurate the response detection process needs to be.

Fig. 8 provides several illustrative examples of the ID-based decoding methods shown above. For this example, the 8 slot tag that was depicted in Fig. 1 is used along with a 7 slot version (Fig. 8b) where the innermost slot resonator has been removed. The responses for both tags are shown in Fig. 8c along with the binary code assignment for Methods 2 and 3 using the notches as the "specified response feature". This demonstrates how the code can be manipulated through intentional changes of the tag structure in order to assign different IDs. Fig. 8c shows how the response of the 8 slot tag can be decoded using Method 9. This method was designed for use in sensing applications and thus can capture various types of changes in the tag response as it changes with changes in the tag environment. However, as mentioned previously, this intensifies the measurement accuracy requirements since more response features are relied on for decoding.

In terms of the extraction of resonance frequencies in a response, a number of methods have been proposed. The methods tend to vary based on whether or not there is a set of expected resonance frequencies and/or a set of potential codes to compare against [305], [320], [321]. For example, in some ID applications the expected code is known and this informs the detection and decoding procedure, while in sensing applications there is not an expected response since changes in the response are being used to determine an unknown sensing parameter [4], [194].

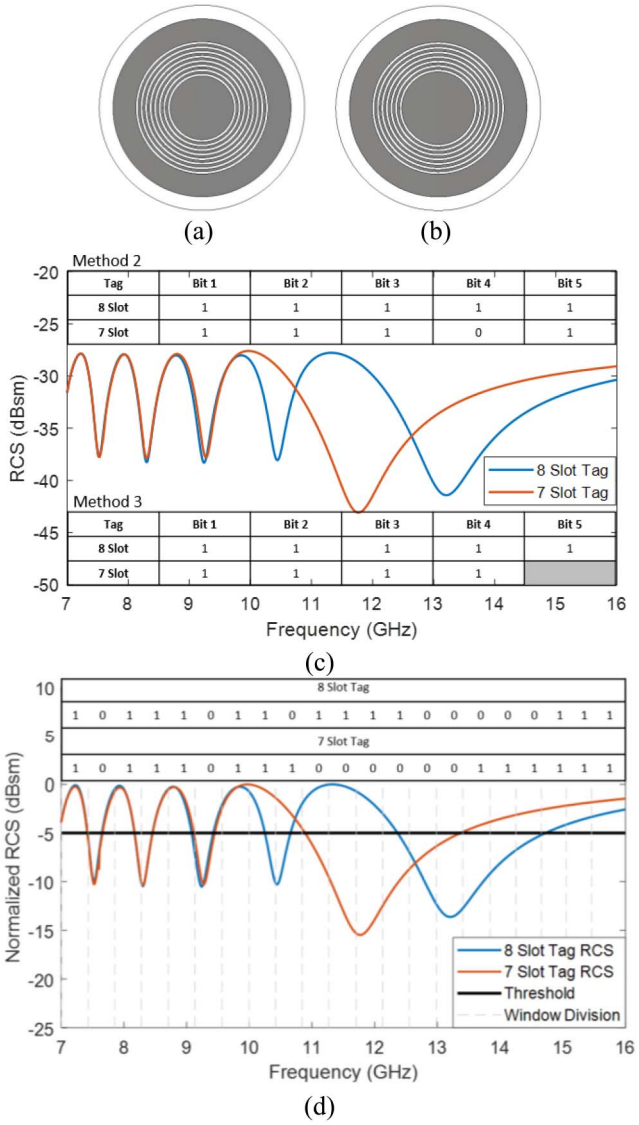

FIGURE 8. Example of binary code assignment as the tag structure is intentionally changed: a) 8 circular slot tag model, b) 7 circular slot tag model, c) Simulated RCS response coding for Methods 2 and 3 using notches as the response feature of interest, and d) 8 slot and 7 slot tag RCS response coding with Method 9.

One of the simplest decoding methods is finding the local minima or maxima in a response and comparing their amplitudes to some preset thresholds. These thresholds can be set by reference tags, which have codes that consist of either all 1's or all 0's, or by analyzing the responses at multiple expected reading distances and selecting a threshold accordingly [65], [135], [258], [281]. This approach works well if the reading distance is known and will stay consistent or within a certain range. However, this is not always the case for practical systems. Reading distance changes can result in response amplitude variations, which could cause bits to be misread [292]. To mitigate this, using the normalized amplitude of the derivative with respect to frequency of the tag mode response for decoding with thresholds has been proposed. This is part of a method to estimates the range to solve the chipless RFID "inverse problem" [241]. However, misalignments can also cause amplitude changes and resonance frequency shifts, which are not necessarily taken care of by this method [4]. Another alternative that has been proposed is the adaptive energy detection (AED) method. The AED method divides the response into windows and performs an energy calculation in each window to determine where to set the decoding threshold. As a result, this approach both takes into account channel effects and tends to have a lower probability of error than the traditional threshold setting method, especially for low SNRs [322]. While these threshold setting methods are applicable for ID applications, they are not suitable for sensing applications.

Alternative response decoding methods for ID applications that can be used when all possible codes are known include, the Maximum Likelihood (ML) and the Signal Space Representation (SSR) methods [240], [294], [307]. In the ML method, the measured response is compared against a set of stored potential responses to calculate the ML values. The response is then decoded as the comparison that produces the highest ML value. This approach is computationally resource-intensive particularly when the code length and set of potential codes increases [292], [323], [324]. In implementations of the ML method, multiple tag readings have been performed and results averaged to mitigate potential interferences [323], the statistical properties of the channel state have been integrated into the calculations [305], the Euclidian distance between codes has been increased through the binary code assignment method which also allows Euclidean distance itself to be used to decode tag measurements [155], [325], [326], and the channel/tag combinations with the highest probability of occurrence has been determined [327]. Additionally, bit-by-bit reading has been proposed to help improve the scalability of this approach for use with higher bit density tags [305], [321].

In the SSR approach each possible tag response, of which there are 2^b where b is the number of notches in the response, is collected and fully described by a linear combination of orthonormal basis functions which are determined through singular value decomposition (SVD). These possible responses are represented as constellation points against which measured responses are compared using a minimum distance calculation. In the end, the response is decoded based on which constellation point it is closest to. The advantages of this approach are that it allows for the response to be more comprehensively considered during decoding (i.e., taking into account the Q-factor of notches rather than just comparing to a threshold) and it has an improved detection error rate (DER) over the threshold method. However, it can be very computationally resource intensive, especially for tags with high bit densities, and the DER tends to increase as the number of notches in the response increases [240], [292], [320], [322].

Improvements to the traditional SSR method have been proposed, namely: the logarithmic SSR (LSSR) and the window based SVD (WB-SVD). In the LSSR method, the basis

functions are derived without the use of SVD and decoding is done by testing the tag response against the constellation one bit at a time. These two changes greatly reduce the computational resource requirements with an increase in the number of tag notches, but come with the tradeoff of increased probability of error with respect to the traditional SSR method [240]. In the WB-SVD method (also referred to as Smart-SVD (SSVD)), fewer points are used than the traditional SSR method which helps to reduce complexity and processing time. Unlike the traditional SSR method, the WB-SVD approach also takes into account channel effects, which results in a lower probability of error. Furthermore, WB-SVD allows for notch bandwidths to be estimated, which is necessary for certain decoding methods (e.g., Method 5 above) [309], [322], [328].

Another method that is similar to the ML and SSR methods, is the dynamic time warping (DTW) method, which compares the tag response to a dataset and computes cost matrices to decode the response. By considering the tag response more comprehensively, the DTW method allows for similar response shapes to be matched even if they are shifted in time or frequency or distorted. The downside to this approach is that it is very computationally intensive. However, it has shown better probability of detection than the WB-SVD method [309]. These methods that compare responses to a set of possible known codes are also mainly suited for ID applications over sensing applications, just like the threshold methods.

Another approach is to extract the complex natural resonances (CNRs) of tags, which are considered to be aspect independent (i.e., they do not change location due to angle of arrival of the interrogating wave or the observation point) [118], [134], [329], [330], [331]. It should be noted that CNRs are sensitive to changes in tag's substrate permittivity and structure effective permittivity, which makes the following discussed CNR extraction methods suitable for sensing, as well as identification, applications [332], [333]. CNRs can be extracted by using methods like the singularity expansion method (SEM), matrix pencil method (MPM), short time matrix pencil method (STMPM), and spectrogram method [19], [245], [304], [329], [333]. The latter three can be considered as more optimized methods to estimate and extract the poles described by SEM theory, of which there is a detailed explanation provided in [299] and [334]. The MPM involves solving a generalized eigenvalue problem in order to find the poles of the response. In order to employ the MPM, the response is transformed to the time-domain (if needed) and then processed. In the case of processing chipless RFID tag responses, the additional steps of background subtraction and deconvolving the background-subtracted tag response with the response of a time windowed large metal plate are taken. The deconvolved response is inverse Fourier transformed to the time-domain and time windowed before the MPM is applied. This means that three measurements are needed, the results are distance dependent, and the challenges with selecting the time window beginning and length discussed previously are relevant here [118], [134], [271]. Another challenge facing the MPM approach is that it cannot separate the reflections from background objects from that of the tag. In an attempt to overcome this, separating the poles based on their time and direction of arrival has been proposed [298]. The MPM inherently includes singular value decomposition (SVD), unlike other CNR extraction methods like Prony's method or Cauchy's method, which helps reduce the effects of noise. Additionally, an autocorrelation function approach and a time-domain averaging approach have been proposed to help further reduce the effects of noise when employing the MPM [330], [334], [335], [336].

An alternative approach that harness the benefits of MPM while helping to overcome some of its challenges is the short time matrix pencil method (STMPM). The STMPM uses a sliding time window and applies MPM at each window location to get a time-frequency plot. By examining the convergence in this plot, one can identify the approximate start time of the tag mode and can find the average resonance frequencies over time, which makes this approach even less susceptible to noise than the MPM while also calculating the CNRs more accurately. One of the limitations of the STMPM, though, is that it has fixed resolution in time and frequency [290], [292], [304], [334]. Improvements to the STMPM method have also been proposed, including a k-nearest neighbor algorithm in order to create decision boundaries and decode the tag response [220].

The Short Time Fourier Transform (STFT) method (also referred to as the spectrogram method) is similar to the STMPM method in that it uses a sliding window over the time domain response to determine the tag response from the tag mode. One of the differences is the data presentation format, namely, the STFT method presents the data in a spectrogram format. Additionally, the STFT method like STMPM and MPM traditionally requires multiple measurements to isolate the tag mode before extracting the poles [19], [245], [334]. However, the temporal separation method has been proposed for the purpose of performing the STFT method with only a single measurement and no calibration process [245]. Averaging of the spectrogram over a window of time is also used to enhance the dynamic range and robustness of the tag response detection. Although, there are still limitations with the STFT method, including fixed resolution in time and frequency, sensitivity to the window length, and limited performance in terms of distinguishing resonant frequencies when they are densely packed in the operational frequency band of the tag [334]. Overall, the STFT method has been shown to be more accurate, require fewer measurements, and require less computation time than the STMPM and MPM methods while still being able to extract the resonant frequency information in an aspect independent fashion [19], [193], [245], [329].

The STMPM and STFT methods can be classified as time-frequency approaches based on how their outputs are viewed and interpreted. Wavelet-based methods are another type of time-frequency approach. By employing the continuous

wavelet transform (CWT) for a set of scaling factors and time translations a time-frequency plot with variable resolution in one domain and multi-resolution in another domain can be generated. This time-frequency plot, just like the ones for the other time-frequency approaches, gives information about the turn-on times and resonant frequencies. Similar to the MPM, this approach has the benefit of denoising the tag response since the CWT acts like a matched filter, but it can still struggle with the detection of densely-packed resonant frequencies due to its limited frequency resolution [244], [294], [295], [334]. In order to help with this, an adaptive wavelet method has been proposed that provides better resolution for high-frequency resonant frequencies while also helping to detect tags when they are attached to highly scattering objects [190], [292], [337]. While wavelet methods have been primarily applied for response detection and decoding in identification applications, they could also potentially be used for sensing applications.

While many methods are focused on determining resonance frequencies, there are additional methods that either consider the tag response more comprehensively or aim to extract other response features than the resonance frequencies in the RCS or S-parameter response. One such example is [308], where the goal is to find the zeros in the falling edge of the derivative with respect to frequency of the group delay. Another example is the use of Principle Component Analysis (PCA), which considers the full response of a tag under different conditions with multiple measurements taken under each condition. The data is then processed using SVD and principle components are generated. The principle components can be associated with different conditions [311], [325]. In [311], for example, PCA was used to detect and characterize cracks in metal samples. Machine learning based techniques have also been considered, including in [338] and [339] where quantile regression is used, in [325] where linear discriminant analysis is used, [43] that sends tag response data to a cloud database where various pattern recognition algorithms are applied for supervised learning purposes, and in [223] the Support Vector Machine approach is found to have the best performance among four machine learning approaches tested, to give just a few examples [207], [340], [341].

C. DECODING METRICS

As evidenced by this section, there are many different approaches for detecting and decoding chipless RFID tag responses. While some comparisons of the different methods have been attempted, they are not often one-to-one comparable due to factors, such as difference in reader hardware, tag design, reading distance, measurement environment (e.g., anechoic chamber vs. "real" environment and whether or not the tag is attached to a highly scattering object), and the design of validation experiments (i.e., the number of trials/measurements, whether misalignments and noise are considered, etc.). Additionally, many of the comparisons use subjective measurement metrics, such as ranking the complexity of a method on a low-medium-high scale, without providing definitions of these classifiers [19], [77], [292], [295], [313].

In terms of quantitative decoding performance metrics, the two most common ones are detection error rate (DER) and throughput. These are related to the number of successful response decodings [65], [305], [308], [322], [342]. However, what constitutes "success" tends to vary from one work to the next, and is not always explicitly stated. Thus, while in some cases a specific threshold, such as resonant depth of at least 5 dB, is used to define which bit a notch is coded with, in others a small fluctuation in the response could be considered a notch. This means that the same response could be decoded differently by different users and therefore, the frequency of success could vary between users [20]. Additionally, similar to other chipless RFID metrics (e.g., bit density, spectral density, coding capacity, etc.) successful decoding can also be dependent on the coding method or sensing parameter assignment method used [58].

DER, also referred to as the probability of error, is expressed as follows:

$$DER = \frac{N_{Failures}}{N_{Total}} \tag{11}$$

In equation 11, $N_{Failures}$ represents the number of failed decodings while N_{Total} represents the number of attempted decodings. It should be noted that DER considers whether or not the entire response is properly decoded, while probability of error can be used to describe both the probability of the whole response being decoded properly or individual bits being decoded properly. Throughput, also referred to as probability of detection, reading accuracy, success rate, and reliability, is the inverse of the DER. As such, throughput can be expressed as follows:

$$Throughput = \frac{N_{success}}{N_{Total}} = 1 - DER \tag{12}$$

DER and throughput can be evaluated as a function of reading distance and SNR, with a higher SNR corresponding to a higher throughput and therefore lower DER [77], [295], [305], [342]. An example of this is provided in Fig. 9 where probability of detection (i.e., the inverse of DER), is plotted as a function of SNR. In this case, as the SNR increases so does the probability of detection. Fig. 9 also demonstrates how different decoding methods perform in relation to each other [309].

DER and throughput have also been calculated over a reading volume in front of the reader antenna. In these cases, the throughput tends to be lower because there are measurements being considered where there are large tag/reader misalignments (i.e., <15% over the total volume as compared to the reported 90%-99% in [292] where the measurements are being made at the same location) [313], [343]. This is an example of how using the same metric does not necessarily mean that a one-to-one comparison can be made. The probability of false negative and probability of false positive have

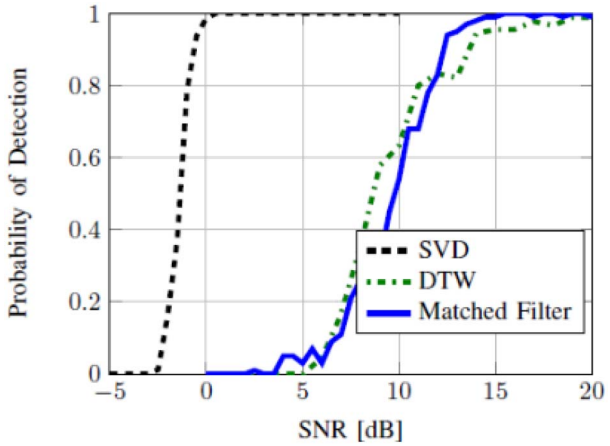

FIGURE 9. Probability of detection as a function of SNR for the SVD, DTW, and Matched Filter detection methods (©*2017, IEEE*) [309].

also been examined as metrics related to the probability of error [344], [345].

Another quantitative metric of interest is bit error rate/bit error ratio (BER). Rather than analyzing decoding performance based on whether or not the full response is properly decoded as in DER, BER considers the decoding performance on a bit-by-bit basis. This metric, unlike bit density and spectral density, considers the RCS level of the tag and provides a measure of the detectability of the tag. This is valuable because increasing the information stored in a tag is pointless if that information cannot be properly decoded. Similar to DER, BER can be calculated as a function of the SNR or clutter level and is also affected by the tag RCS, reading distance, coding method, and measurement setup [16], [346], [347].

Table 5 provides a list of the detection and decoding comparisons that have been made in the literature. Some of the comparisons in Table 5 perform the full comparison with the same measurement setup themselves (e.g., [309], [313], [322], [343]), while others compare the method they are proposing to methods that have proposed in other works (i.e., the measurement setup, tag, etc. varies among the works compared). Another thing to note from Table 5, is that some works refer to methods like background response subtraction and time gating as decoding methods, while other works may refer to these as calibration or pre-processing methods.

D. APPLICATION SPECIFIC POST-PROCESSING

Just as there are application-specific measurement approaches, there are also application-specific post-processing methods. For example, post processing methods have been developed for specific sensor architectures [157], [350], [351], for authentication purposes [189], [207], [325], [345], [352], and for decoding responses measured from moving tags [337], [346], [353], [354], [355]. Another application that has seen many specifically developed post-processing methods is collision avoidance/tag localization in multi-tag environments [247], [248], [356], [357], [358].

TABLE 5. Post-processing method comparisons.

Methods Compared	Comparison Metrics	Year	Ref.
Valley Detection [348] and ML	DER as a function of SNR	‘14	[305]
Valley Detection [348], ML on Frequency-Domain and Time-Domain Data [305], Bit-by-Bit ML	DER as a function of SNR	‘14	[321]
Threshold [349], SVD (SSR) [320], WB-SVD, and AED	Probability of error, complexity, processing time, robustness with different tag types	‘15	[322]
ML, Threshold, and SSR [320]	DER as a function of SNR	‘15	[327]
Matched Filter, WB-SVD, and DTW	Probability of detection as a function of SNR	‘17	[309]
Fixed Frequency Hopping (FFH), Adaptive Frequency Hopping (AFH), Adaptive Sliding Window Frequency Hopping (ASW-FH), and Adaptive Sliding Window Adaptive Hopping (ASW-AH)	Number of frequency points, system latency, detection accuracy, algorithm complexity, dependency on tag type, and latency increment with number of tags	‘17	[263]
Threshold [350], SSR [320], ML [327], Wavelet [337], AC analysis [295]	Reading accuracy, complexity, reader type, and whether the signal processing is done in post or in real-time	‘19	[295]
Background Subtraction and Time Gating	Read success rate over a 3D reading volume	‘19	[343]
Threshold [350], SSR [320], ML [324], Mother Wavelet [292]	Throughput, what type of objects the tag is attached to, and complexity	‘19	[292]
Adaptive Wavelet [337], STMPM [304], Selective Spectral Interrogation (SSI) with Time Gating [271], Calibration with Reference Measurements [67], STFT [245], and Extraction of Antenna Mode with Signal Derivation	Tag type, number of bits, calibration, whether or not reader parameters are known, measurement environment, whether or not the reading distance is known, whether or not applied to an inverse scenario	‘20	[241]
Background Subtraction, Time Gating, STFT, Short Time Prony Analysis (STPA)	Read success rate over a 3D reading volume	‘20	[313]
MPM [118], STMPM [134, 303, 304], ISAR [346], Mother Wavelet [292], Time-Frequency Domain [300], Scalar [87], STFT [193, 245], Mathematical Model [243], and Spectrogram [19]	Whether or not calibration is performed, what type of objects the tag is attached to, whether aspect angles are considered, reading performance over a 3D reading volume	‘21	[19]
MPM and Spectrogram	Variation in RCS, resonance frequency, and Q-factor, and computation time as a function of window length	‘21	[329]
Temporal Separation [245] and Differential Dual-Polarization [75]	Reliability when tag is attached to different objects, memory storage, and design complexity	‘21	[77]

Due to the breadth of application-specific post-processing methods, further discussion will not be provided in this work.

VI. MEASUREMENT AND DETECTION METHOD COMPARISONS

As evidenced in the previous sections, there is significant diversity in the ways chipless RFID measurements are performed, processed, and decoded. While the different system

TABLE 6. Comparison of chipless RFID measurements.

Application	Tag Description	Reader Type	Reader Antenna Setup	Reader Antenna Polarization	Only Measured in Anechoic Chamber?	Calibration Procedure	Quantity Measured	Quantity Examined	Frequency (GHz)	Reading Distance (cm)	Coding/Sensing Parameter	Year	Reference
ID	Co-polar backscatter	VNA	Bistatic patch antenna arrays	Linearly co-polarized	No	Not specified	S_{21}	S_{21} mag.	5-6	100	Method: 2 Bits: 5	'05	[107]
ID	Co-polar backscatter	VNA	Bistatic horn antennas	Linearly co-polarized	No	Background subtraction	RCS	RCS	3-4.5	122	Method: 2 Bits: 3	'06	[108]
ID	Tx/Rx	Custom freq. domain reader	Bistatic horn antennas	Linearly cross-polarized	Yes	Two reference tags	DC voltage out of gain phase detector	Mag. and phase of decoded data	5-9	15	Method: 1 Bits: 8	'10	[114]
ID	Co-polar backscatter	VNA	Bistatic transmission through with two WR-75 waveguides	Linearly co-polarized	No	Not specified	S_{21}	S_{21} mag.	10-15	0	Method: 1	'11	[101]
Sensing	Tx/Rx	VNA	Bistatic Vivaldi antennas	Linearly cross-polarized	Yes	Time gating and using a reference tag	S_{21}	Normalized S_{21} mag. difference with ref. tag	1.25-6	70	Permittivity	'12	[126]
ID	Cross-polar backscatter	Novelda Radar	Monostatic dual-polarized horn antenna	Linearly cross-polarized	No	Averaging, background subtraction, and time gating	RCS	RCS	3-8	20	Method: 5 Bits: 6	'13	[67]
ID	Co-polar backscatter	VNA	Bistatic horn antennas	Linearly co-polarized	No	Ref. measurement subtraction and dividing by the FFT of the time-gated response of a metal plate	RCS	RCS and pole diagram	1-11	60	Method: 2 Bits: 24	'14	[134]
Sensing	Cross-polar backscatter	FMCW Radar	High gain scanning parabolic TX antenna and patch array Rx antenna	Linearly cross-polarized	No	Beam scan to ensure tag is normal to reader	Power	Error estimators	24	5800	Humidity	'17	[157]
ID	Co-polar backscatter	VNA	Monostatic dual-polarized patch antenna	Linearly dual-polarized	No	Background subtraction	S_{11}	S_{11} mag.	4.5-7.2	800	NA	'18	[188]
ID	Co-polar backscatter	VNA	Monostatic WR-90 waveguide with engineered flange	Linearly co-polarized	No	Calibrated VNA up to waveguide aperture	S_{11}	S_{11} mag.	7.5-12.4	0.5	Method: 9 Bits: 116	'19	[58]
ID	Tx/Rx	IR-UWB made with oscilloscope and arbitrary waveform generator	Bistatic horn antennas	Linearly cross-polarized	No	Background subtraction	Power	Power	3-10	40	Method: 2 Bits: 32	'21	[203]
Sensing	Co-polar backscatter	VNA	Bistatic circularly-polarized arrays	Circularly cross-polarized	No	Background subtraction	S21	S21 mag.	5.5-9.5	10	Liquid differentiation	'21	[93]

components are often compared to each other (i.e., reader antennas are compared to other reader antennas and post-processing methods are compared to other post-processing methods), the full systems are not often compared to each other. Since, many factors (e.g., antenna gain, calibration method, detection criteria, reader architecture, frequency range, etc.) can play a role in the achievable reading distance and other metrics, like the DER or throughput, these

component level comparisons do not necessarily paint a full picture.

This section aims to provide a brief comparison of implemented measurement and detection setups across several parameters, namely: the application, tag type, reader hardware, reader antenna hardware and configuration, polarization, measurement environment, calibration procedure, measured quantity, format the measurement was examined in, measurement frequency range, reading distance, decoding method, and the year published. Table 6 provides a non-exhaustive comparison with the entries being listed in chronological publishing order. The entries were selected to showcase a variety of different measurement and detection approaches. Interested readers can see the references associated with Figs. 4 and 6 for more examples of chipless RFID tag measurements [105].

In Table 6, similar to Figs. 4 and 6, the maximum distance at which the tag was successfully measured in each reference is reported. In comparing Figs. 4 and 6 and Tables 1–6, the following statements can be made about the chipless RFID measurement and decoding landscape at the current time: 1) most tags that are currently in the literature are designed to operate below 10 GHz, 2) most tags are measured with a VNA, 3) background subtraction is one of the most common calibration methods, 4) RCS and S-parameters are the measurement quantity of choice an approximately equal amount of time, 5) reading distances tend to be below 1 m for both co-polar and cross-polar tags, and 6) tags are measured in a bistatic configuration slightly more often than in a monostatic configuration.

VII. CONCLUSION

This work provided a review of chipless RFID measurement and response detection methods. Measurement quantities namely RCS and S-parameters, were compared and an overview of measurement approaches, which vary based on the tag type, desired reading distance, and available equipment, was also given. It was shown that despite there being theoretically higher read ranges, most tags are measured at distances below 1 m at this time. Additionally, many tags are designed to operate below 10 GHz to be compliant with various transmit power regulations. As such, the custom readers and reader antennas that have been designed also tend to operate below 10 GHz. Once the tag response has been measured, there are a wide variety of techniques that have been proposed to detect specific response features and decode the response. These techniques vary in complexity from averaging of multiple measurements to machine learning and can also be application specific. In order to compare system level performance, various metrics including the DER, throughput, and BER have been proposed and some comparisons among processing methods and systems have been attempted. However, due to the breadth and diversity in chipless RFID systems, making a comprehensive comparison is an ongoing challenge. In order to address this challenge, standardization efforts, including standard tags for comparison purposes along with specific benchmark tests that clearly define the success criteria, could be undertaken.

REFERENCES

[1] T. Athauda and N. Karmakar, "Chipped versus chipless RF identification: A comprehensive review," *IEEE Microw. Mag.*, vol. 20, no. 9, pp. 47–57, Sep. 2019, doi: 10.1109/MMM.2019.2922118.

[2] F. Costa, S. Genovesi, M. Borgese, A. Michel, F. A. Dicandia, and G. Manara, "A review of RFID sensors, the New Frontier of Internet of Things," *Sensors*, vol. 21, no. 9, p. 3138, 2021, doi: 10.3390/s21093138.

[3] S. Tedjini, F. Costa, S. Genovesi, and G. Manara, "Chipless RFID, from principles to applications," in *Proc. Int. Conf. Electromagn. Adv. Appl. (ICEAA)*, Sep. 2017, pp. 1906–1908, doi: 10.1109/ICEAA.2017.8065679.

[4] K. Brinker, "Passively-coded embedded microwave sensors for materials characterization and structural health monitoring (SHM)," M.S. thesis, Master Sci. Elect. Eng., Missouri Univ. Sci. Technol., Rolla, MO, USA, 2019.

[5] D. H. Nguyen, M. Zomorrodi, and N. C. Karmarka, "Spatial-based chipless RFID system," *IEEE J. Radio Freq. Identif.*, vol. 3, no. 1, pp. 46–55, Mar. 2019, doi: 10.1109/JRFID.2018.2887162.

[6] M. Forouzandeh and N. C. Karmakar, "Chipless RFID tags and sensors: A review on time-domain techniques," *Wireless Power Transfer*, vol. 2, no. 2, pp. 62–77, 2015, doi: 10.1017/wpt.2015.10.

[7] K. Brinker and R. Zoughi, "Utilization of microwave imaging for chipless RFID tag reading and verification—A hybrid approach," in *Proc. Antenna Meas. Techn. Assoc. (AMTA) Symp.*, Nov. 2020, pp. 1–9.

[8] V. Sharma and M. Hashmi, "Advances in the design techniques and applications of chipless RFIDs," *IEEE Access*, vol. 9, pp. 79264–79277, 2021, doi: 10.1109/ACCESS.2021.3084056.

[9] J. Havlíček, M. Svanda, J. Machac, and P. Milan, "Improvement of reading performance of frequency-domain chipless RFID transponders," *Radioengineering*, vol. 25, pp. 219–229, Apr. 2016, doi: 10.13164/re.2016.0219.

[10] C. Herrojo, F. Paredes, J. Mata-Contreras, and F. Martín, "Chipless-RFID: A review and recent developments," *Sensors*, vol. 19, no. 15, p. 3385, 2019, doi: 10.3390/s19153385.

[11] K. Mekki, O. Necibi, H. Dinis, P. Mendes, and A. Gharsallah, "Investigation on the chipless RFID tag with a UWB pulse using a UWB IR-based reader," *Int. J. Microw. Wireless Technol.*, vol. 14, no. 2, pp. 166–175, 2021, doi: 10.1017/S1759078721000313.

[12] R. Koswatta and N. C. Karmakar, "Investigation into antenna performance on read range improvement of chipless RFID tag reader," in *Proc. Asia–Pac. Microw. Conf.*, Dec. 2010, pp. 1300–1303.

[13] K. Mc Gee, P. Anandarajah, and D. Collins, "A review of chipless remote sensing solutions based on RFID technology," *Sensors*, vol. 19, no. 22, p. 4829, 2019, doi: 10.3390/s19224829.

[14] N. C. Karmaker, "Tag, you're it radar cross section of chipless RFID tags," *IEEE Microw. Mag.*, vol. 17, no. 7, pp. 64–74, Jul. 2016, doi: 10.1109/MMM.2016.2549160.

[15] N. Barbot, O. Rance, and E. Perret, "Classical RFID versus chipless RFID read range: Is linearity a friend or a foe?" *IEEE Trans. Microw. Theory Techn.*, vol. 69, no. 9, pp. 4199–4208, Sep. 2021, doi: 10.1109/TMTT.2021.3077019.

[16] M. Borgese, S. Genovesi, G. Manara, and F. Costa, "Radar cross section of chipless RFID tags and ber performance," *IEEE Trans. Antennas Propag.*, vol. 69, no. 5, pp. 2877–2886, May 2021, doi: 10.1109/TAP.2020.3037800.

[17] F. Zheng, Y. Chen, T. Kaiser, and A. J. H. Vinck, "On the coding of chipless tags," *IEEE J. Radio Freq. Identif.*, vol. 2, no. 4, pp. 170–184, Dec. 2018, doi: 10.1109/JRFID.2018.2877054.

[18] S. R. Patre, "Passive chipless RFID sensors: Concept to applications—A review," *IEEE J. Radio Freq. Identif.*, vol. 6, pp. 64–76, 2021, doi: 10.1109/JRFID.2021.3114104.

[19] Z. Ali, E. Perret, N. Barbot, and R. Siragusa, "Extraction of aspect-independent parameters using spectrogram method for chipless frequency-coded RFID," *IEEE Sensors J.*, vol. 21, no. 5, pp. 6530–6542, Mar. 2021, doi: 10.1109/JSEN.2020.3041574.

[20] K. R. Brinker and R. Zoughi, "Corner reflector based misalignment-tolerant chipless RFID tag design methodology," *IEEE J. Radio Freq. Identif.*, vol. 5, no. 1, pp. 94–105, Mar. 2021, doi: 10.1109/JRFID.2020.3034483.

[21] A. Subrahmannian and S. K. Behera, "Chipless RFID: A unique technology for mankind," *IEEE J. Radio Freq. Identif.*, vol. 6, pp. 151–163, 2022, doi: 10.1109/JRFID.2022.3146902.

[22] F. Babaeian and N. Karmakar, "A cross-polar orientation insensitive chipless RFID tag," in *Proc. IEEE Int. Conf. RFID Technol. Appl. (RFID-TA)*, Sep. 2019, pp. 116–119, doi: 10.1109/RFID-TA.2019.8892193.

[23] M. Garbati, E. Perret, R. Siragusa, and C. Halopè, "Toward chipless RFID reading systems independent of tag orientation," *IEEE Microw. Wireless Compon. Lett.*, vol. 27, no. 12, pp. 1158–1160, Dec. 2017, doi: 10.1109/LMWC.2017.2750417.

[24] O. Rance, N. Barbot, and E. Perret, "Comments on "development of cross-polar orientation-insensitive chipless RFID tags,"' *IEEE Trans. Antennas Propag.*, vol. 70, no. 5, pp. 3922–3923, May 2022, doi: 10.1109/TAP.2021.3133661.

[25] M. El-Hadidy and Y. E. S. B. Yasser, "Realistic chipless RFID tag modeling, mathematical framework and 3D EM simulation," in *Proc. IEEE Int. Conf. RFID Technol. Appl. (RFID-TA)*, Sep. 2019, pp. 201–206, doi: 10.1109/RFID-TA.2019.8892178.

[26] R. Rezaiesarlak and M. Manteghi, "A new technique for positioning of chipless RFID tags," in *Proc. IEEE Antennas Propag. Soc. Int. Symp. (APSURSI)*, Jul. 2014, pp. 1680–1681, doi: 10.1109/APS.2014.6905166.

[27] M. Borgese, F. Costa, S. Genovesi, and G. Manara, "Depolarizing chipless tags with polarization insensitive capabilities," *Electronics*, vol. 10, no. 4, p. 478, 2021, doi: 10.3390/electronics10040478.

[28] G. T. Ruck, *Radar Cross Section Handbook*. New York, NY, USA: Springer, 1970.

[29] O. Rance, E. Perret, R. Siragusa, and P. Lemaître-Auger, "3—Theory of chipless RFID tags," in *RCS Synthesis for Chipless RFID*, O. Rance, E. Perret, R. Siragusa, and P. Lemaître-Auger, Eds. Amsterdam, The Netherlands: Elsevier, 2017, pp. 51–85.

[30] S. K. Behera and N. C. Karmakar, "Wearable chipless radio-frequency identification tags for biomedical applications: A review [antenna applications corner]," *IEEE Antennas Propag. Mag.*, vol. 62, no. 3, pp. 94–104, Jun. 2020, doi: 10.1109/MAP.2020.2983978.

[31] R. B. Dybdal, "Radar cross section measurements," *Proc. IEEE*, vol. 75, no. 4, pp. 498–516, Apr. 1987, doi: 10.1109/PROC.1987.13757.

[32] K. Brinker and R. Zoughi, "Embedded chipless RFID measurement methodology for microwave materials characterization," in *Proc. IEEE Int. Instrum. Meas. Technol. Conf. I2MTC)*, May 2018, pp. 1–6, doi: 10.1109/I2MTC.2018.8409670.

[33] K. Brinker and R. Zoughi, "Measurement of inkjet-printing parameters for accurate chipless RFID tag EM simulation," in *Proc. IEEE Int. Instrum. Meas. Technol. Conf.*, Auckland, New Zealand, 2019, pp. 1–6.

[34] M. Kempin, M. T. Ghasr, J. T. Case, and R. Zoughi, "Modified waveguide flange for evaluation of stratified composites," *IEEE Trans. Instrum. Meas.*, vol. 63, no. 6, pp. 1524–1534, Jun. 2014, doi: 10.1109/TIM.2013.2291952.

[35] M. Grace, *Measurement of Radar Cross Section Using the 'VNA Master' Handheld VNA: Application Note*, Anritsu, Atsugi, Japan, 2011.

[36] M. I. Skolnik, *Introduction to Radar Systems*. New York, NY, USA: McGraw-Hill, 2001.

[37] T. Singh, S. Tedjini, E. Perret, and A. Vena, "A frequency signature based method for the RF identification of letters," in *Proc. IEEE Int. Conf. RFID*, Apr. 2011, pp. 1–5, doi: 10.1109/RFID.2011.5764628.

[38] F. Costa, S. Genovesi, and A. Monorchio, "A chipless RFID based on multiresonant high-impedance surfaces," *IEEE Trans. Microw. Theory Techn.*, vol. 61, no. 1, pp. 146–153, Jan. 2013, doi: 10.1109/TMTT.2012.2227777.

[39] D. Betancourt, M. Barahona, K. Haase, G. Schmidt, A. Hübler, and F. Ellinger, "Design of printed chipless-RFID tags with QR-code appearance based on genetic algorithm," *IEEE Trans. Antennas Propag.*, vol. 65, no. 5, pp. 2190–2195, May 2017, doi: 10.1109/TAP.2017.2684193.

[40] P. Fathi, J. Aliasgari, and N. C. Karmakar, "Analysis on polarization responses of resonators for frequency-coded chipless RFID tags," *IEEE Trans. Antennas Propag.*, vol. 70, no. 2, pp. 1198–1210, Feb. 2022, doi: 10.1109/TAP.2021.3111526.

[41] W. Wiesbeck and D. Kahny, "Single reference, three target calibration and error correction for monostatic, polarimetric free space measurements," *Proc. IEEE*, vol. 79, no. 10, pp. 1551–1558, Oct. 1991, doi: 10.1109/5.104229.

[42] R. C. Wittmann, M. H. Francis, L. A. Muth, and R. L. Lewis, *Proposed Uncertainty Analysis for RCS Measurements*, NIST, Gaithersburg, MD, USA, 1994.

[43] L. M. Arjomandi, G. Khadka, Z. Xiong, and N. C. Karmakar, "Document verification: A cloud-based computing pattern recognition approach to chipless RFID," *IEEE Access*, vol. 6, pp. 78007–78015, 2018, doi: 10.1109/ACCESS.2018.2884651.

[44] A. Vena, *Contribution au Développement de la Technologie RFID Sans Puce à Haute Capacité De Codage*, Université de Grenoble, Grenoble, France, 2014.

[45] A. Vena, E. Perret, and S. Tedjini, "High-capacity chipless RFID tag insensitive to the polarization," *IEEE Trans. Antennas Propag.*, vol. 60, no. 10, pp. 4509–4515, Oct. 2012, doi: 10.1109/TAP.2012.2207347.

[46] A. Vena, E. Perret, and S. Tedjini, "A fully printable chipless RFID tag with detuning correction technique," *IEEE Microw. Wireless Compon. Lett.*, vol. 22, no. 4, pp. 209–211, Apr. 2012, doi: 10.1109/LMWC.2012.2188785.

[47] M. Polivka, J. Havlicek, M. Svanda, and J. Machac, "Improvement in robustness and recognizability of RCS response of U-shaped strip-based chipless RFID tags," *IEEE Antennas Wireless Propag. Lett.*, vol. 15, pp. 2000–2003, 2016, doi: 10.1109/LAWP.2016.2549638.

[48] J. Havlicek, M. Svanda, M. Polivka, J. Machac, and J. Kracek, "Chipless RFID tag based on electrically small spiral capacitively loaded dipole," *IEEE Antennas Wireless Propag. Lett.*, vol. 16, pp. 3051–3054, 2017, doi: 10.1109/LAWP.2017.2760059.

[49] M. Polivka, M. Scanda, J. Havlicek, and J. Machac, "Detuned dipole array backed by rectangular plate applied as chipless RFID tag," in *Proc. Progr. Electromagn. Res. Symp*, 2017, pp. 1–9.

[50] D. Hotte, R. Siragusa, Y. Duroc, and S. Tedjini, "Radar cross-section measurement in millimeter-wave for passive millimeter-wave identification tags," *IET Microw. Antennas Propag.*, vol. 9, no. 15, pp. 1733–1739, 2015, doi: 0.1049/iet-map.2015.0281.

[51] A. Vena, L. Sydänheimo, M. M. Tentzeris, and L. Ukkonen, "A fully inkjet-printed wireless and chipless sensor for CO_2 and temperature detection," *IEEE Sensors J.*, vol. 15, no. 1, pp. 89–99, Jan. 2015, doi: 10.1109/JSEN.2014.2336838.

[52] F. Costa, S. Genovesi, and A. Monorchio, "Chipless RFIDs for metallic objects by using cross polarization encoding," *IEEE Trans. Antennas Propag.*, vol. 62, no. 8, pp. 4402–4407, Aug. 2014.

[53] M. Polivka, M. Svanda, and J. Machac, "Chipless RFID tag with an improved RCS response," in *Proc. 44th Eur. Microw. Conf.*, Oct. 2014, pp. 770–773, doi: 10.1109/EuMC.2014.6986548.

[54] K. Brinker and R. Zoughi, "Chipless RFID tags as microwave sensors for delamination detection in layered structures," in *Proc. IEEE Int. Instrum. Meas. Technol. Conf. (I2MTC)*, May 2021, pp. 1–6, doi: 10.1109/I2MTC50364.2021.9459795.

[55] F. Zohra, O. Salim, S. Dey, H. Masoumi, and N. Karmakar, "Investigation of chipless RFID tag performance in coal mining conveyor belt," in *Proc. 4th Aust. Microw. Symp. (AMS)*, Feb. 2020, pp. 1–2, doi: 10.1109/AMS48904.2020.9059330.

[56] F. Costa, S. Genovesi, A. Monorchio, and G. Manara, "Calibration method for periodic surface based chipless tags," in *Proc. IEEE RFID Technol. Appl. Conf. (RFID-TA)*, Sep. 2014, pp. 78–81, doi: 10.1109/RFID-TA.2014.6934204.

[57] F. Villa-Gonzalez, A. Rezola, A. Estevez, J. Diaz, and D. Valderas, "Chipless RFID tag detection with a single measurement in presence of multipath," in *Proc. IEEE Int. Symp. Antennas Propag. USNC-URSI Radio Sci. Meeting (APS/URSI)*, Dec. 2021, pp. 389–390, doi: 10.1109/APS/URSI47566.2021.9704656.

[58] K. R. Brinker, M. Vaccaro, and R. Zoughi, "Application-adaptable chipless RFID tag: Design methodology, metrics, and measurements," *IEEE Trans. Instrum. Meas.*, vol. 69, no. 6, pp. 3882–3895, Jun. 2020, doi: 10.1109/TIM.2019.2938131.

[59] I. Balbin and N. Karmakar, "Novel chipless RFID tag for conveyor belt tracking using multi-resonant dipole antenna," in *Proc. Eur. Microw. Conf. (EuMC)*, Sep./Oct. 2009, pp. 1109–1112, doi: 10.23919/EUMC.2009.5296395.

[60] M. Khaliel, A. El-Awamry, A. F. Megahed, and T. Kaiser, "A novel design approach for co/cross-polarizing chipless RFID tags of high coding capacity," *IEEE J. Radio Freq. Identif.*, vol. 1, no. 2, pp. 135–143, Jun. 2017, doi: 10.1109/JRFID.2017.2765560.

[61] J. Aliasgari, P. Fathi, M. Forouzandeh, and N. Karmakar, "IR-UWB chipless RFID reader based on frequency translation technique for decoding frequency-coded tags," *IEEE Trans. Instrum. Meas.*, vol. 70, pp. 1–11, 2021, doi: 10.1109/TIM.2021.3094239.

[62] Y. H. Cho, F. P. Lai, and Y. S. Chen, "Orientation-insensitive chipless RFID achieved in multiple rotational degrees of freedom," *IEEE Trans. Antennas Propag.*, vol. 70, no. 7, pp. 5266–5277, Jul. 2022, doi: 10.1109/TAP.2022.3145446.

[63] R. E-Azim, P. Kalansuriya, N. C. Karmakar, and R. Koswatta, *Chipless RFID Reader Architecture*. London, U.K.: Artech House, 2013.

[64] O. Rance, E. Perret, R. Siragusa, and P. Lemaître-Auger, "4—Magnitude coding," in *RCS Synthesis for Chipless RFID*, O. Rance, E. Perret, R. Siragusa, and P. Lemaître-Auger, Eds. Amsterdam, Netherlands: Elsevier, 2017, pp. 87–145.

[65] S. Preradovic and N. C. Karmakar, "Design of short range chipless RFID reader prototype," in *Proc. Int. Conf. Intell. Sensors Sensor Netw. Inf. Process. (ISSNIP)*, Dec. 2009, pp. 307–312, doi: 10.1109/ISSNIP.2009.5416768.

[66] P. Fathi, J. Aliasgari, F. Babaeian, N. C. Karmakar, M. Bhattacharya, and S. Bhattacharya, "Chipless RFID tags: Co- or cross-polar tag?" in *Proc. IEEE Asia–Pac. Microw. Conf. (APMC)*, Dec. 2019, pp. 117–119, doi: 10.1109/APMC46564.2019.9038368.

[67] A. Vena, E. Perret, and S. Tedjni, "A depolarizing chipless RFID tag for robust detection and its FCC compliant UWB reading system," *IEEE Trans. Microw. Theory Techn.*, vol. 61, no. 8, pp. 2982–2994, Aug. 2013, doi: 10.1109/TMTT.2013.2267748.

[68] A. Vena, E. Perret, and S. Tedjini, *Chipless RFID Based on RF Encoding Particle: Realization, Coding and Reading System*. London, U.K.: ISTE Press, 2016, pp. 1–245.

[69] C. Liu, K. Brinker, and R. Zoughi, "Single antenna dual circularly-polarized chipless RFID reading methodology," in *Proc. Antenna Meas. Techn. Assoc. (AMTA) Symp.*, Nov. 2020, pp. 1–6.

[70] M. A. Islam and N. Karmakar, "A linearly polarized (LP) reader antenna for LP and orientation insensitive (OI) chipless RFID tags," in *Proc. 9th Int. Conf. Elect. Comput. Eng. (ICECE)*, Dec. 2016, pp. 431–434, doi: 10.1109/ICECE.2016.7853949.

[71] M. A. Islam, Y. Yap, and N. Karmakar, "'Δ' slotted compact printable orientation insensitive chipless RFID tag for long range applications," in *Proc. 9th Int. Conf. Elect. Comput. Eng. (ICECE)*, Dec. 2016, pp. 283–286, doi: 10.1109/ICECE.2016.7853911.

[72] Q. Li, R. S. Anwar, H. Ning, J. Wang, and L. Mao, "Electromagnetic spectrum chipless radio frequency identification: A review," *Digit. Commun. Netw.*, vol. 6, no. 3, pp. 377–388, 2020, doi: https://doi.org/10.1016/j.dcan.2019.12.002.

[73] Z. Ali, O. Rance, N. Barbot, and E. Perret, "Depolarizing chipless RFID tag made orientation insensitive by using ground plane interaction," *IEEE Trans. Antennas Propag.*, vol. 70, no. 7, pp. 5235–5245, Jul. 2022, doi: 10.1109/TAP.2022.3145479.

[74] F. Babaeian and N. Karmakar, "Development of cross-polar orientation-insensitive chipless RFID tags," *IEEE Trans. Antennas Propag.*, vol. 68, no. 7, pp. 5159–5170, Jul. 2020, doi: 10.1109/TAP.2020.2975639.

[75] F. Costa, S. Genovesi, and A. Monorchio, "Normalization-free chipless RFIDs by using dual-polarized interrogation," *IEEE Trans. Microw. Theory Techn.*, vol. 64, no. 1, pp. 310–318, Jan. 2016, doi: 10.1109/TMTT.2015.2504529.

[76] H. Huang and L. Su, "A compact dual-polarized chipless RFID tag by using nested concentric square loops," *IEEE Antennas Wireless Propag. Lett.*, vol. 16, pp. 1036–1039, 2017, doi: 10.1109/LAWP.2016.2618928.

[77] J.-A. Lin, J.-Y. Jhang, F.-P. Lai, B.-L. Lin, Y.-M. Jhang, and Y.-S. Chen, "Analysis of calibration-free detection techniques for frequency-coded chipless RFID," *IEEE Trans. Antennas Propag.*, vol. 69, no. 3, pp. 1681–1691, Mar. 2021, doi: 10.1109/TAP.2020.3016160.

[78] M. A. Islam and N. C. Karmakar, "Real-world implementation challenges of a novel dual-polarized compact printable chipless RFID tag," *IEEE Trans. Microw. Theory Techn.*, vol. 63, no. 12, pp. 4581–4591, Dec. 2015, doi: 10.1109/TMTT.2015.2495285.

[79] S. Preradovic, I. Balbin, N. C. Karmakar, and G. Swiegers, "A novel chipless RFID system based on planar multiresonators for barcode replacement," in *Proc. IEEE Int. Conf. RFID*, Apr. 2008, pp. 289–296, doi: 10.1109/RFID.2008.4519383.

[80] M. A. Islam and N. C. Karmakar, "A 4 × 4 dual polarized mm-Wave ACMPA array for a universal mm-Wave chipless RFID tag reader," *IEEE Trans. Antennas Propag.*, vol. 63, no. 4, pp. 1633–1640, Apr. 2015, doi: 10.1109/TAP.2015.2398355.

[81] M. Martinez and D. V. D. Weide, "Circular polarization on depolarizing chipless RFID tags," in *Proc. IEEE Radio Wireless Symp. (RWS)*, Jan. 2016, pp. 145–147, doi: 10.1109/RWS.2016.7444388.

[82] A. Vena, E. Perret, B. Sorli, and S. Tedjini, "Theoretical study on detection distance for chipless RFID systems according to transmit power regulation standards," in *Proc. 9th Eur. Conf. Antennas Propag. (EuCAP)*, Apr. 2015, pp. 1–4.

[83] S. Shrestha and N. C. Karmakar, "Analysis of real-world implementation challenges of chipless RFID tag," *IET Microw. Antennas Propag.*, vol. 13, no. 9, pp. 1318–1324, 2019, doi: 10.1049/iet-map.2018.5605.

[84] M. Garbati, A. Ramos, R. Siragusa, E. Perret, and C. Halopé, "Chipless RFID reading system independent of polarization," in *Proc. IEEE MTT-S Int. Microw. Symp. (IMS)*, May 2016, pp. 1–3, doi: 10.1109/MWSYM.2016.7540406.

[85] F. Costa, S. Genovesi, and G. Manara, "Reader antennas requirements in chipless RFID systems with linear and circular polarization," in *Proc. Int. Workshop Antenna Technol. (iWAT)*, Feb. 2020, pp. 1–4, doi: 10.1109/iWAT48004.2020.1570609801.

[86] R. R. Antayhua, C. R. Rambo, and F. R. D. Sousa, "Self-interference cancellation in chipless RFID readers for reading range enhancement," in *Proc. IEEE Int. Instrum. Meas. Technol. Conf. (I2MTC)*, May 2018, pp. 1–6, doi: 10.1109/I2MTC.2018.8409774.

[87] J. Kracek, M. Svanda, and K. Hoffmann, "Scalar method for reading of chipless RFID tags based on limited ground plane backed dipole resonator array," *IEEE Trans. Microw. Theory Techn.*, vol. 67, no. 11, pp. 4547–4558, Nov. 2019, doi: 10.1109/TMTT.2019.2918287.

[88] G. Dong, Y. Shen, H. He, J. Virkki, and S. Hu, "Chipless graphene tag and dual-CP reader for Internet of Things," in *Proc. Int. Appl. Comput. Electromagn. Soc. Symp. (ACES)*, Aug. 2017, pp. 1–2.

[89] S. Genovesi, F. Costa, F. A. Dicandia, M. Borgese, and G. Manara, "Orientation-insensitive and normalization-free reading chipless RFID system based on circular polarization interrogation," *IEEE Trans. Antennas Propag.*, vol. 68, no. 3, pp. 2370–2378, Mar. 2020, doi: 10.1109/TAP.2019.2949417.

[90] C. A. Balanis, *Antenna Theory: Analysis and Design*. New York, NY, USA: Wiley, 2012.

[91] C. A. Balanis, *Advanced Engineering Electromagnetics*. New York, NY, USA: Wiley, 1989.

[92] S. Genovesi, F. Costa, F. A. Dicandia, M. Borgese, and G. Manara, "Circular polarization advantages for chipless RFID and sensor design," in *Proc. 34th Gen. Assembly Sci. Symp. Int. Union Radio Sci. (URSI GASS)*, Aug./Sep. 2021, pp. 1–3, doi: 10.23919/URSIGASS51995.2021.9560645.

[93] Y. Shen, N. Chen, J. Wang, and S. Hu, "Triple-resonance chipless RFID tag with dual circularly-polarized wideband reader antenna for wirelessly differentiating liquid," *IEEE J. Radio Freq. Identif.*, vol. 5, no. 2, pp. 154–162, Jun. 2021, doi: 10.1109/JRFID.2020.3035190.

[94] Y. Shen and C. L. Law, "A low-cost UWB-RFID system utilizing compact circularly polarized chipless tags," *IEEE Antennas Wireless Propag. Lett.*, vol. 11, pp. 1382–1385, 2012, doi: 10.1109/LAWP.2012.2225822.

[95] O. Rance, N. Barbot, and E. Perret, "Comparison between cross-polarization and circular polarization interrogation for robust chipless RFID reading," in *Proc. 51st Eur. Microw. Conf. (EuMC)*, Apr. 2022, pp. 668–671, doi: 10.23919/EuMC50147.2022.9784342.

[96] M. Svanda, M. Polivka, J. Havlicek, J. Machac, and D. H. Werner, "Platform tolerant, high encoding capacity dipole array-plate chipless RFID tags," *IEEE Access*, vol. 7, pp. 138707–138720, 2019, doi: 10.1109/ACCESS.2019.2935258.

[97] N. Barbot, O. Rance, and E. Perret, "Chipless RFID reading method insensitive to tag orientation," *IEEE Trans. Antennas Propag.*, vol. 69, no. 5, pp. 2896–2902, May 2021, doi: 10.1109/TAP.2020.3028187.

[98] C. Chen, Y. Chen, T. Li, Y. Yu, and W. Wu, "A chipless RFID system based on polarization characteristics," in *Proc. 7th IEEE Int. Symp. Microw. Antenna Propag. EMC Technol. (MAPE)*, Oct. 2017, pp. 324–329, doi: 10.1109/MAPE.2017.8250866.

[99] F. Sakai, M. Makimoto, and K. Wada, "Multimode stepped impedance resonators and their application in chipless RFID tags," in *Proc. 46th Eur. Microw. Conf. (EuMC)*, Oct. 2016, pp. 604–607, doi: 10.1109/EuMC.2016.7824415.

[100] M. A. Islam, Y. Yap, N. Karmakar, and A. K. M. Azad, "Orientation independent compact chipless RFID tag," in *Proc. IEEE Int. Conf. RFID Technol. Appl. (RFID-TA)*, Nov. 2012, pp. 137–141, doi: 10.1109/RFID-TA.2012.6404499.

[101] W. S. Lee, H. S. Jang, K. S. Oh, and J. W. Yu, "Design of chipless tag with electromagnetic code for paper-based banknote classification," in *Proc. Asia–Pac. Microw. Conf.*, Dec. 2011, pp. 1406–1409.

[102] M. A. Islam, M. S. Bhuiyan, and N. Karmakar, "A novel compact chipless RFID tag and near-field reader," in *Proc. Asia–Pac. Microw. Conf.*, Dec. 2011, pp. 1518–1521.

[103] S. Terranova, F. Costa, S. Genovesi, and G. Manara, "Detection of chipless tags through near field interrogation with waveguide antennas," in *Proc. IEEE Int. Conf. RFID Technol. Appl. (RFID-TA)*, Sep. 2019, pp. 63–66, doi: 10.1109/RFID-TA.2019.8892230.

[104] W. S. Lee, H. S. Jang, W. S. Lee, K. S. Oh, and J. W. Yu, "Design of near-field chipless RFID tags and reader based on transmission line," in *Proc. Asia–Pac. Microw. Conf. (APMC)*, Nov. 2013, pp. 911–913, doi: 10.1109/APMC.2013.6694971.

[105] K. Brinker. "Chipless RFID measurements reported in the literature." doi: 10.21227/1v7w-3c83. (Accessed: May 5, 2022).

[106] E. Çetin, M. B. Sahin, and Ö. Ergül, "Array strategies for improving the performances of chipless RFID tags," in *Proc. IEEE Int. Symp. Antennas Propag. USNC/URSI Nat. Radio Sci. Meeting*, Jul. 2018, pp. 2015–2016, doi: 10.1109/APUSNCURSINRSM.2018.8608653.

[107] I. Jalaly and I. D. Robertson, "Capacitively-tuned split microstrip resonators for RFID barcodes," in *Proc. Eur. Microw. Conf.*, vol. 2, Oct. 2005, p. 1164, doi: 10.1109/EUMC.2005.1610138.

[108] M. John, H. Ahmad, and E. Nader, "Theory and experiments on Peano and Hilbert curve RFID tags," in *Proc. SPIE*, 2006, p. 6248, [Online]. Available: https://doi.org/10.1117/12.666911

[109] J. McVay, A. Hoorfar, and N. Engheta, "Space-filling curve RFID tags," in *Proc. IEEE Radio Wireless Symp.*, Oct. 2006, pp. 199–202, doi: 10.1109/RWS.2006.1615129.

[110] S. Preradovic, I. Balbin, N. C. Karmakar, and G. F. Swiegers, "Multiresonator-based chipless RFID system for low-cost item tracking," *IEEE Trans. Microw. Theory Techn.*, vol. 57, no. 5, pp. 1411–1419, May 2009, doi: 10.1109/TMTT.2009.2017323.

[111] S. Preradovic, S. Roy, and N. Karmakar, "Fully printable multi-bit chipless RFID transponder on flexible laminate," in *Proc. Asia–Pac. Microw. Conf.*, Dec. 2009, pp. 2371–2374, doi: 10.1109/APMC.2009.5385460.

[112] S. Mukherjee and C. Goutam, "Chipless RFID using stacked multilayer patches," in *Proc. Appl. Electromagn. Conf. (AEMC)*, Dec. 2009, pp. 1–4, doi: 10.1109/AEMC.2009.5430585.

[113] L. Reichardt, G. Adamiuk, G. Jereczek, and T. Zwick, "Chipless RFID systems for car-to-infrastructure communication," in *Proc. IEEE Int. Conf. Commun. Workshops*, May 2010, pp. 1–5, doi: 10.1109/ICCW.2010.5503936.

[114] S. Preradovic, N. Karmakar, and M. Zenere, "UWB chipless tag RFID reader design," in *Proc. IEEE Int. Conf. RFID-Technol. Appl.*, Jun. 2010, pp. 257–262, doi: 10.1109/RFID-TA.2010.5529922.

[115] S. Preradovic and N. C. Karmakar, "Multiresonator based chipless RFID tag and dedicated RFID reader," in *Proc. IEEE MTT-S Int. Microw. Symp.*, May 2010, pp. 1520–1523, doi: 10.1109/MWSYM.2010.5515168.

[116] A. Vena, E. Perret, and S. Tedjini, "Chipless RFID tag using hybrid coding technique," *IEEE Trans. Microw. Theory Techn.*, vol. 59, no. 12, pp. 3356–3364, Dec. 2011, doi: 10.1109/TMTT.2011.2171001.

[117] A. Vena, E. Perret, and S. Tedjini, "RFID chipless tag based on multiple phase shifters," in *Proc. IEEE MTT-S Int. Microw. Symp.*, Jun. 2011, pp. 1–4, doi: 10.1109/MWSYM.2011.5972712.

[118] A. T. Blischak and M. Manteghi, "Embedded singularity chipless RFID tags," *IEEE Trans. Antennas Propag.*, vol. 59, no. 11, pp. 3961–3968, Nov. 2011, doi: 10.1109/TAP.2011.2164191.

[119] S. Preradovic, S. M. Roy, and N. C. Karmakar, "RFID system based on fully printable chipless tag for paper-/plastic-ltem tagging," *IEEE Antennas Propag. Mag.*, vol. 53, no. 5, pp. 15–32, Oct. 2011, doi: 10.1109/MAP.2011.6138421.

[120] N. C. Karmakar and C. K. Pern, "mm-Wave chipless RFID tag for low-cost item tagging," in *Proc. Asia–Pac. Microw. Conf.*, Dec. 2011, pp. 1462–1465.

[121] D. Girbau, J. Lorenzo, A. Lazaro, C. Ferrater, and R. Villarino, "Frequency-coded chipless RFID tag based on dual-band resonators," *IEEE Antennas Wireless Propag. Lett.*, vol. 11, pp. 126–128, 2012, doi: 10.1109/LAWP.2012.2185032.

[122] A. Vena, E. Perret, and S. Tedjini, "A compact chipless RFID tag using polarization diversity for encoding and sensing," in *Proc. IEEE Int. Conf. RFID (RFID)*, Apr. 2012, pp. 191–197, doi: 10.1109/RFID.2012.6193050.

[123] C. M. Nijas *et al.*, "Chipless RFID tag using multiple microstrip open stub resonators," *IEEE Trans. Antennas Propag.*, vol. 60, no. 9, pp. 4429–4432, Sep. 2012, doi: 10.1109/TAP.2012.2207081.

[124] A. Vena, E. Perret, and S. Tedjini, "Design of compact and auto-compensated single-layer chipless RFID tag," *IEEE Trans. Microw. Theory Techn.*, vol. 60, no. 9, pp. 2913–2924, Sep. 2012, doi: 10.1109/TMTT.2012.2203927.

[125] A. Vena, E. Perret, S. Tedjini, D. Kaddour, A. Potie, and T. Barron, "A compact chipless RFID tag with environment sensing capability," in *IEEE/MTT-S Int. Microw. Symp. Dig.*, Jun. 2012, pp. 1–3, doi: 10.1109/MWSYM.2012.6258420.

[126] D. Girbau, A. Lázaro, and R. Villarino, "Passive wireless permittivity sensor based on frequency-coded chipless RFID tags," in *IEEE/MTT-S Int. Microw. Symp. Dig.*, Jun. 2012, pp. 1–3, doi: 10.1109/MWSYM.2012.6259412.

[127] H. E. Matbouly, N. Boubekeur, and F. Domingue, "A novel chipless identification tag based on a substrate integrated cavity resonator," *IEEE Microw. Wireless Compon. Lett.*, vol. 23, no. 1, pp. 52–54, Jan. 2013, doi: 10.1109/LMWC.2012.2236081.

[128] B. Shao, Y. Amin, Q. Chen, R. Liu, and L. Zheng, "Directly printed packaging-paper-based chipless RFID tag with coplanar LC resonator," *IEEE Antennas Wireless Propag. Lett.*, vol. 12, pp. 325–328, Feb. 2013, doi: 10.1109/LAWP.2013.2247556.

[129] Y. F. Weng, S. W. Cheung, T. I. Yuk, and L. Liu, "Design of chipless UWB RFID system using A CPW multi-resonator," *IEEE Antennas Propag. Mag.*, vol. 55, no. 1, pp. 13–31, May 2013, doi: 10.1109/MAP.2013.6474480.

[130] A. Vena, A. A. Babar, L. Sydänheimo, M. M. Tentzeris, and L. Ukkonen, "A novel near-transparent ASK-reconfigurable inkjet-printed chipless RFID tag," *IEEE Antennas Wireless Propag. Lett.*, vol. 12, pp. 753–756, 2013, doi: 10.1109/LAWP.2013.2270932.

[131] A. Vena *et al.*, "Design and realization of stretchable sewn chipless RFID tags and sensors for wearable applications," in *Proc. IEEE Int. Conf. RFID (RFID)*, Apr./May 2013, pp. 176–183, doi: 10.1109/RFID.2013.6548152.

[132] A. Vena *et al.*, "Design of chipless RFID tags printed on paper by flexography," *IEEE Trans. Antennas Propag.*, vol. 61, no. 12, pp. 5868–5877, Dec. 2013, doi: 10.1109/TAP.2013.2281742.

[133] A. Vena, L. Sydänheimo, M. M. Tentzeris, and L. Ukkonen, "A novel inkjet printed carbon nanotube-based chipless RFID sensor for gas detection," in *Proc. Eur. Microw. Conf.*, Oct. 2013, pp. 9–12, doi: 10.23919/EuMC.2013.6686577.

[134] R. Rezaiesarlak and M. Manteghi, "Complex-natural-resonance-based design of chipless RFID tag for high-density data," *IEEE Trans. Antennas Propag.*, vol. 62, no. 2, pp. 898–904, Feb. 2014, doi: 10.1109/TAP.2013.2290998.

[135] C. M. Nijas *et al.*, "Low-cost multiple-bit encoded chipless RFID tag using stepped impedance resonator," *IEEE Trans. Antennas Propag.*, vol. 62, no. 9, pp. 4762–4770, Sep. 2014, doi: 10.1109/TAP.2014.2330586.

[136] J. Kim, Z. Wang, and W. S. Kim, "Stretchable RFID for wireless strain sensing with silver nano ink," *IEEE Sensors J.*, vol. 14, no. 12, pp. 4395–4401, Dec. 2014, doi: 10.1109/JSEN.2014.2335743.

[137] R. Nair *et al.*, "A fully printed passive chipless RFID tag for low-cost mass production," in *Proc. 8th Eur. Conf. Antennas Propag. (EuCAP)*, Apr. 2014, pp. 2950–2954, doi: 10.1109/EuCAP.2014.6902446.

[138] A. Vena, L. Sydänheimo, L. Ukkonen, and M. M. Tentzeris, "A fully inkjet-printed chipless RFID gas and temperature sensor on paper," in *Proc. IEEE RFID Technol. Appl. Conf. (RFID-TA)*, Sep. 2014, pp. 115–120, doi: 10.1109/RFID-TA.2014.6934211.

[139] M. S. Bhuiyan and N. Karmakar, "A spectrally efficient chipless RFID tag based on split-wheel resonator," in *Proc. Int. Workshop Antenna Technol. Small Antennas Novel EM Structures Mater. Appl. (iWAT)*, Mar. 2014, pp. 1–4, doi: 10.1109/IWAT.2014.6958582.

[140] M. Polivka and J. Machac, "Improvement of backscatter properties of C-shaped dipole scatterer for chipless RFID," in *Proc. Asia–Pac. Microw. Conf.*, Nov. 2014, pp. 962–964.

[141] M. Barahona, D. Betancourt, and F. Ellinger, "Decoding of multiple same-coded in-line placed chipless RFID tags," in *Proc. IEEE Conf. Antenna Meas. Appl. (CAMA)*, Nov. 2014, pp. 1–4, doi: 10.1109/CAMA.2014.7003353.

[142] C. Feng, W. Zhang, L. Li, L. Han, X. Chen, and R. Ma, "Angle-based chipless RFID tag with high capacity and insensitivity to polarization," *IEEE Trans. Antennas Propag.*, vol. 63, no. 4, pp. 1789–1797, Apr. 2015, doi: 10.1109/TAP.2015.2393851.

[143] M. Garbati, R. Siragusa, E. Perret, A. Vena, and C. Halopé, "High performance chipless RFID reader based on IR-UWB technology," in *Proc. 9th Eur. Conf. Antennas Propag. (EuCAP)*, Apr. 2015, pp. 1–5.

[144] M. A. Islam and N. Karmakar, "On a compact printable dual-polarized chipless RFID tag using slot length variation encoding technique for barcode replacement," in *IEEE MTT-S Int. Microw. Symp.*, May 2015, pp. 1–4, doi: 10.1109/MWSYM.2015.7167100.

[145] M. Khaliel, M. El-Hadidy, and T. Kaiser, "Printable depolarizing chipless RFID tag based on DGS resonators for suppressing the clutter effects," in *Proc. 9th Eur. Conf. Antennas Propag. (EuCAP)*, Apr. 2015, pp. 1–5.

[146] D. Betancourt *et al.*, "Square-shape fully printed chipless RFID tag and its applications in evacuation procedures," in *Proc. 9th Eur. Conf. Antennas Propag. (EuCAP)*, Apr. 2015, pp. 1–5.

[147] M. A. Islam and N. C. Karmakar, "Compact printable chipless RFID systems," *IEEE Trans. Microw. Theory Techn.*, vol. 63, no. 11, pp. 3785–3793, Nov. 2015, doi: 10.1109/TMTT.2015.2482968.

[148] M. Polivka, J. Havlicek, M. Svanda, and J. Machac, "Improvement of RCS response of U-shaped strip-based chipless RFID tags," in *Proc. Eur. Microw. Conf. (EuMC)*, Sep. 2015, pp. 107–110, doi: 10.1109/EuMC.2015.7345711.

[149] S. Genovesi, F. Costa, A. Monorchio, and G. Manara, "Chipless RFID tag exploiting multifrequency delta-phase quantization encoding," *IEEE Antennas Wireless Propag. Lett.*, vol. 15, pp. 738–741, 2016, doi: 10.1109/LAWP.2015.2471101.

[150] M. M. Khan, F. A. Tahir, M. F. Farooqui, A. Shamim, and H. M. Cheema, "3.56-bits/cm compact Inkjet printed and application specific chipless RFID tag," *IEEE Antennas Wireless Propag. Lett.*, vol. 15, pp. 1109–1112, 2016, doi: 10.1109/LAWP.2015.2494864.

[151] D. Betancourt, K. Haase, A. Hübler, and F. Ellinger, "Bending and folding effect study of flexible fully printed and late-stage codified octagonal chipless RFID tags," *IEEE Trans. Antennas Propag.*, vol. 64, no. 7, pp. 2815–2823, Jul. 2016, doi: 10.1109/TAP.2016.2559522.

[152] J. Havlicek, M. Polivka, M. Svanda, and J. Machac, "Capacitively loaded dipoles for chipless RFID transponder," in *Proc. 26th Int. Conf. Radioelektronika (RADIOELEKTRONIKA)*, Apr. 2016, pp. 446–449, doi: 10.1109/RADIOELEK.2016.7477349.

[153] S. Preradovic and A. Menicanin, "Printed 3-D stacked chipless RFID tag with spectral and polarization encoding capacity," in *Proc. 39th Int. Spring Seminar Electron. Technol. (ISSE)*, May 2016, pp. 500–505, doi: 10.1109/ISSE.2016.7563249.

[154] E. Perret, "Permittivity characterization based on Radar Cross measurements," in *Proc. URSI Int. Symp. Electromagn. Theory (EMTS)*, Aug. 2016, pp. 457–460, doi: 10.1109/URSI-EMTS.2016.7571425.

[155] M. Barahona, D. Betancourt, and F. Ellinger, "On the decoding of equiprobable UWB chipless RFID tags using a minimum distance detector," in *Proc. Int. Symp. Antennas Propag. (ISAP)*, Oct. 2016, pp. 1006–1007.

[156] M. Barahona, D. Betancourt, and F. Ellinger, "Comparison of UWB chipless tags on flexible substrates fabricated using either aluminum, copper or silver," in *Proc. IEEE-APS Topical Conf. Antennas Propag. Wireless Commun. (APWC)*, Sep. 2016, pp. 78–81, doi: 10.1109/APWC.2016.7738123.

[157] D. Henry, J. G. D. Hester, H. Aubert, P. Pons, and M. M. Tentzeris, "Long-range wireless interrogation of passive humidity sensors using Van-Atta cross-polarization effect and different beam scanning techniques," *IEEE Trans. Microw. Theory Techn.*, vol. 65, no. 12, pp. 5345–5354, Dec. 2017, doi: 10.1109/TMTT.2017.2769055.

[158] E. Perret, "Displacement sensor based on radar cross-polarization measurements," *IEEE Trans. Microw. Theory Techn.*, vol. 65, no. 3, pp. 955–966, Mar. 2017, doi: 10.1109/TMTT.2016.2638842.

[159] M. Borgese, F. A. Dicandia, F. Costa, S. Genovesi, and G. Manara, "An inkjet printed chipless RFID sensor for wireless humidity monitoring," *IEEE Sensors J.*, vol. 17, no. 15, pp. 4699–4707, Aug. 2017, doi: 10.1109/JSEN.2017.2712190.

[160] M. Martinez and D. V. D. Weide, "Chipless RFID temperature threshold sensor and detection method," in *Proc. IEEE Int. Conf. RFID (RFID)*, May 2017, pp. 61–66, doi: 10.1109/RFID.2017.7945588.

[161] M. Borgese, F. A. Dicandia, F. Costa, S. Genovesi, and G. Manara, "Exploitation of chipless RFID technology for humidity monitoring," in *Proc. 32nd Gen. Assembly Sci. Symp. Int. Union Radio Sci. (URSI GASS)*, Aug. 2017, pp. 1–4, doi: 10.23919/URSIGASS.2017.8104972.

[162] C. Schuster, P. Schumacher, M. Schüßler, A. Jiménez-Sáez, and R. Jakoby, "Passive chipless wireless pressure sensor based on dielectric resonators," in *Proc. IEEE SENSORS*, Oct./Nov. 2017, pp. 1–3, doi: 10.1109/ICSENS.2017.8234269.

[163] S. Dey and N. C. Karmakar, "An IoT empowered flexible chipless RFID tag for low cost item identification," in *Proc. IEEE Region 10 Humanitarian Technol. Conf. (R10-HTC)*, Dec. 2017, pp. 179–182, doi: 10.1109/R10-HTC.2017.8288933.

[164] K. Xie and Y. Xue, "A 12 bits chipless RFID tag based on 'I-shaped' slot resonators," in *Proc. 6th Int. Conf. Comput. Sci. Netw. Technol. (ICCSNT)*, Oct. 2017, pp. 320–324, doi: 10.1109/ICCSNT.2017.8343710.

[165] L. Wang, T. Liu, J. Sidén, and G. Wang, "Design of chipless RFID tag by using miniaturized open-loop resonators," *IEEE Trans. Antennas Propag.*, vol. 66, no. 2, pp. 618–626, Feb. 2018, doi: 10.1109/TAP.2017.2782262.

[166] A. M. J. Marindra and G. Y. Tian, "Chipless RFID sensor tag for metal crack detection and characterization," *IEEE Trans. Microw. Theory Techn.*, vol. 66, no. 5, pp. 2452–2462, May 2018, doi: 10.1109/TMTT.2017.2786696.

[167] Y. Liu and X. Yang, "Chipless radio frequency identification tag design with modified interdigital hairpin resonators," in *Proc. Int. Conf. Intell. Transp. Big Data Smart City (ICITBS)*, Jan. 2018, pp. 645–648, doi: 10.1109/ICITBS.2018.00168.

[168] F. Costa *et al.*, "A depolarizing chipless RF label for dielectric permittivity sensing," *IEEE Microw. Wireless Compon. Lett.*, vol. 28, no. 5, pp. 371–373, May 2018, doi: 10.1109/LMWC.2018.2820604.

[169] A. Lázaro *et al.*, "Chipless dielectric constant sensor for structural health testing," *IEEE Sensors J.*, vol. 18, no. 13, pp. 5576–5585, Jul. 2018, doi: 10.1109/JSEN.2018.2839689.

[170] A. M. J. Marindra, R. Sutthaweekul, and G. Y. Tian, "Depolarizing chipless RFID sensor tag for characterization of metal cracks based on dual resonance features," in *Proc. 10th Int. Conf. Inf. Technol. Elect. Eng. (ICITEE)*, Jul. 2018, pp. 73–78, doi: 10.1109/ICITEED.2018.8534943.

[171] V. Sharma, S. Malhotra, and M. Hashmi, "Orientation independent printable backscattering chipless RFID tags based on L-resonator," in *Proc. 48th Eur. Microw. Conf. (EuMC)*, Sep. 2018, pp. 989–992, doi: 10.23919/EuMC.2018.8541425.

[172] H. Huang and L. Su, "A high capacity and bending-insensitive minimized chipless tag," in *Proc. Int. Conf. Microw. Mil. Wave Technol. (ICMMT)*, May 2018, pp. 1–3, doi: 10.1109/ICMMT.2018.8563929.

[173] M. Polivka, M. Svanda, J. Havlicek, and J. Machac, "Semi-platform tolerant 20-bit chipless RFID tag composed of dipole array closely coupled to plate," in *Proc. 12th Eur. Conf. Antennas Propag. (EuCAP)*, Apr. 2018, pp. 1–3, doi: 10.1049/cp.2018.0482.

[174] Y. J. Zhang, R. X. Gao, Y. He, and M. S. Tong, "Effective design of microstrip-line chipless RFID tags based on filter theory," *IEEE Trans. Antennas Propag.*, vol. 67, no. 3, pp. 1428–1436, Mar. 2019, doi: 10.1109/TAP.2018.2879854.

[175] Y. S. Chen, T. Y. Jiang, and F. P. Lai, "Automatic topology generation of 21 bit chipless radio frequency identification tags using a non-iterative technique," *IEEE Antennas Wireless Propag. Lett.*, vol. 18, no. 2, pp. 293–297, Feb. 2019, doi: 10.1109/LAWP.2018.2889322.

[176] V. Sharma, S. Malhotra, and M. Hashmi, "Slot resonator based novel orientation independent chipless RFID tag configurations," *IEEE Sensors J.*, vol. 19, no.3, pp. 5153–5160, Jul. 2019, doi: 10.1109/JSEN.2019.2902622.

[177] V. Ferro, P. Rebello, M. Quadros, and W. Staehler, "L-shaped chipless tag design analysis and optimization for fully inkjet printing," in *Proc. IEEE Int. Conf. RFID (RFID)*, Apr. 2019, pp. 1–8, doi: 10.1109/RFID.2019.8719282.

[178] M. Added, N. Boulejfen, M. Svanda, F. M. Ghannouchi, and T. P. Vuong, "High-performance chipless radio-frequency identification tags: Using a slow-wave approach for miniaturized structure," *IEEE Antennas Propag. Mag.*, vol. 61, no. 4, pp. 46–54, Jul. 2019, doi: 10.1109/MAP.2019.2920664.

[179] N. Tariq *et al.*, "Orientation independent chipless RFID tag using novel trefoil resonators," *IEEE Access*, vol. 7, pp. 122398–122407, 2019, doi: 10.1109/ACCESS.2019.2937131.

[180] H. Li, B. Wang, M. Wu, J. Zhu, and C. Zhou, "Design and analysis of chipless RFID Tags Based on Retro-Radiators," *IEEE Access*, vol. 7, pp. 148208–148217, 2019, doi: 10.1109/ACCESS.2019.2946614.

[181] W. M. Abdulkawi and A. A. Sheta, "K-state resonators for high-coding-capacity chipless RFID applications," *IEEE Access*, vol. 7, pp. 185868–185878, 2019, doi: 10.1109/ACCESS.2019.2961565.

[182] G. A. Eyebe and F. Domingue, "Towards substrate-sensitive chipless tags for sensing applications," in *Proc. IEEE SENSORS*, Oct. 2019, pp. 1–4, doi: 10.1109/SENSORS43011.2019.8956618.

[183] Z. Li and S. Bhadra, "A flexible printed chipless RFID tag for concentration measurements of liquid solutions," in *Proc. IEEE SENSORS*, Oct. 2019, pp. 1–4, doi: 10.1109/SENSORS43011.2019.8956830.

[184] F. Babaeian, J. Feng, and N. Karmakar, "Realisation of a high spectral efficient chipless RFID tag using hairpin resonators," in *Proc. IEEE Asia–Pac. Microw. Conf. (APMC)*, Dec. 2019, pp. 114–116, doi: 10.1109/APMC46564.2019.9038844.

[185] D. P. Mishra, T. K. Das, P. Sethy, and S. K. Behera, "Design of a multi-bit chipless RFID tag using square split-ring resonators," in *Proc. IEEE Indian Conf. Antennas Propag. (InCAP)*, Dec. 2019, pp. 1–4, doi: 10.1109/InCAP47789.2019.9134626.

[186] M. Forouzandeh and N. Karmakar, "Self-interference cancelation in frequency-domain chipless RFID readers," *IEEE Trans. Microw. Theory Techn.*, vol. 67, no. 5, pp. 1994–2009, Aug. 2019, doi: 10.1109/TMTT.2018.2890638.

[187] H. E. Matbouly, S. Tedjini, K. Zannas, and Y. Duroc, "Chipless sensing system compliant with the standard radio frequency regulations," *IEEE J. Radio Freq. Identif.*, vol. 3, no. 2, pp. 83–90, Jun. 2019, doi: 10.1109/JRFID.2019.2909092.

[188] F. Babaeian and N. C. Karmakar, "A high gain dual polarized ultra-wideband array of antenna for chipless RFID applications," *IEEE Access*, vol. 6, pp. 73702–73712, 2018, doi: 10.1109/ACCESS.2018.2883439.

[189] Z. Ali *et al.*, "Authentication using metallic inkjet-printed chipless RFID tags," *IEEE Trans. Antennas Propag.*, vol. 68, no. 5, pp. 4137–4142, May 2020, doi: 10.1109/TAP.2019.2948740.

[190] M. A. Bibile, G. Khadka, and N. C. Karmakar, "Detection of chipless RFID tag using a single antenna RFID reader system," in *Proc. 5th Int. Conf. Innov. Technol. Intell. Syst. Ind. Appl. (CITISIA)*, Nov. 2020, pp. 1–6, doi: 10.1109/CITISIA50690.2020.9371834.

[191] L. Shahid *et al.*, "Chipless RFID tag for touch event sensing and localization," *IEEE Access*, vol. 8, pp. 502–513, 2020, doi: 10.1109/ACCESS.2019.2961691.

[192] D. P. Mishra, T. K. Das, and S. K. Behera, "Design of a 3-bit chipless RFID tag using circular split-ring resonators for retail and healthcare applications," in *Proc. Nat. Conf. Commun. (NCC)*, Feb. 2020, pp. 1–4, doi: 10.1109/NCC48643.2020.9056018.

[193] A. Ramos, Z. Ali, A. Vena, M. Garbati, and E. Perret, "Single-layer, flexible, and depolarizing chipless RFID tags," *IEEE Access*, vol. 8, pp. 72929–72941, 2020, doi: 10.1109/ACCESS.2020.2988116.

[194] K. Brinker and R. Zoughi, "Multi-bit chipless RFID sensing methodology for rotation determination," in *Proc. IEEE Int. Instrum. Meas. Technol. Conf. (I2MTC)*, May 2020, pp. 1–6.

[195] R. A. A. R. Felix, W. C. Felix, and E. C. Gurjão, "Multi-layer flexible chipless RFID tag based on group delay encoding," in *Proc. IEEE 6th World Forum Internet Things (WF-IoT)*, Jun. 2020, pp. 1–6, doi: 10.1109/WF-IoT48130.2020.9221216.

[196] S. Dey, E. M. Amin, and N. C. Karmakar, "Paper based chipless RFID leaf wetness detector for plant health monitoring," *IEEE Access*, vol. 8, pp. 191986–191996, 2020, doi: 10.1109/ACCESS.2020.3033191.

[197] N. Javed, M. A. Azam, I. Qazi, Y. Amin, and H. Tenhunen, "Data-dense chipless RFID multisensor for aviculture industry," *IEEE Microw. Wireless Compon. Lett.*, vol. 30, no. 12, pp. 1193–1196, Dec. 2020, doi: 10.1109/LMWC.2020.3032027.

[198] F. Babaeian and N. C. Karmakar, "A semi-omnidirectional resonator for chipless RFID backscattered tag design," in *Proc. 27th Int. Conf. Telecommun. (ICT)*, Oct. 2020, pp. 1–5, doi: 10.1109/ICT49546.2020.9239460.

[199] P. Kadera, A. Jiménez-Sáez, T. Burmeister, J. Lacik, M. Schüßler, and R. Jakoby, "Gradient-index-based frequency-coded retroreflective lenses for mm-Wave indoor localization," *IEEE Access*, vol. 8, pp. 212765–212775, 2020, doi: 10.1109/ACCESS.2020.3039986.

[200] F. Babaeian, N. Karmakar, Z. Komeily-Nia, and A. Sutti, "Towards an Objective and Precise Moisture Content Measurement of Textiles Using a Chipless RFID Tag-Sensor," in *Proc. IEEE SENSORS*, Oct. 2020, pp. 1–4, doi: 10.1109/SENSORS47125.2020.9278905.

[201] M. U. A. Khan, R. Raad, J. Foroughi, P. I. Theoharis, S. Liu, and J. Masud, "A silver-coated conductive fibre HC12 sewed chipless RFID tag on cotton fabric for wearable applications," in *Proc. IEEE 23rd Int. Multitopic Conf. (INMIC)*, Nov. 2020, pp. 1–5, doi: 10.1109/INMIC50486.2020.9318155.

[202] A. A. Awan, M. N. Salimi, M. A. Riaz, H. Shahid, M. A. Asghar, and Y. Amin, "An RFID enabled miniaturized chipless tag for IoT applications," in *Proc. IEEE 23rd Int. Multitopic Conf. (INMIC)*, Nov. 2020, pp. 1–5, doi: 10.1109/INMIC50486.2020.9318131.

[203] R. E. Ghiri and K. Entesari, "Time-domain ultrawideband chipless RFID readers," *IEEE Trans. Instrum. Meas.*, vol. 70, pp. 1–10, 2021, doi: 10.1109/TIM.2021.3091472.

[204] M. A. Islam and N. C. Karmakar, "An 8×8 mm-Wave LP ACMPA Array for a long-range mm-Wave chipless RFID tag-sensor reader," *IEEE J. Radio Freq. Identif.*, vol. 5, no. 1, pp. 53–63, Mar. 2021, doi: 10.1109/JRFID.2020.3036721.

[205] N. Barbot, O. Rance, and E. Perret, "Cross-polarization chipless tag for orientation sensing," in *Proc. 50th Eur. Microw. Conf. (EuMC)*, Jan. 2021, pp. 1119–1122, doi: 10.23919/EuMC48046.2021.9338174.

[206] R. D. Amorim, N. Barbot, R. Siragusa, and E. Perret, "Millimeter-wave chipless RFID tag for authentication applications," in *Proc. 50th Eur. Microw. Conf. (EuMC)*, Jan. 2021, pp. 800–803, doi: 10.23919/EuMC48046.2021.9338082.

[207] R. D. Amorim, R. Siragusa, N. Barbot, G. Fontgalland, and E. Perret, "Millimeter wave chipless RFID authentication based on spatial diversity and 2-D classification approach," *IEEE Trans. Antennas Propag.*, vol. 69, no. 9, pp. 5913–5923, Sep. 2021, doi: 10.1109/TAP.2021.3060126.

[208] M. E. B. Jalil *et al.*, "High capacity and miniaturized flexible chipless RFID tag using modified complementary split ring resonator," *IEEE Access*, vol. 9, pp. 33929–33943, 2021, doi: 10.1109/ACCESS.2021.3061792.

[209] J. Sánchez-Pastor, A. Jiménez-Sáez, M. Schüßler, and R. Jakoby, "Gridded square-ring frequency selective surface for angular-stable response on chipless indoor location tag landmarks," in *Proc. 15th Eur. Conf. Antennas Propag. (EuCAP)*, Mar. 2021, pp. 1–5, doi: 10.23919/EuCAP51087.2021.9411424.

[210] T. Burmeister *et al.*, "Chipless frequency-coded RFID tags integrating high-Q resonators and dielectric rod antennas," in *Proc. 15th Eur. Conf. Antennas Propag. (EuCAP)*, Mar. 2021, pp. 1–5, doi: 10.23919/EuCAP51087.2021.9410915.

[211] R. E. Ghiri and K. Entesari, "A 50.7-bit retransmission-based chipless RFID tag with miniaturized resonators," in *Proc. IEEE Topical Conf. Wireless Sensors Sensor Netw. (WiSNeT)*, Jan. 2021, pp. 12–14, doi: 10.1109/WiSNeT51848.2021.9413790.

[212] N. Javed, M. A. Azam, and Y. Amin, "Chipless RFID multisensor for temperature sensing and crack monitoring in an IoT environment," *IEEE Sensors Lett.*, vol. 5, no. 6, pp. 1–4, Jun. 2021, doi: 10.1109/LSENS.2021.3083218.

[213] M. Elgeziry, F. Costa, and S. Genovesi, "Wireless monitoring of displacement using spiral resonators," *IEEE Sensors J.*, vol. 21, no. 16, pp. 17838–17845, Aug. 2021, doi: 10.1109/JSEN.2021.3085191.

[214] F. Villa-Gonzalez, R. Bhattacharyya, and S. Sarma, "Single and bulk identification of plastics in the recycling chain using chipless RFID tags," in *Proc. IEEE Int. Conf. RFID (RFID)*, Apr. 2021, pp. 1–8, doi: 10.1109/RFID52461.2021.9444372.

[215] P. Sethy, D. P. Mishra, and S. K. Behera, "A 3-bit chipless RFID tag for IOT applications," in *Proc. 2nd Int. Conf. Emerg. Technol. (INCET)*, May 2021, pp. 1–4, doi: 10.1109/INCET51464.2021.9456349.

[216] K. Mekki, O. Necibi, H. Dinis, P. Mendes, and A. Gharsallah, "Backscatter analysis in UWB chipless RFID based on UWB-IR," in *Proc. IEEE Texas Symp. Wireless Microw. Circuits Syst. (WMCS)*, May 2021, pp. 1–5, doi: 10.1109/WMCS52222.2021.9493268.

[217] A. A. Abbas, Y. Zantah, K. Solbach, and T. Kaiser, "Frequency-coded lens by photonic crystal resonator for mm-Wave chipless RFID applications," in *Proc. 4th Int. Workshop Mobile Terahertz Syst. (IWMTS)*, Jul. 2021, pp. 1–5, doi: 10.1109/IWMTS51331.2021.9486828.

[218] J. Sánchez-Pastor, A. Jiménez-Sáez, M. Schüßler, and R. Jakoby, "Frequency-coded spherical retroreflector for wide-angle indoor localization tag landmarks," in *Proc. 4th Int. Workshop Mobile Terahertz Syst. (IWMTS)*, Jul. 2021, pp. 1–5, doi: 10.1109/IWMTS51331.2021.9486810.

[219] A. A. Abbas, M. H. Hassan, A. Abuelhaija, D. Erni, K. Solbach, and T. Kaiser, "Retrodirective dielectric resonator tag with polarization twist signature for clutter suppression in self-localization system," *IEEE Trans. Microw. Theory Techn.*, vol. 69, no. 12, pp. 5291–5299, Dec. 2021, doi: 10.1109/TMTT.2021.3108151.

[220] F. Kheawprae, A. Boonpoonga, and P. Akkaraekthalin, "Robust chipless RFID detection using complex natural frequency along with the k-nearest neighbor algorithm," *IEEE Access*, vol. 9, pp. 136217–136230, 2021, doi: 10.1109/ACCESS.2021.3116268.

[221] J. M. Purushothama, S. Lopez-Soriano, A. Vena, B. Sorli, and E. Perret, "Application of additive manufacturing based thermal printing techniques for realization of electronically rewritable chipless RFID tags on flexible substrates," in *Proc. 34th Gen. Assembly Sci. Symp. Int. Union Radio Sci. (URSI GASS)*, Aug./Sep. 2021, pp. 1–4, doi: 10.23919/URSIGASS51995.2021.9560362.

[222] Z. Ali and E. Perret, "A simple RCS calibration approach for depolarizing chipless RFID tags," in *Proc. IEEE MTT-S Int. Microw. Symp. (IMS)*, Jun. 2021, pp. 165–168, doi: 10.1109/IMS19712.2021.9574947.

[223] S. Jeong, J. Hester, R. Bahr, and M. M. Tentzeris, "A machine learning approach-based chipless RFID system for robust detection in real-world implementations," in *Proc. IEEE MTT-S Int. Microw. Symp. (IMS)*, Jun. 2021, pp. 661–664, doi: 10.1109/IMS19712.2021.9574849.

[224] A. Azarfar, N. Barbot, and E. Perret, "Towards chipless RFID technology based on micro-doppler effect for long range applications," in *Proc. IEEE MTT-S Int. Microw. Symp. (IMS)*, Jun. 2021, pp. 819–822, doi: 10.1109/IMS19712.2021.9575006.

[225] D. P. Mishra and S. K. Behera, "A novel technique for dimensional space reduction in passive RFID transponders," in *Proc. 2nd Int. Conf. Range Technol. (ICORT)*, Aug. 2021, pp. 1–4, doi: 10.1109/ICORT52730.2021.9581971.

[226] X. Wang, Y. Tao, J. Sidén, and G. Wang, "Design of high-data-density chipless RFID tag embedded in QR code," *IEEE Trans. Antennas Propag.*, vol. 70, no. 3, pp. 2189–2198, Mar. 2022, doi: 10.1109/TAP.2021.3111335.

[227] A. K. Gorur, E. Dogan, G. Ayas, C. Karpuz, and A. Gorur, "Multibit chipless RFID tags based on the transition among closed- and open-loop resonators," *IEEE Trans. Microw. Theory Techn.*, vol. 70, no. 1, pp. 101–111, Jan. 2022, doi: 10.1109/TMTT.2021.3122795.

[228] P. Fathi, S. Bhattacharya, and N. C. Karmakar, "Dual-polarized keratin-based UWB chipless RFID relative humidity sensor," *IEEE Sensors J.*, vol. 22, no. 3, pp. 1924–1932, Feb. 2022, doi: 10.1109/JSEN.2021.3135500.

[229] R. Raju and G. E. Bridges, "A compact wireless passive harmonic sensor for ammonia sensing in packaged food," *IEEE Sensors Lett.*, vol. 6, no. 4, pp. 1–4, Apr. 2022, doi: 10.1109/LSENS.2022.3159622.

[230] W. S. Li, C. Z. Peng, F. P. Lai, P. S. Lai, and Y. S. Chen, "Independent component analysis for the multi-tag detection of frequency-coded chipless RFID," *IEEE Trans. Antennas Propag.*, early access, Mar. 28, 2022, doi: 10.1109/TAP.2022.3161483.

[231] P. Kadera *et al.*, "Wide-angle ceramic retroreflective luneburg lens based on quasi-conformal transformation optics for mm-Wave indoor localization," *IEEE Access*, vol. 10, pp. 41097–41111, 2022, doi: 10.1109/ACCESS.2022.3166509.

[232] F. Babaeian and N. C. Karmakar, "4×4 element UWB dual-polarized aperture coupled microstrip patch antenna array for chipless RFID," in *Proc. IEEE Int. RF Microw. Conf. (RFM)*, Dec. 2020, pp. 1–4, doi: 10.1109/RFM50841.2020.9344752.

[233] F. Babaeian and N. Karmakar, "A UWB antenna for chipless RFID tag detection," in *Proc. Int. Conf. Elect. Commun. Comput. Eng. (ICECCE)*, Jun. 2020, pp. 1–6, doi: 10.1109/ICECCE49384.2020.9179191.

[234] Y. Gao, M. Mahmoodi, and R. Zoughi, "Design of a novel frequency-coded chipless RFID tag," *IEEE Open J. Instrum. Meas.*, vol. 1, 2022, Art. no. 8000109.

[235] M. M. Forouzandeh and N. Karmakar, "Towards the improvement of frequency-domain chipless RFID readers," in *Proc. IEEE Wireless Power Transf. Conf. (WPTC)*, Jun. 2018, pp. 1–4, doi: 10.1109/WPT.2018.8639263.

[236] M. Garbati, E. Perret, and R. Siragusa, *Chipless RFID Reader Design for Ultra-Wideband Technology*. New York, NY, USA: ISTE Press, 2018.

[237] N. Barbot and E. Perret, "Impact of the polarization over the read range in chipless RFID," in *Proc. IEEE Int. Conf. RFID Technol. Appl. (RFID-TA)*, Oct. 2021, pp. 139–141, doi: 10.1109/RFID-TA53372.2021.9617398.

[238] E. M. Amin, M. S. Bhuiyan, N. C. Karmakar, and B. Winther-Jensen, "Development of a low cost printable chipless RFID humidity sensor," *IEEE Sensors J.*, vol. 14, no. 1, pp. 140–149, Jan. 2014, doi: 10.1109/JSEN.2013.2278560.

[239] A. Guillet, A. Vena, E. Perret, and S. Tedjini, "Design of a chipless RFID sensor for water level detection," in *Proc. Int. Symp. Antenna Technol. Appl. Electromagn.*, Jun. 2012, pp. 1–4, doi: 10.1109/ANTEM.2012.6262372.

[240] P. Kalansuriya, "Signal processing methods for chipless RFID," Ph.D. dissertation, Dept. Elect. Comput. Syst. Eng., Monash Univ., Melbourne, VIC, Australia, 2014. [Online]. Available: https://bridges.monash.edu/articles/thesis/Signal_processing_methods_for_chipless_RFID/4684024

[241] F. Babaeian, M. Forouzandeh, and N. Karmakar, "Solving a chipless RFID inverse problem based on tag range estimation," *IET Microw. Antennas Propag.*, vol. 14, no. 12, pp. 1361–1370, Oct. 2020, doi: https://doi.org/10.1049/iet-map.2019.1030..

[242] A. Fawky, M. Khaliel, A. El-Awamry, M. El-Hadidy, and T. Kaiser, "Novel pseudo-noise coded chipless RFID system for clutter removal and tag detection," in *Proc. IEEE Int. Conf. RFID (RFID)*, Apr. 2015, pp. 100–104, doi: 10.1109/RFID.2015.7113079.

[243] J. Aliasgari and N. C. Karmakar, "Mathematical model of chipless RFID tags for detection improvement," *IEEE Trans. Microw. Theory Techn.*, vol. 68, no. 10, pp. 4103–4115, Oct. 2020, doi: 10.1109/TMTT.2020.2996953.

[244] A. Lazaro, A. Ramos, D. Girbau, and R. Villarino, "Chipless UWB RFID tag detection using continuous wavelet transform," *IEEE Antennas Wireless Propag. Lett.*, vol. 10, pp. 520–523, 2011, doi: 10.1109/LAWP.2011.2157299.

[245] A. Ramos, E. Perret, O. Rance, S. Tedjini, A. Lázaro, and D. Girbau, "Temporal separation detection for chipless depolarizing frequency-coded RFID," *IEEE Trans. Microw. Theory Techn.*, vol. 64, no. 7, pp. 2326–2337, Jul. 2016, doi: 10.1109/TMTT.2016.2568180.

[246] R. T. D. Alencar, N. Barbot, M. Garbati, and E. Perret, "Characterization of chipless RFID tag in a 3-dimensional reading zone," in *Proc. IEEE Int. Symp. Antennas Propag. USNC-URSI Radio Sci. Meeting*, Jul. 2019, pp. 639–640, doi: 10.1109/APUSNCURSINRSM.2019.8888559.

[247] R. Anee and N. C. Karmakar, "Chipless RFID tag localization," *IEEE Trans. Microw. Theory Techn.*, vol. 61, no. 11, pp. 4008–4017, Nov. 2013, doi: 10.1109/TMTT.2013.2282280.

[248] A. Fawky, M. Khaliel, A. El-Awamry, and T. Kaiser, "Frequency coded chipless RFID tag localization using multiple antennas," in *Proc. 11th Eur. Conf. Antennas Propag. (EUCAP)*, Mar. 2017, pp. 2075–2079, doi: 10.23919/EuCAP.2017.7928650.

[249] E. M. Amin, N. C. Karmakar, and B. W. Jensen, "Fully printable chipless RFID multi-parameter sensor," *Sensors Actuators A Phys.*, vol. 248, pp. 223–232, Sep. 2016, [Online]. Available: https://doi.org/10.1016/j.sna.2016.06.014

[250] T. Athauda, R. Bhattacharyya, N. Karmakar, and S. Sarma, "Electromagnetic characterization of a food safe, organic smart material for customizable temperature threshold sensing in cold chain applications," in *Proc. IEEE Int. Conf. RFID (RFID)*, Apr. 2019, pp. 1–6, doi: 10.1109/RFID.2019.8719251.

[251] V. Sharma and M. Hashmi, "On the seamless integration and coexistence of chipless RFID in broad IoT framework," *IEEE Access*, ol. 9, pp. 69839–69849, 2021, doi: 10.1109/ACCESS.2021.3078318.

[252] W. M. Adbulkawi and A. A. Sheta, "Printable chipless RFID tags for IoT applications," in *Proc. 1st Int. Conf. Comput. Appl. Inf. Security (ICCAIS)*, Apr. 2018, pp. 1–4, doi: 10.1109/CAIS.2018.8441955.

[253] S. Tedjini, N. Karmakar, E. Perret, A. Vena, R. Koswatta, and R. E. Azim, "Hold the chips: Chipless technology, an alternative technique for RFID," *IEEE Microw. Mag.*, vol. 14, no. 5, pp. 56–65, Jul./Aug. 2013, doi: 10.1109/MMM.2013.2259393.

[254] J. Aliasgari, M. Forouzandeh, and N. Karmakar, "Chipless RFID readers for frequency-coded tags: Time-domain or frequency-domain?" *IEEE J. Radio Freq. Identif.*, vol. 4, no. 2, pp. 146–158, Jun. 2020, doi: 10.1109/JRFID.2020.2982822.

[255] M. Garbati, E. Perret, R. Siragusa, and C. Halope, "Ultrawideband chipless RFID: Reader technology from SFCW to IR-UWB," *IEEE Microw. Mag.*, vol. 20, no. 6, pp. 74–88, Jun. 2019, doi: 10.1109/MMM.2019.2904408.

[256] R. V. Koswatta, "Readers for frequency signature-based chipless RFID tags," Ph.D. dissertation, Dept. Elect. Comput. Syst. Eng., Monash Univ., Melbourne, VIC, Australia, 2013. [Online]. Available: https://bridges.monash.edu/articles/thesis/Readers_for_frequency_signature-based_chipless_RFID_tags/4704928

[257] K. Brinker, M. Dvorsky, M. T. A. Qaseer, and R. Zoughi, "Review of advances in microwave and millimeter-wave NDT&E: Principles and applications," *Philos. Trans. Roy. Soc. A Math. Phys. Eng. Sci.*, to be published.

[258] R. V. Koswatta and N. C. Karmakar, "A novel reader architecture based on UWB chirp signal interrogation for multiresonator-based chipless RFID tag reading," *IEEE Trans. Microw. Theory Techn.*, vol. 60, no. 9, pp. 2925–2933, Sep. 2012, doi: 10.1109/TMTT.2012.2203929.

[259] L. Boggioni, L. Monti, S. Terranova, F. Costa, S. Genovesi, and G. Manara, "Low-cost portable reader for frequency domain chipless tags: Architecture and experimental results on depolarizing tags," *Electronics*, vol. 8, no. 1, p. 35, 2019, doi: 10.3390/electronics8010035.

[260] M. M. Forouzandeh, J. Aliasgari, and N. Karmakar, "A wideband directive filter for LO leakage reduction in UWB frequency-domain chipless RFID readers," in *Proc. IEEE Int. Conf. RFID (RFID)*, Apr. 2021, pp. 1–5, doi: 10.1109/RFID52461.2021.9444323.

[261] M. Forouzandeh, J. Aliasgari, and N. Karmakar, "On the improvement of baseband section of frequency-domain vector chipless RFID readers," *IEEE J. Radio Freq. Identif.*, vol. 6, pp. 140–150, 2022, doi: 10.1109/JRFID.2022.3145585.

[262] A. El-Awamry, A. Fawky, M. Khaliel, and T. Kaiser, "A novel adaptive spectrum scanning technique for reducing the identification time of the UWB chipless RFID system," in *Proc. IEEE 14th Int. Conf. Netw. Sens. Control (ICNSC)*, May 2017, pp. 356–361, doi: 10.1109/ICNSC.2017.8000118.

[263] A. El-Awamry, M. Khaliel, A. Fawky, and T. Kaiser, "Adaptive spectrum scanning techniques for reducing the identification time of the frequency coded chipless RFID system," *Trans. Emerg. Telecommun. Technol.*, vol. 28, no. 11, Nov. 2017, Art. no. e3173, doi: https://doi.org/10.1002/ett.3173..

[264] M. Forouzandeh and N. Karmakar, "Application of wideband differential phase shifters with wide phase range in chipless RFID readers," *IEEE Trans. Microw. Theory Techn.*, vol. 67, no. 9, pp. 3636–3650, Sep. 2019, doi: 10.1109/TMTT.2019.2929042.

[265] R. Koswatta and N. C. Karmakar, "Moving average filtering technique for signal processing in digital section of UWB chipless RFID reader," in *Proc. Asia–Pac. Microw. Conf.*, Dec. 2010, pp. 1304–1307.

[266] A. Vena, E. Perret, B. Sorli, and S. Tedjini, "Toward reliable readers for chipless RFID systems," in *Proc. 31st URSI Gen. Assembly Sci. Symp. (URSI GASS)*, Aug. 2014, pp. 1–4, doi: 10.1109/URSIGASS.2014.6929209.

[267] Z. Linlin, S. Rodriguez, Z. Lu, S. Botao, and Z. Li-Rong, "Design and implementation of a fully reconfigurable chipless RFID tag using Inkjet printing technology," in *Proc. IEEE Int. Symp. Circuits Syst. (ISCAS)*, May 2008, pp. 1524–1527, doi: 10.1109/ISCAS.2008.4541720.

[268] M. Garbati, R. Siragusa, E. Perret, and C. Halopé, "Impact of an IR-UWB reading approach on chipless RFID tag," *IEEE Microw. Wireless Compon. Lett.*, vol. 27, no. 7, pp. 678–680, Jul. 2017, doi: 10.1109/LMWC.2017.2711561.

[269] M. Barahona, D. Betancourt, and F. Ellinger, "Using UWB IR radar technology to decode multiple chipless RFID tags," in *Proc. IEEE Int. Conf. Ubiquitous Wireless Broadband (ICUWB)*, Oct. 2016, pp. 1–6, doi: 10.1109/ICUWB.2016.7790415.

[270] P. Kalansuriya and N. Karmakar, "UWB-IR based detection for frequency-spectra based chipless RFID," in *IEEE/MTT-S Int. Microw. Symp. Dig.*, Jun. 2012, pp. 1–3, doi: 10.1109/MWSYM.2012.6259704.

[271] P. Kalansuriya, N. C. Karmakar, and E. Viterbo, "On the detection of frequency-spectra-based chipless RFID using UWB impulsed interrogation," *IEEE Trans. Microw. Theory Techn.*, vol. 60, no. 12, pp. 4187–4197, Dec. 2012, doi: 10.1109/TMTT.2012.2222920.

[272] Z. W. Xia, L. Y. Tang, G. C. Wan, and M. S. Tong, "Design of recognition system for chipless RFID tags based on spectral characteristics," in *Proc. Progr. Electromagn. Res. Symp. (PIERS-Toyama)*, Aug. 2018, pp. 1884–1886, doi: 10.23919/PIERS.2018.8598015.

[273] M. Garbati, R. Siragusa, E. Perret, and C. Halopé, "Low cost low sampling noise UWB Chipless RFID reader," in *Proc. IEEE MTT-S Int. Microw. Symp.*, May 2015, pp. 1–4, doi: 10.1109/MWSYM.2015.7166944.

[274] M. Garbati, E. Perret, R. Siragusa, and C. Halopé, "Ultra-Low-jitter fully tunable baseband pulse generator for UWB applications," *IEEE Trans. Microw. Theory Techn.*, vol. 66, no. 1, pp. 420–430, Jan. 2018, doi: 10.1109/TMTT.2017.2728041.

[275] J. Aliasgari and N. C. Karmakar, "A pulse distortion approach for decoding frequency-coded tags in multicarrier chipless RFID systems," *IEEE Trans. Microw. Theory Techn.*, vol. 70, no. 3, pp. 1856–1870, Mar. 2022, doi: 10.1109/TMTT.2021.3128598.

[276] V. Sharma, A. Vithalkar, and M. Hashmi, "Power saving method in chipless RFID reader for IoT applications," in *Proc. IEEE Asia–Pac. Conf. Antennas Propag. (APCAP)*, Aug. 2018, pp. 374–375, doi: 10.1109/APCAP.2018.8538088.

[277] A. Fawky, M. Mohammed, M. El-Hadidy, and T. Kaiser, "UWB chipless RFID system performance based on real world 3D-deterministic channel model and ZF equalization," in *Proc. 8th Eur. Conf. Antennas Propag. (EuCAP)*, Apr. 2014, pp. 1765–1768, doi: 10.1109/EuCAP.2014.6902135.

[278] K. Mahmud and S. P. Majumder, "Improvement of the detection range of a chipless RFID for UWB system using receiver diversity with maximal ratio combining," in *Proc. 8th Int. Conf. Elect. Comput. Eng.*, Dec. 2014, pp. 761–764, doi: 10.1109/ICECE.2014.7026956.

[279] M. A. Islam and N. C. Karmakar, "A dual polarised universal reader for frequency domain-based chipless RFID tags and sensors," *IET Microw. Antennas Propag.*, vol. 15, no. 3, pp. 342–355, Feb. 2021, doi: https://doi.org/10.1049/mia2.12042..

[280] J. G. D. Hester and M. M. Tentzeris, "Inkjet-printed flexible mm-Wave Van-Atta reflect arrays: A solution for ultralong-range dense multitag and multisensing chipless RFID implementations for IoT smart skins," *IEEE Trans. Microw. Theory Techn.*, vol. 64, no. 12, pp. 4763–4773, Dec. 2016, doi: 10.1109/TMTT.2016.2623790.

[281] R. Koswatta and N. C. Karmakar, "Development of digital control section of RFID reader for multi-bit chipless RFID tag reading," in *Proc. Int. Conf. Elect. Comput. Eng. (ICECE)*, Dec. 2010, pp. 554–557, doi: 10.1109/ICELCE.2010.5700752.

[282] N. B. Buchanan and V. Fusco, "Single VCO chipless RFID near-field reader," *Electron. Lett.*, vol. 52, no. 23, pp. 1958–1960, Nov. 2016, [Online]. Available: https://doi.org/10.1049/el.2016.1834

[283] V. Sharma and M. Hashmi, "Chipless RFID reader for wide range applications," in *Proc. IEEE Int. Conf. Consum. Electron. Asia (ICCE-Asia)*, Jun. 2019, pp. 39–40, doi: 10.1109/ICCE-Asia46551.2019.8942208.

[284] M. Forouzandeh and N. Karmakar, "Low-cost chipless Rfid reader for polarizer tags," in *Proc. 4th Aust. Microw. Symp. (AMS)*, Feb. 2020, pp. 1–2, doi: 10.1109/AMS48904.2020.9059513.

[285] M. A. Islam, N. Karmakar, and A. K. M. Azad, "Aperture coupled UWB microstrip patch antenna array for mm-Wave chipless RFID tag reader," in *Proc. IEEE Int. Conf. RFID Technol. Appl. (RFID-TA)*, Nov. 2012, pp. 208–211, doi: 10.1109/RFID-TA.2012.6404514.

[286] M. Khaliel, A. Fawky, M. El-Hadidy, and T. Kaiser, "UWB reflectarray antenna for chipless RFID applications," in *Proc. 31st Nat. Radio Sci. Conf. (NRSC)*, Apr. 2014, pp. 17–20, doi: 10.1109/NRSC.2014.6835055.

[287] M. Khaliel, A. El-Awamry, A. Fawky, and T. Kaiser, "Long reading range for the frequency coded Chipless RFID system based on reflectarray antennas," *Int. J. Microw. Wireless Technol.*, vol. 10, no. 2, pp. 187–195, 2018, doi: 10.1017/S1759078718000442.

[288] H. M. Elkady, H. H. Abdullah, and S. M. Darwish, "A novel UWB quadrifilar plannar spiral antenna," in *Proc. Progr. Electromagn. Res. Symp. (PIERS-Toyama)*, Aug. 2018, pp. 1555–1559, doi: 10.23919/PIERS.2018.8598155.

[289] Y. X. Lin and Y. S. Chen, "Broadband and high-gain antenna for frequency-coded chipless RFID handheld readers," in *Proc. Int. Workshop Electromagn. Appl. Student Innov. Competition (iWEM)*, Aug. 2020, pp. 1–2, doi: 10.1109/iWEM49354.2020.9237395.

[290] Y. A. Alshoudokhi, S. A. Alshebeili, M. A. Ashraf, M. R. AlShareef, and H. M. Behairy, "Recent developments in chipless ultra-wideband (UWB) radio frequency identification (RFID) systems," in *Proc. IEEE 2nd Adv. Inf. Technol. Electron. Autom. Control Conf. (IAEAC)*, Mar. 2017, pp. 535–538, doi: 10.1109/IAEAC.2017.8054072.

[291] R. Anee and N. C. Karmakar, "Anti-collision methods for chipless RFID systems," in *Proc. Asia–Pac. Microw. Conf. (APMC)*, vol. 2, Dec. 2015, pp. 1–3, doi: 10.1109/APMC.2015.7413055.

[292] G. Khadka, M. A. Bibile, L. M. Arjomandi, and N. C. Karmakar, "Analysis of artifacts on chipless RFID backscatter tag signals for real world implementation," *IEEE Access*, vol. 7, pp. 66821–66831, 2019, doi: 10.1109/ACCESS.2019.2917757.

[293] M. El-Hadidy *et al.*, "Evaluation of UWB chipless RFID system performance considering indoor multipath propagation channel and real world aspects," in *Proc. Progr. Electromagn. Res. Symp.*, Jan. 2013, pp. 616–620.

[294] N. Karmakar, P. Kalansuriya, R. Azim, and R. Koswatta, *Chipless Radio Frequency Identification Reader Signal Processing*. Hoboken, NJ, USA: Wiley, 2016, pp. 1–267.

[295] G. Khadka, M. S. Arefin, and N. C. Karmakar, "A robust detection algorithm using AC characteristics of backscatter signal for chipless RFID system," in *Proc. IEEE MTT-S Int. Microw. Symp. (IMS)*, Jun. 2019, pp. 404–407, doi: 10.1109/MWSYM.2019.8700978.

[296] P. Kalansuriya and N. Karmakar, "Time domain analysis of a backscattering frequency signature based chipless RFID tag," in *Proc. Asia–Pac. Microw. Conf.*, Dec. 2011, pp. 183–186.

[297] J. Aliasgari and N. C. Karmakar, "Estimation of backscattered signals of frequency-coded chipless RFID tag," in *Proc. IEEE Asia–Pac. Microw. Conf. (APMC)*, Dec. 2019, pp. 111–113, doi: 10.1109/APMC46564.2019.9038715.

[298] M. Manteghi, "A space–time–frequency target identification technique for chipless RFID applications," in *Proc. IEEE Int. Symp. Antennas Propag. (APSURSI)*, Jul. 2011, pp. 3350–3351, doi: 10.1109/APS.2011.6058703.

[299] C. E. Baum, E. J. Rothwell, K. Chen, and D. P. Nyquist, "The singularity expansion method and its application to target identification," *Proc. IEEE*, vol. 79, no. 10, pp. 1481–1492, Oct. 1991, doi: 10.1109/5.104223.

[300] F. Babaeian and N. C. Karmakar, "Time and frequency domains analysis of chipless RFID back-scattered tag reflection," *Internet Things*, vol. 1, no. 1, pp. 109–127, 2020, doi: 10.3390/iot1010007.

[301] C. Hargrave, V. Clarkson, A. Abbosh, and N. Shuley, "Radar target identification: Estimating the start of the late time resonant response," in *Proc. Int. Conf. Radar*, Sep. 2013, pp. 335–340, doi: 10.1109/RADAR.2013.6652009.

[302] S. Jang, W. Choi, T. K. Sarkar, M. Salazar-Palma, K. Kyungjung, and C. E. Baum, "Exploiting early time response using the fractional Fourier transform for analyzing transient radar returns," *IEEE Trans. Antennas Propag.*, vol. 52, no. 11, pp. 3109–3121, Nov. 2004, doi: 10.1109/TAP.2004.835165.

[303] R. Rezaiesarlak and M. Manteghi, "Accurate extraction of early-/late-time responses using short-time matrix pencil method for transient analysis of scatterers," *IEEE Trans. Antennas Propag.*, vol. 63, no. 11, pp. 4995–5002, Nov. 2015, doi: 10.1109/TAP.2015.2477096.

[304] R. Rezaiesarlak and M. Manteghi, "Short-time matrix pencil method for chipless RFID detection applications," *IEEE Trans. Antennas Propag.*, vol. 61, no. 5, pp. 2801–2806, May 2013, doi: 10.1109/TAP.2013.2238497.

[305] C. Divarathne and N. Karmakar, "ML detection based SISO Chipless RFID tag reading," in *Proc. 44th Eur. Microw. Conf.*, Oct. 2014, pp. 762–765, doi: 10.1109/EuMC.2014.6986546.

[306] J. Alam, M. Khaliel, A. Fawky, A. El-Awamry, and T. Kaiser, "Frequency-coded chipless RFID tags: Notch model, detection, angular orientation, and coverage measurements," *Sensors*, vol. 20, no. 7, p. 1843, 2020, doi: 10.3390/s20071843.

[307] N. Karmakar, S. Shrestha, and M. A. Bibile, "TagID generation and detection of Chipless RFID system," in *Proc. FERMAT*, vol. 21, 2017, p. 3.

[308] W. Dullaert, L. Reichardt, and H. Rogier, "Improved detection scheme for chipless RFIDs using prolate spheroidal wave function-based noise filtering," *IEEE Antennas Wireless Propag. Lett.*, vol. 10, pp. 472–475, 2011, doi: 10.1109/LAWP.2011.2155023.

[309] A. Fawky, A. El-Awamry, M. Khaliel, and T. Kaiser, "Novel notch detection techniques for Frequency Coded chipless RFID," in *Proc. IEEE 14th Int. Conf. Netw. Sens. Control (ICNSC)*, May 2017, pp. 345–350, doi: 10.1109/ICNSC.2017.8000116.

[310] Y. L. Lu, L. Y. Liu, and W. Liu, "Chipless RFID tag design and detection with adaptive direct path cancellation," in *Proc. Asia–Pac. Microw. Conf. (APMC)*, vol. 2, Dec. 2015, pp. 1–3, doi: 10.1109/APMC.2015.7413045.

[311] A. M. J. Marindra and G. Y. Tian, "Multiresonance chipless RFID sensor tag for metal defect characterization using principal component analysis," *IEEE Sensors J.*, vol. 19, no. 18, pp. 8037–8046, Sep. 2019, doi: 10.1109/JSEN.2019.2917840.

[312] A. Habib, M. A. Afzal, H. Sadia, Y. Amin, and H. Tenhunen, "Chipless RFID tag for IoT applications," in *Proc. IEEE 59th Int. Midwest Symp. Circuits Syst. (MWSCAS)*, Oct. 2016, pp. 1–4, doi: 10.1109/MWSCAS.2016.7870033.

[313] R. T. Alencar, Z. Ali, N. Barbot, M. Garbati, and E. Perret, "Practical performance comparison of 1-D and 2-D decoding methods for a chipless RFID system in a real environment," *IEEE J. Radio Freq. Identif.*, vol. 4, no. 4, pp. 532–544, Dec. 2020, doi: 10.1109/JRFID.2020.2997988.

[314] F. Babaeian and N. C. Karmakar, "Hybrid chipless RFID tags—A pathway to EPC global standard," *IEEE Access*, vol. 6, pp. 67415–67426, 2018, doi: 10.1109/ACCESS.2018.2879050.

[315] K. Brinker and R. Zoughi, "Tunable chipless RFID pressure sensor utilizing additive manufacturing," in *Proc. IEEE Int. Instrum. Meas. Technol. Conf. (I2MTC)*, May 2022, pp. 1–6.

[316] E. Perret, "Micrometrie displacement sensor based on chipless RFID," in *Proc. IEEE MTT-S Int. Microw. Symp. (IMS)*, Jun. 2017, pp. 605–608, doi: 10.1109/MWSYM.2017.8058640.

[317] A. Vena, M. Tedjini, T. Björninen, L. Sydänheimo, L. Ukkonen, and M. M. Tentzeris, "A novel inkjet-printed wireless chipless strain and crack sensor on flexible laminates," in *Proc. IEEE Antennas Propag. Soc. Int. Symp. (APSURSI)*, Jul. 2014, pp. 1294–1295, doi: 10.1109/APS.2014.6904974.

[318] R. Suwalak, C. Phongcharoenpanich, D. Torrungrueng, and P. Akkaraekthalin, "Dielectric material determination using the radar equation in RFID sensor applications," in *Proc. IEEE Conf. Antenna Meas. Appl. (CAMA)*, Nov./Dec. 2015, pp. 1–4, doi: 10.1109/CAMA.2015.7428131.

[319] S. Mukherjee, "Chipless radio frequency identification by remote measurement of complex impedance," in *Proc. Eur. Microw. Conf.*, Oct. 2007, pp. 1007–1010, doi: 10.1109/EUMC.2007.4405366.

[320] P. Kalansuriya, N. Karmakar, and E. Viterbo, "Signal space representation of chipless RFID tag frequency signatures," in *Proc. IEEE Global Telecommun. Conf. (GLOBECOM)*, Dec. 2011, pp. 1–5, doi: 10.1109/GLOCOM.2011.6133629.

[321] C. Divarathne and N. Karmakar, "A feasible detection technique for chipless RFID systems based on likelihood," in *Proc. 1st Aust. Microw. Symp. (AMS)*, Jun. 2014, pp. 5–6, doi: 10.1109/AUSMS.2014.7017338.

[322] A. El-Awamry, A. Fawky, M. El-Hadidy, and T. Kaiser, "Smart notch detection techniques for robust frequency coded chipless RFID systems," in *Proc. 9th Eur. Conf. Antennas Propag. (EuCAP)*, Apr. 2015, pp. 1–5.

[323] M. Barahona, D. Betancourt, F. Ellinger, K. Haase, G. C. Schmidt, and A. C. Hübler, "Automatic IR UWB chipless RFID system for short range applications," in *Proc. IEEE-APS Topical Conf. Antennas Propag. Wireless Commun. (APWC)*, Sep. 2017, pp. 274–279, doi: 10.1109/APWC.2017.8062300.

[324] C. Divarathne and N. Karmakar, "A maximum likelihood based tag detection technique for MIMO chipless RFID systems," in *Proc. IEEE Int. Microw. RF Conf. (IMaRC)*, Dec. 2014, pp. 5–8, doi: 10.1109/IMaRC.2014.7038958.

[325] K. Yang, U. Botero, H. Shen, D. Forte, and M. Tehranipoor, "A split manufacturing approach for unclonable chipless RFIDs for pharmaceutical supply chain security," in *Proc. Asian Hardw. Orient. Security Trust Symp. (AsianHOST)*, Oct. 2017, pp. 61–66, doi: 10.1109/AsianHOST.2017.8353996.

[326] G. Wan, M. Zhang, W. Li, and L. Chen, "A novel detection method based on maximum-likelihood estimation decoding of a 6-bit chipless radio frequency identification coded tag," *IEEE Trans. Instrum. Meas.*, vol. 70, pp. 1–11, 2021, doi: 10.1109/TIM.2020.3019616.

[327] C. Divarathne and N. Karmakar, "An advanced tag detection technique for chipless RFID systems," in *Proc. Eur. Microw. Conf. (EuMC)*, Sep. 2015, pp. 251–254, doi: 10.1109/EuMC.2015.7345747.

[328] A. El-Awamry, M. Khaliel, A. Fawky, M. El-Hadidy, and T. Kaiser, "Novel notch modulation algorithm for enhancing the chipless RFID tags coding capacity," in *Proc. IEEE Int. Conf. RFID (RFID)*, Apr. 2015, pp. 25–31, doi: 10.1109/RFID.2015.7113069.

[329] Z. Ali and E. Perret, "Notes on the extraction of aspect-independent parameters of chipless RFID tags," in *Proc. 6th Int. Conf. Smart Sustain. Technol. (SpliTech)*, Sep. 2021, pp. 1–6, doi: 10.23919/SpliTech52315.2021.9566393.

[330] T. K. Sarkar and O. Pereira, "Using the matrix pencil method to estimate the parameters of a sum of complex exponentials," *IEEE Antennas Propag. Mag.*, vol. 37, no. 1, pp. 48–55, Feb. 1995, doi: 10.1109/74.370583.

[331] A. Blischak and M. Manteghi, "Pole residue techniques for chipless RFID detection," in *Proc. IEEE Antennas Propag. Soc. Int. Symp.*, Jun. 2009, pp. 1–4, doi: 10.1109/APS.2009.5172097.

[332] Y. He, L. Xu, and C. Y. Zou, "Effect of dielectric substrate on pole characteristic of chipless tag," in *Proc. Int. Conf. Control Eng. Commun. Technol.*, Dec. 2012, pp. 564–567, doi: 10.1109/ICCECT.2012.259.

[333] S. Nongpromma, A. Boonpoonga, P. Akkaraekthalin, L. Bannawat, and T. Lertwiriyaprapa, "Simple chipless RFID sensor for dielectric sensing using shot-time matrix pencil method," in *Proc. 9th Int. Elect. Eng. Congr. (iEECON)*, Mar. 2021, pp. 583–586, doi: 10.1109/iEECON51072.2021.9440250.

[334] R. Rezaiesarlak and M. Manteghi, *Chipless RFID, Design Procedure and Detection Techniques*. Cham, Switzerland: Springer, 2015, pp. 1–159.

[335] M. Manteghi, "A novel approach to improve noise reduction in the matrix pencil algorithm for chipless RFID tag detection," in *Proc. IEEE Antennas Propag. Soc. Int. Symp.*, Jul. 2010, pp. 1–4, doi: 10.1109/APS.2010.5562223.

[336] C. M. Nijas, V. R. Sajitha, R. Vivek, P. Mohanan, B. Paul, and S. Mridula, "Spectral extraction of chipless RFID tag using time domain analysis," in *Proc. IEEE Int. Symp. Antennas Propag. USNC/URSI Nat. Radio Sci. Meeting*, Jul. 2015, pp. 169–170, doi: 10.1109/APS.2015.7304470.

[337] M. A. Bibile and N. C. Karmakar, "Moving chipless RFID tag detection using adaptive wavelet-based detection algorithm," *IEEE Trans. Antennas Propag.*, vol. 66, no. 6, pp. 2752–2760, Jun. 2018, doi: 10.1109/TAP.2018.2819725.

[338] M. Manekiya, M. Donelli, A. Kumar, and S. K. Menon, "A novel detection technique for a chipless RFID system using quantile regression," *Electronics*, vol. 7, no. 12, p. 409, 2018, doi: 10.3390/electronics7120409.

[339] M. Donelli, M. Manekiya, and S. K. Menon, "Enhanced chipless RFID with Van-Atta and quantile regression," in *Proc. 34th Gen. Assembly Sci. Symp. Int. Union Radio Sci. (URSI GASS)*, Aug./Sep. 2021, pp. 1–4, doi: 10.23919/URSIGASS51995.2021.9560214.

[340] S. Jeong, J. G. D. Hester, W. Su, and M. M. Tentzeris, "Read/interrogation enhancement of chipless RFIDs using machine learning techniques," *IEEE Antennas Wireless Propag. Lett.*, vol. 18, no. 11, pp. 2272–2276, Nov. 2019, doi: 10.1109/LAWP.2019.2937055.

[341] L. M. Arjomandi, G. Khadka, and N. C. Karmakar, "mm-Wave chipless RFID decoding: Introducing image-based deep learning techniques," *IEEE Trans. Antennas Propag.*, vol. 70. no. 5, pp. 3700–3709, May 2022, doi: 10.1109/TAP.2021.3137197.

[342] M. A. Bibile and N. A. Karmakar, "Detection error rate analysis using coloured noise for the movement of chipless RFID tag," in *Proc. Aust. Microw. Symp. (AMS)*, Feb. 2018, pp. 1–2, doi: 10.1109/AUSMS.2018.8346952.

[343] R. T. D. Alencar, N. Barbot, M. Garbati, and E. Perret, "Practical comparison of decoding methods for chipless RFID system in real environment," in *Proc. IEEE Int. Conf. RFID Technol. Appl. (RFID-TA)*, Sep. 2019, pp. 207–211, doi: 10.1109/RFID-TA.2019.8892020.

[344] Z. Ali *et al.*, "Chipless RFID tag discrimination and the performance of resemblance metrics to be used for it," in *Proc. IEEE/MTT-S Int. Microw. Symp. (IMS)*, Jun. 2018, pp. 363–366, doi: 10.1109/MWSYM.2018.8439855.

[345] Z. Ali *et al.*, "Detection of natural randomness by chipless RFID approach and its application to authentication," *IEEE Trans. Microw. Theory Techn.*, vol. 67, no. 9, pp. 3867–3881, Sep. 2019, doi: 10.1109/TMTT.2019.2914102.

[346] F. Costa *et al.*, "Robust reading approach for moving chipless RFID tags by using ISAR processing," *IEEE Trans. Microw. Theory Techn.*, vol. 66, no. 5, pp. 2442–2451, May 2018, doi: 10.1109/TMTT.2017.2779801.

[347] M. Borgese, S. Genovesi, G. Manara, and F. Costa, "System Level Performance in Chipless RFID," in *Proc. URSI GASS*, Rome, Italy, 2021, pp. 1–6.

[348] C. Divarathne and N. Karmakar, "MIMO based chipless RFID system," in *Proc. IEEE Int. Conf. RFID Technol. Appl. (RFID-TA)*, Nov. 2012, pp. 423–428, doi: 10.1109/RFID-TA.2012.6404560.

[349] G. Pevtsov, A. Yatsutsenko, Y. Trofimenko, D. Karlov, and M. Bortsova, "Theoretical basics of radar signals energy detection," in *Proc. Int. Conf. Math. Methods Electromagn. Theory*, Aug. 2012, pp. 324–327, doi: 10.1109/MMET.2012.6331269.

[350] A. Lazaro, A. Ramos, D. Girbau, and R. Villarino, "Signal processing techniques for chipless UWB RFID thermal threshold detector detection," *IEEE Antennas Wireless Propag. Lett.*, vol. 15, pp. 618–621, 2016, doi: 10.1109/LAWP.2015.2464680.

[351] A. M. J. Marindra and G. Y. Tian, "Chipless RFID sensor for corrosion characterization based on frequency selective surface and feature fusion," *Smart Mater. Struct.*, vol. 29, no. 12, Oct. 2020, Art. no. 125010, doi: 10.1088/1361-665x/abbff4.

[352] K. Yang, D. Forte, and M. M. Tehranipoor, "UCR: An unclonable chipless RFID tag," in *Proc. IEEE Int. Symp. Hardw. Orient. Security Trust (HOST)*, May 2016, pp. 7–12, doi: 10.1109/HST.2016.7495548.

[353] F. Costa *et al.*, "On the reading of moving chipless RFID tags," in *Proc. 2nd URSI Atlantic Radio Sci. Meeting (AT-RASC)*, May/Jun. 2018, pp. 1–3, doi: 10.23919/URSI-AT-RASC.2018.8471593.

[354] F. Costa *et al.*, "Detection of moving chipless tags by using SAR processing," in *Proc. IEEE Int. Conf. RFID Technol. Appl. (RFID-TA)*, Sep. 2017, pp. 229–232, doi: 10.1109/RFID-TA.2017.8098890.

[355] M. A. Bibile and N. A. Karmakar, "Detection performance of a chipless RFID tag in motion," in *Proc. IEEE MTT-S Int. Microw. RF Conf. (IMaRC)*, Dec. 2016, pp. 1–4, doi: 10.1109/IMaRC.2016.7939629.

[356] N. Zhang, X. Liu, and T. Chang, "A chipless RFID Unit Based on interference for tag location," in *Proc. 6th Asia–Pac. Conf. Antennas Propag. (APCAP)*, Oct. 2017, pp. 1–3, doi: 10.1109/APCAP.2017.8420377.

[357] A. A. Abbas, M. El-Absi, A. Abualhijaa, K. Solbach, and T. Kaiser, "Dielectric resonator-based passive chipless tag with angle-of-arrival sensing," *IEEE Trans. Microw. Theory Techn.*, vol. 67, no. 5, pp. 2010–2017, May 2019, doi: 10.1109/TMTT.2019.2901447.

[358] M. El-Hadidy, A. El-Awamry, A. Fawky, M. Khaliel, and T. Kaiser, "Real-world testbed for multi-tag UWB chipless RFID system based on a novel collision avoidance MAC protocol," *Trans. Emerg. Telecommun. Technol.*, vol. 27, no. 12, pp. 1707–1714, 2016, doi: https://doi.org/10.1002/ett.3124..

KATELYN R. BRINKER (Graduate Student Member, IEEE) received the B.S. degree in electrical engineering and computer engineering and the M.S. degree in electrical engineering from the Missouri University of Science and Technology (Missouri S&T), Rolla, MO, USA, in 2017 and 2019, respectively. She is currently pursuing the Ph.D. degree in electrical engineering with the support of the NASA Space Technology Research Fellowship (2017–2021), Iowa State University. She was a recipient of the 2017 IEEE-HKN Alton B. Zerby and Carl T. Koerner Outstanding Student Award, the 2017 IEEE-USA recipient of the DiscoverE New Faces of Engineering Award, and the 2018 IEEE St. Louis Section Outstanding Graduate Student Award. She has served as a Student Governor and PR & Communications Committee Chair to the Board of Governors for IEEE-HKN and she is currently serving as a Member-At-Large to the AdCom of the IEEE Instrumentation and Measurement Society.

REZA ZOUGHI (Fellow, IEEE) received the B.S.E.E., M.S.E.E., and Ph.D. degrees in electrical engineering (radar remote sensing, radar systems, and microwaves) from the University of Kansas.

From 1981 to 1987, he was with the Radar Systems and Remote Sensing Laboratory, University of Kansas. He is the Kirby Gray (Battelle) Chair of Engineering and a Professor with Electrical and Computer Engineering, Iowa State University, where he is also the Director of Center for Nondestructive Evaluation. He served as the Schlumberger Endowed Professor with the Electrical and Computer Engineering, Missouri University of Science and Technology (Missouri S&T) from January 2001 to August 2019. Prior to joining Missouri S&T and in 1987, he was with the Electrical and Computer Engineering Department, Colorado State University (CSU), where he was a Professor and established the Applied Microwave Nondestructive Testing Laboratory (amntl) (http://amntl.mst.edu/). He held the position of Business Challenge Endowed Professor with Electrical and Computer Engineering from 1995 to 1997, CSU. He has authored a textbook titled *Microwave Nondestructive Testing and Evaluation Principles* (KLUWER Academic Publishers, 2000), and coauthored a Chapter on Microwave Techniques in the book titled *Nondestructive Evaluation: Theory, Techniques, and Applications* (Marcel and Dekker, Inc., 2002). He has coauthored more than over 177 refereed journal papers, 358 conference proceedings and presentations and 120 technical reports. He has 19 issued U.S. patents to his credit (in addition to several issued abroad) in the field of microwave nondestructive testing and evaluation. He received Nine Teaching Awards, including the State Board of Agriculture, Excellence in Undergraduate Teaching Award and the Abell Faculty Teaching Award, while at CSU. He has received 17 Outstanding Teaching Awards and Commendations, while at Missouri S&T. He is a recipient of the 2007 IEEE Instrumentation and Measurement Society Distinguished Service Award, the 2009 American Society for Nondestructive Testing (ASNT) Research Award for Sustained Excellence, and the 2011 IEEE Joseph F. Keithley Award in Instrumentation and Measurement. In 2013 and 2020, he and his coauthors received the H. A. Wheeler Applications Prize Paper Award from the IEEE Antennas and Propagation Society. He has delivered numerous Invited and Keynote presentations on the subject of microwave and millimeter wave nondestructive testing and imaging. He served as the Editor-in-Chief of the IEEE TRANSACTIONS ON INSTRUMENTATION AND MEASUREMENT from 2007 to 2011, three terms as an at-large AdCom Member of the IEEE Instrumentation and Measurement (I&M) Society, as an I&M Society President from 2014 to 2015, and serves as an I&M Society Distinguished Lecturer. He served as the General Co-Chair of the 2013 IEEE Instrumentation and Measurement Technology Conference. He has been elected as an at-large Member of IEEE Publications Services & Products Board (PSPB) for two terms from 2016 to 2018 and in 2019, and served on the IEEE TAB/PSPB in 2015 and from 2017 to 2019. He is also a Fellow of ASNT.